Layer-by-Layer Deposition and Silane SAMs: Thin Film Interactions with DNA Nanostructures

by

Jason T. Smith

B.S. in Chemistry, University of Florida, 2018

Submitted to the Graduate Faculty of

The Kenneth P. Dietrich School of Arts and Sciences in partial fulfillment

of the requirements for the degree of

Masters of Science

University of Pittsburgh

2022

UNIVERSITY OF PITTSBURGH

KENNETH P. DIETRICH SCHOOL OF ARTS AND SCIENCES

This thesis was presented

by

Jason T. Smith

It was defended on

May 13th, 2022

and approved by

Lei Li, Ph.D., Associate Professor, Department of Chemical and Petroleum Engineering

Jill Millstone, Ph.D., Professor of Chemistry, Department of Chemistry

Dissertation Advisor: Haitao Liu, Ph.D., Associate Professor, Department of Chemistry

Layer-by-Layer Deposition and Silane SAMs: Thin Film Interactions with DNA Nanostructures

Jason T. Smith, M.S.

University of Pittsburgh, 2022

Abstract

DNA molecules possess a variety of properties aside from genetics. These include structural stability, programmability of sequences, and predictable self-assembly. Because of these non-genetic properties, DNA nanotechnology has been studied and harnessed for a variety of applications. These include X-ray crystallography, spectroscopy, medicine, therapeutics, and machinery. Recently, many researchers have investigated how DNA nanostructures interact with various materials. This research of DNA nanostructure-material interaction has been used to develop a variety of applications. These applications include drug-delivery, biosensors, electronics, and magnetic devices.

This thesis focuses on analyzing the interactive behavior of DNA origami nanostructures with various materials, particularly thin films. Chapter one discusses the history and background of DNA nanotechnology with a particular focus on DNA origami and the interaction between DNA origami and thin films. Chapter two investigates the idea of growing inorganic materials on top of DNA nanostructures using the thin film technique layer-by-layer deposition. This chapter also discusses the history of layer-by-layer deposition along with the relationship it has with DNA origami. The third chapter discusses the interactions between DNA nanostructures and various organosilane self-assembled monolayers grown on SiO_2 wafers. This chapter also discusses the history of self-assembled monolayers (SAMs) and their relationship with DNA origami. Ultimately, this thesis' goal is to encourage future work regarding DNA nanostructures and their interactions with various materials to further the endeavors of mankind.

Table of Contents

List of Tables

List of Figures

1.0 INTRODUCTION

1.1: DNA NANOTECHNOLOGY

DNA, an abbreviation for deoxyribonucleic acid, is a molecule that houses genetic information. It is this molecule that is used to carry, organize, and convey all genetic information for every living organism. DNA is either composed of two or one polynucleotide chains. Depending on whether two or one polynucleotides are used, DNA can be classified as either double stranded (dsDNA) or single stranded (ssDNA) respectively.[1] In dsDNA, these chains coil around each other and form a double helix structure. DNA is a polymer built up of monomers called nucleotides. Each nucleotide in the DNA structure consists of a base, a sugar (specifically called deoxyribose), and a negatively charged phosphate group (Figure 1a).[2] The alternating sugar and phosphate groups form the backbone of DNA. This backbone forms the outer part of the double helix while the bases pair up and form the "rungs" of the helix structure (Figure 1b). Each base is bound to the deoxyribose sugar part of the backbone and comes in four different varieties. These four base types are: adenine (A), cytosine (C), guanine (G), and thymine (T). These bases are further classified into one of two groups, being categorized by the aromatic heterocyclic structure each base possesses. This leads to the bases being classified as either purines (A and G) or pyrimidines (C and T).[2 – 3]

What makes DNA special is Watson-Crick base pairing between the different bases. In this model, one particular type of purines binds to one particular type of pyrimidines through hydrogen bonding (Figure 1c). This base pairing is such that adenine always pairs with thymine and guanine always pairs with cytosine.[3] Because of Watson-Crick base pairing, the hybridization of DNA is both precise and predictable. The precise and predictable hybridization possessed by DNA enables it to be programmable in terms of self-assembly. This makes DNA

not only a great hereditary material, but also an ideal molecule for designing nanometer-scale structures.[4]

Dimensionally, a DNA helix has an approximate diameter of 2 nm with a linear length of 3.5 nm every full circular turn. Additionally, the helix makes a full circular turn every 10 base pairs. These dimensions, combined with precise and predictable molecular recognition, allows DNA to be used for fabricating arbitrarily-shaped multi-dimensional nanostructures with a theoretical resolution of 2 – 3 nm.[5 – 10] When compared to other self-assembled structures made of other materials, such as proteins or block copolymers, DNA nanostructures possess a degree of control over shape and size that is unmatched.[11 – 12] Furthermore, DNA nanostructures have an edge in the realm of economics. The fast growth of biomedical research has lowered the current market price of custom synthetic oligonucleotides down to $17.50 per base per 10 μmol. With this price, it would cost less than $6.00 to cover an area of 1 m^2 of substrate with a monolayer of DNA.[13]

Given their dimensional, programmable, and economical advantages, DNA nanostructures have received attention as an alternative to the expensive current state-of-the-art photolithography techniques used to generate ultra-high-resolution patterns. In this section of the thesis, DNA nanotechnology relevant to this project will be examined by reviewing the history of DNA nanotechnology, an in-depth discussion of DNA origami, and an analysis of past projects focused on the interactive behavior between DNA origami nanostructures and various substrates relevant to the project.

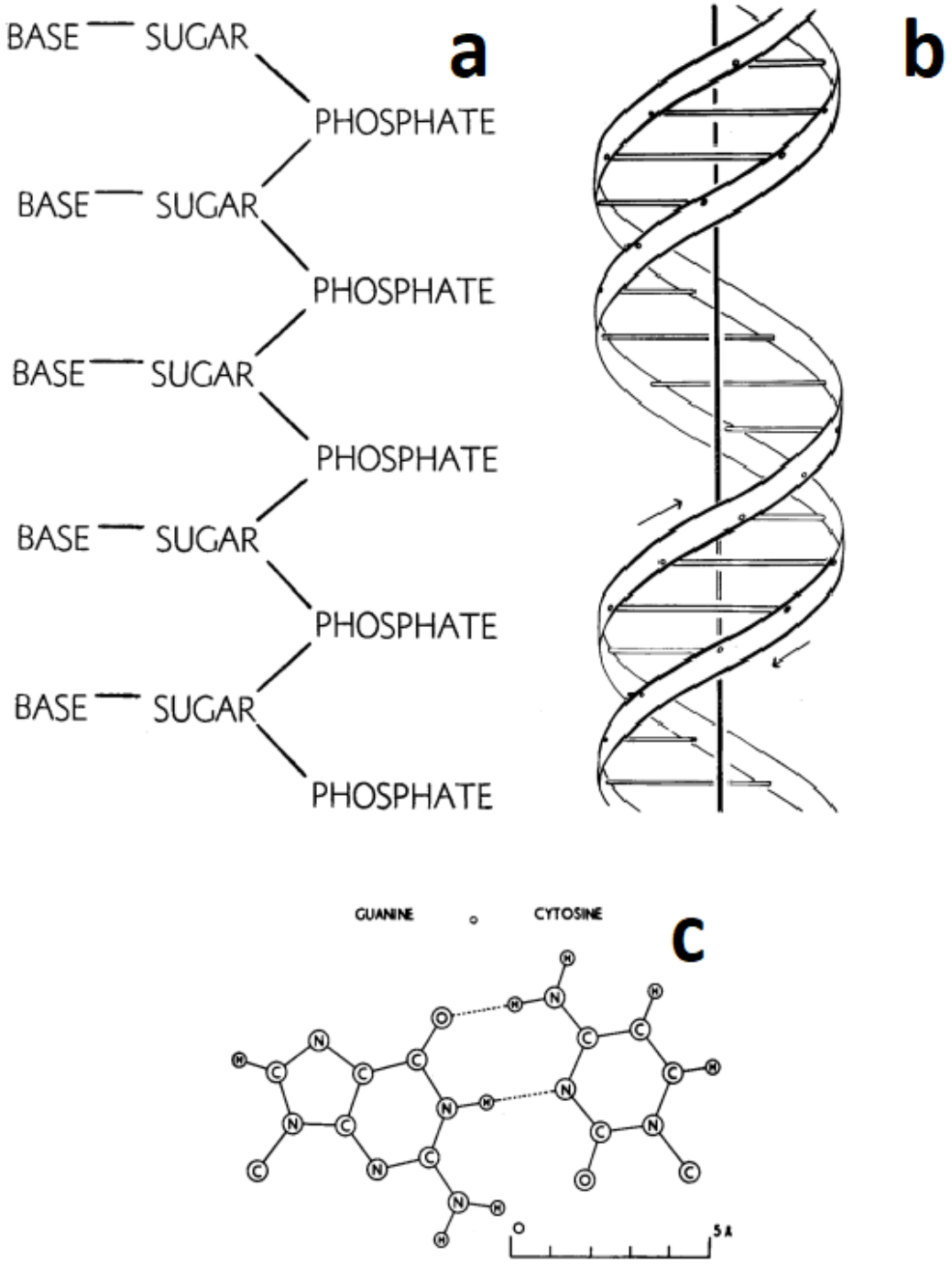

Figure 1. Characteristics of DNA. (a) Schematic showing the structural arrangement of nucleotides which form the DNA structure. (b) Example of DNA double helix structure along with seeing the rungs of the helix and phosphate backbone. (c) Representation of Watson-Crick base pairing model. Here guanine is shown to interact with cytosine through hydrogen bonding. Reprinted by permission from Springer Nature: *Nature*, *Nature*, Molecular Structure of Nucleic Acids: A Structure for Deoxyribose Nucleic Acid, J. D. Watson et al. © 1953.

1.2: HISTORY OF DNA NANOTECHNOLOGY

DNA nanotechnology was initially proposed by Nadrian Seeman in 1982. Seeman saw a unique woodcut titled *Depth (*Figure 2).[14] In this piece of art, flying fish were arrayed in a pattern where their wings created six-arm junctions. To Seeman, this pattern of flying fish looked similar to an array of DNA six-arm junctions. With this in mind, he considered using 3D lattices of DNA to orient hard-to-crystallize molecules. He proposed that this was possible by creating immobile DNA junctions using properly designed strand sequences within the DNA molecules themselves. This would allow the DNA to be combined into rigid crystalline lattices.[15]

Seeman produced the first DNA nanostructures which were in the form of immobile branched Holliday junction-like constructs (Figure 2). Here, ssDNA strands were linked together in a crossroad-like pattern forming the Holliday junctions. Additionally, these junctions possessed an overhang at the end of each arm called a sticky-end. These sticky-ends allowed for the junctions to be stitched together to form larger patterns. Through utilizing these junctions and sticky-ends, various structures could potentially be constructed on both the 2D and 3D planes.[16 – 17] Seeman proved this theory in 1991 when he developed the very first 3D DNA nanostructure. This structure consisted of a cube formed by turning the junctions' branch points into vertices and the branched molecules' sticky-ends into the cube's edges.[18]

Since Seeman pioneered the idea of utilizing a sequence of DNA to build mechanically robust nanostructures in 1982, the field of structural DNA nanotechnology has rapidly advanced. Within approximately forty years, DNA nanostructures have evolved from simple "single-stranded tiles" and Holliday junctions, to complex shapes and designs ranging from 2D to 3D.[19 – 20] The fabrication of DNA has evolved into a variety of different forms with a variety of different methods to create them. In the main, the vast majority of these new methods are able

to create more complex patterns, lattices, and shapes. One of the most successful, versatile, and effective methods for creating DNA nanostructures is DNA origami which will be discussed in-depth in the following section.

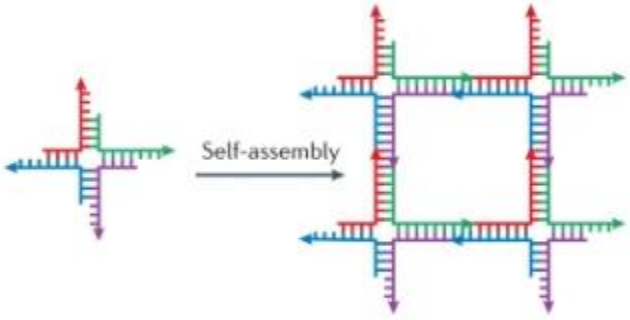

Figure 2. Origin of DNA nanotechnology. Schematic representation of a four-arm branched DNA molecule with sticky-end tails to form larger arrangements. Reprinted by permission from Springer Nature Customer Service Centre GmbH: Nature, *Nature Review Materials*, DNA nanotechnology, Nadrian C. Seeman et al. © 2017.

1.3: DNA ORIGAMI

DNA origami was developed in 2006 by Paul Rothemund. In summary, DNA origami is a nanoscale folding process in which complementary base pairing of DNA is used to form arbitrary two- and three-dimensional shapes. To produce a desired shape, certain structures are drawn with a raster fill of a single long DNA molecule. The design is then fed into a computer program which determines the placement of individual strands called staple strands. Each staple strand binds to a specific region of the DNA scaffold strand according to the Watson-Crick base pairing. The DNA is then heated to anneal the DNA and then cooled. As the DNA cools the various staples bend the DNA scaffold strand into the desired shape. DNA origami has been used to produce a variety of shapes including squares, smiley faces, and triangles (Figure 3).[21] In 2009, a milestone advancement was achieved when Shih and coworkers constructed bundled DNA helices into a 3D array of honeycomb lattices. This accomplishment revealed that DNA origami could also be used to construct 3D structures as well.[22]

DNA origami is a very powerful form of DNA nanofabrication. It is considered a major breakthrough in DNA nanotechnology due to two min advantages. First, DNA origami is capable of making a variety of different patterns and architectures. The number of different patterns and shapes produced via DNA origami has shown that practically any given shape or design is possible due to the magnificent folding properties of the method (Figure 4). Additionally, DNA origami nanostructures possess details and complexities which are magnitudes higher than any other current DNA nanofabrication method.[23 – 25] The second major advantage of DNA origami is its simplicity in experimentation. Most DNA nanofabrication methods require highly purified DNA strands along with precise measurements in the concentrations. Additionally, the annealing processes for these other methods are usually time consuming and can take days. Unlike these methods, DNA origami is capable of fabricating

DNA nanostructures from unpurified staple strands at varying stoichiometric measurements.[26 – 27] The annealing process of DNA origami is also much faster, usually taking only a couple of hours for completion. Aside from these two major achievements, DNA origami has other advantages such as high yields and enhanced structural stability.[28]

As mentioned earlier, DNA origami has been extensively used in the process of nanofabrication. DNA origami nanostructures have been used in a variety of different ways throughout many different areas of scientific research. These uses range from masking materials for nanolithography to template structures for biomolecules. Additionally, these devices fabricated by DNA origami have been used in a variety of applications including nanoplasmonics, nanophotonics, biosensing, and drug delivery.

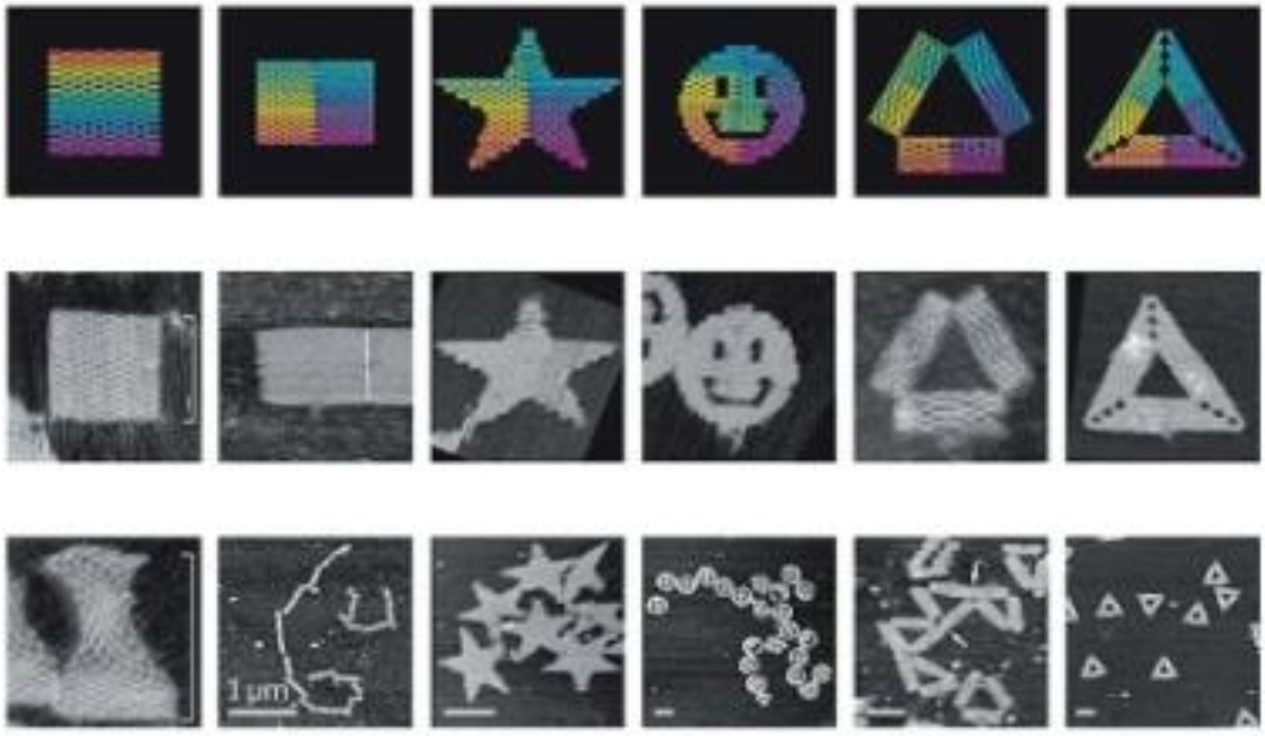

Figure 3. Examples of DNA origami. Simple DNA origami structures which have been designed include (left to right) squares, rectangles, stars, smiley faces, trapezoids, and triangles. Reprinted by permission from Springer Nature Customer Service Centre GmbH: Nature, *Nature*, Folding DNA to create nanoscale shapes and patterns, Paul W. K. Rothemund. © 2006.

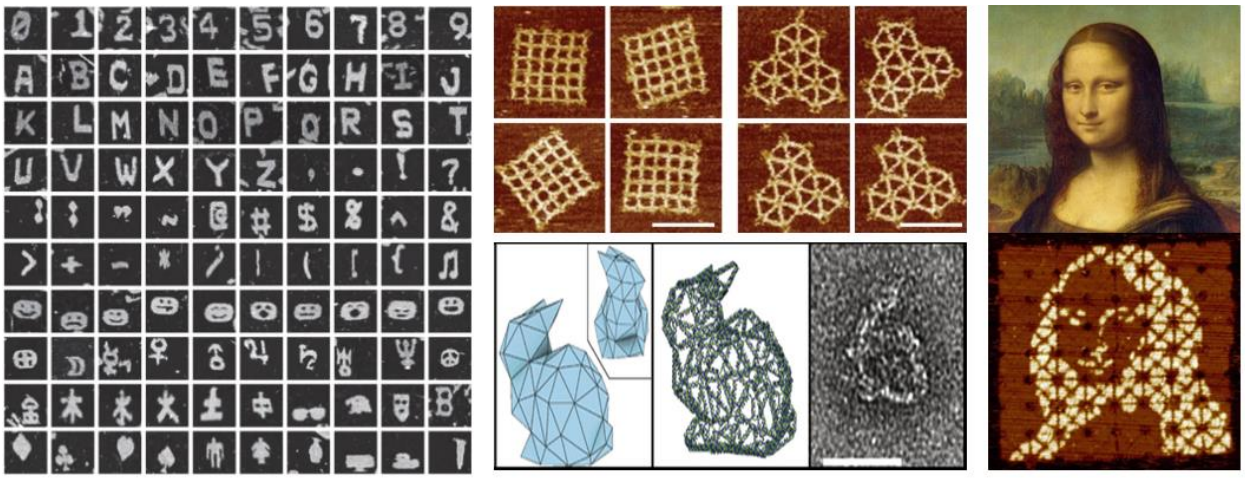

Figure 4. Examples of complex DNA origami structures. Examples of more arbitrary and complex DNA origami nanostructures such as figures and letters (left). Example of DNA origami tessellation patterns (upper center). Example of 3D DNA origami (bottom center). DNA origami Mona Lisa (right). Reprinted by permission from Springer Nature: *Nature*, *Nature*, Complex shapes self-assembled from single-stranded DNA tiles, Bryan Wei, et al. © 2012 (a), Reprinted by permission from Springer Nature: Nature Nanotechnology, *Nature Nanotechnology*, Complex wireframe DNA origami nanostructures with multi-arm junction vertices, Fei Zhang et al. © 2015 (b), Reprinted by permission from Springer Nature: *Nature*, *Nature*, DNA rendering of polyhedral meshes at the nanoscale, Erik Benson et al. © 2015 (c), Reprinted by permission from Springer Nature: Nature, *Nature*, Fractal assembly of micrometre-scale DNA origami arrays with arbitrary patterns, Grigory Tikhomirov et al. © 2017 (d).

1.4: DNA ORIGAMI TEMPLATES AND NANOPARTICLE INTERACTION

DNA origami has been studied in a variety of ways. One growing research area is DNA origami-nanoparticle interactions. This focus on DNA origami consists of projects mainly revolving around using the DNA nanostructure as a template or surface where certain nanoparticles can grow onto it. Utilizing DNA nanostructures in this way has resulted in various applications. The investigation of DNA origami templates ranges from protein assembly to nanoscale metallization.[29 – 30] Due to the vast number of projects revolving around DNA origami templates, this section will limit its focus to discussing metallization and protein assembly.

Metallization with DNA origami templates is by far one of the more popular uses of DNA origami templates. The idea of using DNA to template the direct assembly of metal ions started in 1998 when Braun et al. used DNA molecules incubated with Ag^+ ions to develop semi-

continuous electrically conductive nanowires.[31] Since then, the metallization of DNA nanostructures has evolved to where DNA origami structures are used to plate various metals, particularly gold and silver. Often, these DNA nanostructures are enhanced with various compounds or chemical species such as 4-aminomethyltrioxsalen. These species help maintain the DNA's structure and chemical stability.[32] Additionally, the DNA nanostructures can be chemically modified with other various chemicals to enable specific interaction between and certain metal ions. There are a wide range of various metallization projects, but several will be noted here.

Often metallization of DNA origami involves covering the whole DNA origami structure with ions of a certain metal species. This results in the metal ions forming together and taking the shape of the DNA origami. One example of this was performed in 2011 where Liu et al. used Ag-seeded electroless deposition to deposit Au onto T-shaped DNA origami (Figure 5a).[33] Another example was performed by Shen et al. in 2015 where custom-shaped metal nanostructures were made by patterning various metal ions onto DNA nanostructures.[34] A more recent example of metallization was conducted in 2022 by Sandeepa et al. where linear DNA origami structures were modified to metalize and pattern silver nanowires.[35]

Metallization of DNA origami nanostructures does not always involve covering the whole structure. Often, it is more desirable to cover certain areas of the structure with metal while leaving other areas bare. This form of metallization is called site-specific metallization.[36–38] Here, DNA origami nanostructures are often modified with areas called binding sites. These binding sites accept certain metal ions, but reject others. This allows for select deposition on the DNA's surface instead of the whole surface being covered. One example of site-specific metallization was performed by LaBean et al. in 2011. In this project, DNA origami structures

were modified with unique coded sequences which produced binding sites for gold nanoparticles functionalized with cDNA. These modified nanostructures produced various metallic structures in a variety of designs including rings, bars, and letters (Figure 5b).[39] A recent example of site-specific metallization was performed in 2021 where Zhao et al. produced programmable DNA origami nanostructures with site-specific patterning for silver and silica.[40]

Outside the realms of metallization, DNA origami structures are used as templates for a variety of purposes. One such area is in biochemistry where DNA origami nanostructures are used as templates to assemble various proteins and enzymes.[41] Early examples of this include Kuzyk et al. in 2009.[42] Kuzyk developed two general approaches to assemble proteins with DNA origami. The first method involved using DNA origami as a prefabricated template for protein assembly. The second method was where materials were assembled simultaneously with the DNA origami, i.e. the DNA origami technique is used to drive the assembly of materials. Another example was performed by Aslan et al. in 2016. Aslan was able to pattern proteins using modified DNA origami nanostructures as templates. This approach involved employing DNA origami nanostructures to arrange Bovine Serum Albumin (BSA) protein (Figure 5c). This process was found to be fast and cheap and could be used in potential technological applications.

Using DNA origami as templates has been being studied for many years. Since then, the projects used to investigate this area have advanced the range of potential applications. DNA origami nanostructures are ideal for creating or fabricating other materials with desired shapes, designs, and structures. One such project will be discussed in this thesis where DNA origami is used as a template for creating inorganic salts with layer-by-layer deposition.

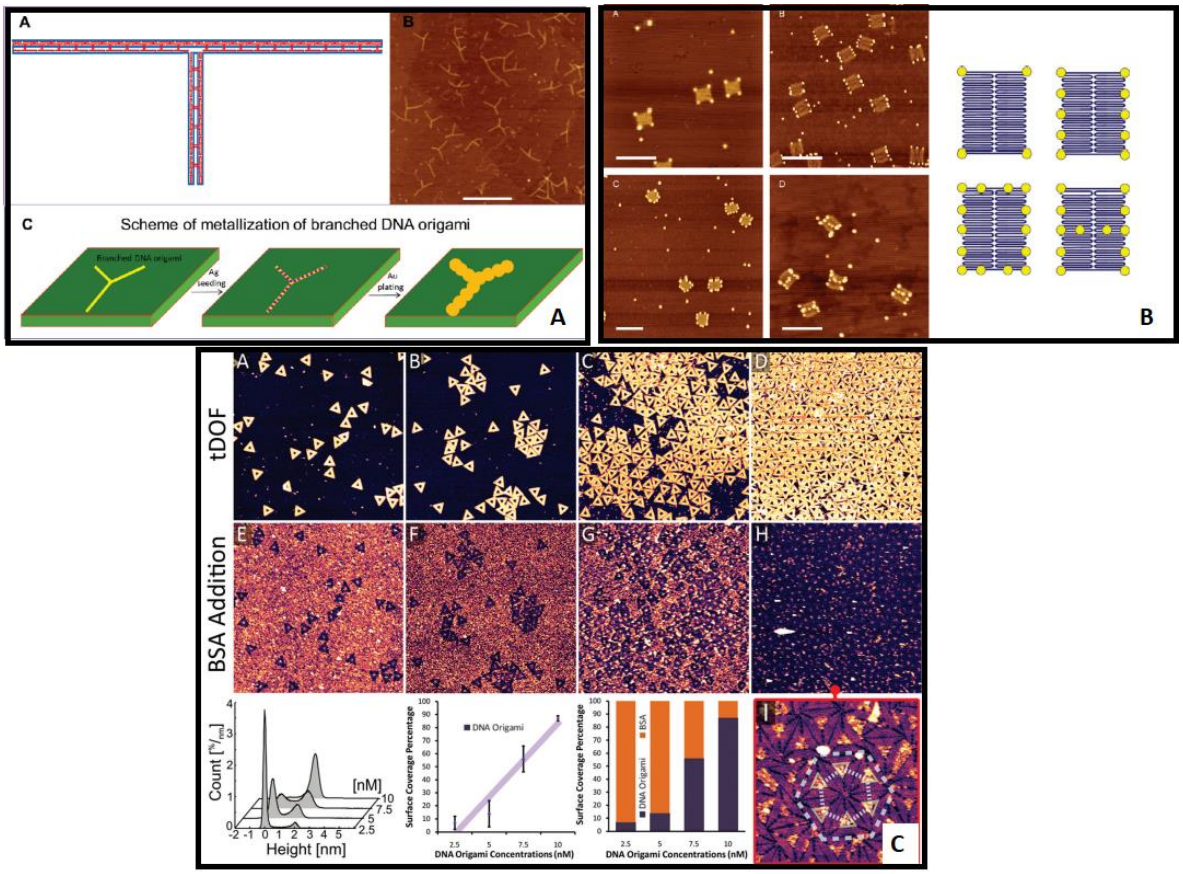

Figure 5. Examples of DNA origami interactions with nanoparticles. Metallization of T-shaped DNA origami (a); Site-specific metallization of DNA origami (b); DNA origami templates used to assemble protein patterns (c). Reprinted with permission from Liu, J.; Geng, Y.; Pound, E.; Gyawali, S.; Ashton, J. R.; Hickey, J.; Woolley, A. T.; Harb, J. N. Metallization of Branched DNA Origami for Nanoelectronic Circuit Fabrication. *ACS Nano* **2011**, *5* (3), 2240–2247. © 2011. American Chemical Society (a), Reprinted with permission from Pilo-Pais, M.; Goldberg, S.; Samano, E.; LaBean, T. H.; Finkelstein, G. Connecting the Nanodots: Programmable Nanofabrication of Fused Metal Shapes on DNA Templates. *Nano Letters* **2011**, *11* (8), 3489–3492. © 2011. American Chemical Society (b), and reference 42 Copyright © 2016 Nanoscale (c)

1.5: DNA ORIGAMI AND SUBSTRATE INTERACTIONS

DNA origami necessarily involves the investigation of how DNA origami nanostructures interact with various substrates. The study of DNA-nanostructure-substrate interactions is important because DNA nanostructures behave differently depending on the substrate the nanostructures adhere to. Additionally, certain applications might require that the DNA origami nanostructures adhere to and interact with specific substrates. With these two factors in mind, many researchers have devoted research to analyzing how DNA nanostructures interact with various substrates along with how these substrates affect the properties of the nanostructures such as chemical stability. Currently, substrates which have been heavily investigated include SiO_2, mica, and highly oriented pyrolytic graphite (HOPG).[43 – 45]

SiO_2 is an extremely common substrate that has been studied regarding its interactions with DNA nanostructure. SiO_2 has been utilized with DNA origami in a variety of ways primarily in regards to molecular lithography, masking and patterning. Pattern transfer is a chemical process where the shape of the template is copied into the substrate. Due to their chemical nature, DNA nanostructures are challenging in regards to pattern transfer. In 2011, our team reported a direct pattern transfer of DNA nanostructure to SiO_2 by vapor-phase HF etching reaction (Figure 6a). Kinetically, the vapor-phase HF etching of SiO_2 was modulated by the DNA nanostructures. Furthermore, we found that by tuning the reaction conditions regarding certain factors such as humidity and water concentration, both positive-tone and negative-tone pattern transfers were possible. This pattern transfer was possible due to carrying out the etching process in the vapor-phase only. The use of vapor-phase allowed us to avoid lifting the DNA templates off the SiO_2.[46]

Since our discovery of using vapor-phase HF etching, many researchers have applied this method to achieve various forms of patterning with DNA origami on SiO2. In 2016, Diagne, et

al. performed a pattern transfer of DNA origami into SiO_2 to demonstrate that various nanoscale features were achievable. In this project, a DNA nanostructure was synthesized in the shape of a rectangle measuring 52x53 nm. In the center of the rectangle was a 9x14 nm hole. The goal was to see if the nanostructure's pattern could be effectively transferred onto SiO_2 with the hole being clearly defined. Using an etching rate of 0.2 nm/sec, Diagne was able to successfully transfer the DNA's shape onto SiO_2 within a process time between 30 - 60 sec. The resulting pattern transfer possessed all the details of the original DNA nanostructure including the hole in the rectangle. Furthermore, Diagne found that longer etching times, those past 600 seconds, resulted in corrosion of the SiO_2 pattern along with the etching reaction being blocked. These findings provided the team with a system of fabrication rules, process time windows, and limits for the DNA-based lithography.[47]

As time went on, DNA nanostructures became more complex, and their use as a tool for lithography became more prevalent. After Diagne's project, more researchers tried to push the limits regarding the level of detail DNA origami pattern transfer could achieve. In 2020, Thomas et al. built upon the results of Diagne's project by trying to use DNA origami nanostructures and SiO_2 to transfer patterns onto pure silicon. Thomas developed a 105 x 68 nm rectangle from DNA origami with three different holes in the rectangle, two measuring 10 x 10 nm and one measuring 20 x 20 nm. To transfer the pattern of the DNA onto silicon, Thomas developed a three-step procedure. First, DNA origami was deposited onto SiO_2. Next, the DNA origami's pattern was transferred onto the SiO_2 using HF vapor phase etching. Finally, the SiO_2, which served as an intermediate mask, had its pattern etched into silicon using HBr/O_2 plasma. The resulting pattern on the silicon could be effectively analyzed by atomic force

microscopy, scanning electron microscopy, focused ion beam−transmission electron microscopy, and ellipsometry measurements.[48]

Another surface that has been commonly used for DNA origami is mica. Mica is not an individual compound like SiO_2, but rather groups of phyllosilicate minerals which crystallize in a monoclinic system.[49] These crystals can easily be split into thin elastic sheets. DNA origami has a strong interaction with mica and prior to 2009, all high-resolution AFM images of DNA origami were performed on mica.[50] This was due to the atomic-level flatness that mica sheets possess.

The interactions between DNA and mica have been studied since the early 2000s. In 2006, Pastre et al. investigated the interaction between DNA molecules and mica in respect to various salt concentrations. Before this, scientists knew that DNA molecules adsorbed onto mica when multivalent counterions such as Mg^{2+} were added to the buffer. However, it was not very well known about the correlation between cations and DNA adsorption on mica. Pastre investigated this phenomenon by analyzing AFM images of DNA molecules on mica. With this information, he created a phase diagram of DNA molecules interacting with the mica surface established in the terms of monovalent, divalent, and multivalent salt concentrations. Pastre found that DNA adsorption onto mica was determined by ionic strength. DNA molecules did not adsorb very well when high ranges of monovalent salt concentrations were present ([MX] > 0.1 M, where MX is the monovalent salt compound). Instead, he found that lower concentrations of divalent or multivalent salts were effective in allowing DNA adsorption onto mica. Furthermore, Pastre found that DNA adsorption onto mica took place when the energy gained by the counterion correlations overcame a certain energy barrier. This energy barrier was caused by several factors including the entropy loss in confining DNA in a thin adsorbed layer, the entropy

loss in the interpenetration of the clouds of mica and DNA counterions, and the electrostatic repulsion between DNA and mica.[51]

Pastre's work revealed that the surface density of cations, particularly divalent cations such as Mg^{2+}, was a key parameter in DNA adsorption and behavior on mica. Since then, other researchers have explored the relationship between DNA and mica interaction regarding cationic density and concentration. In 2014, Woo and Rothermund decided to quantitatively study the cationic-dependent binding between DNA origami and mica. Their mission was to investigate the competition between monovalent and divalent cations. In this project, Woo and Rothermund analyzed the self-assembly of DNA origami into 2D checkerboard lattices based on stepwise control of surface diffusion mediated by exploiting the competition between Mg^{2+} and Na^{+} in DNA–mica binding. They found that while low concentrations of divalent cations were suitable for DNA-mica adsorption, high ionic strength was required for DNA lattice formation.[52]

The previously explained projects, along with many others, have shown that DNA adsorption onto mica, and other silicon surfaces, require the presence of divalent cations in the buffer solution. Typically, DNA nanostructures are adsorbed and immobilized by adding millimolar concentrations of divalent cations, particularly Mg^{2+}, to the buffer solution. However, the use of Mg^{2+} in DNA buffer solutions present potential limitations for certain projects. This is because the Mg^{2+} concentrations used are normally non-physiological.[53 – 54] As a result, these concentrations interfere with certain reactions and processes that might be under investigation. Research has recently been done to see if DNA origami can be adsorbed onto mica without the need of Mg^{2+}.

In 2021, Xin et al. presented three different approaches to adsorb DNA origami nanostructures onto mica without the use of magnesium cation (Figure 6b). In this project, DNA

origami nanostructures were synthesized in Mg^{2+}-containing TAE buffer, but were then immediately transferred to either phosphate-buffered saline (PBS), or pure H2O. The nanostructures were then deposited onto mica which had one of three different cations pre-adsorbed onto its surface: Ni^{2+}, poly-L-lysine (PLL), or spermidine (Spdn). Xin found different results depending on the type of cation pre-adsorbed onto the mica along with which solvent the DNA nanostructures were transferred to. First, the Ni^{2+}-modified mica showed the worst performance. For both PBS and water, the nanostructures adsorbed onto the Ni^{2+}-modified mica were heavily deformed and many were denatured. Unlike the Ni^{2+}-containing mica, the PLL and Spdn modified mica surfaces produced better results. Regarding the PBS, the nanostructures deposited onto both PLL and Spdn exhibited superior adsorption when compared to the Ni^{2}+ and even Mg^{2+} mediated adsorption in terms of surface coverage. It was noted that the Spdn was slightly better in terms of adsorption and surface coverage. In pure water, the results were extremely different. Here, the PLL and Spdn modified surfaces showed DNA adsorption, but inferior when compared to Mg^{2+}-mediated adsorption. Xin further noted that the PLL-modified surface performed slightly better than the Spdn, with the latter resulting in severe AFM artifacts. Xin's work was a huge breakthrough because up to this point, most DNA nanostructure adsorptions were carried out with Mg^{2+} cation. However, the results collected demonstrated that there is great potential in using polyelectrolyte-coated mica to serve as a DNA adsorbing substrate without the need of Mg^{2+}.[55]

One final substrate that warrants mentioning in detail is HOPG or highly oriented pyrolytic graphite. Originally, HOPG was viewed as a promising substrate for imaging DNA. A number of factors including its ultra-flat surface, quickness in providing clean surfaces, and its conductivity contributed to this belief. The conductivity was desired because early DNA

imaging was performed by scanning tunneling microscopy which requires a tunneling current for imaging. However, by 1992, the popularity of HOPG for DNA imaging had significantly decreased. Multiple research articles were published which deterred the use of HOPG for DNA imaging. These articles centered around the fact that graphite could mimic the structure of DNA and therefore produce artifacts. Additionally, a new form of imaging tool, atomic force microscopy, arose which did not require conductivity to image objects. [56 – 57] Before long, mica and SiO_2 took over the realm of DNA interacting substrates and HOPG was put on the back shelf regarding research.

Despite its lack of popularity, HOPG has been making a comeback in the realm of DNA origami. This comeback is occurring for a number of reasons. HOPG displays remarkable mechanical strength, flexibility, and biocompatibility. Additionally, the simultaneous development of DNA origami has led many researchers to believe that DNA origami combined with HOPG might open up a new realm of applications including in the fields of nanoelectronics, biosensors, and nano-optics.[58 – 60] While the interaction between DNA and HOPG is not well studied, the interaction between DNA and single-walled carbon nanotubes is.

ssDNA has been shown to wrap helically around single-walled carbon nanotubes which forms a bridge between the hydrophobic carbon nanotube and the aqueous media. Furthermore, the DNA's negatively charged phosphate backbone faces the solution which produces a hydrophilic coating. With this coating, the DNA aids in the effective dispersion of the carbon nanotube into the aqueous phase. It is thought that ssDNA might have a similar interaction with HOPG due to an enhanced π–π stacking interaction between the HOPG surface and the planar aromatic nucleotide bases, which is augmented by the additional ionic contribution from the DNA's phosphate backbone.[61 – 63]

While promising, there are some complications with this idea regarding DNA origami. The main problem is that most DNA origami structures are formed from double-stranded DNA (dsDNA). In order for the π–π stacking interactions with the graphite surface to occur, the dsDNA would need to reorganize its structure so that the DNA's intrinsic π–π stacking and hydrogen bonds would be disrupted enough to interact with the HOPG's surface. Recent publications have tried to bind dsDNA to HOPG and all of them report that only limited interaction between the DNA and HOPG occurs.[64]

Researchers have had some success in binding DNA to HOPG using various methods. One example was performed by Dubrovin et al. in 2010. Here, Dubrovin and his team wanted to discover a method to immobilize DNA molecules onto HOPG. Their approach was to modify the surface of HOPG substrates with certain chemical species. These species would tune the properties of the HOPG which in turn would make the surface "DNA-friendly." The species they chose to use for surface modification was octadecylamine (ODA). They decided upon this polymer because ODA was known to self-assemble onto HOPG in various patterns. These patterned areas could then be tested to see if DNA would adsorb on those areas. Using ODA vapor, they coated various HOPG substrates with the polymer. They found that DNA molecules would adsorb onto the ODA covered areas along with following the patterns in which the ODA had self-assembled onto the HOPG.[65]

Another method of adsorbing DNA onto HOPG was explored by Zhao et al. in 2011. Zhao and his team decided to try on improving the adsorption of DNA onto HOPG by adding particular divalent cations to the DNA buffer solution. They worked with three different cations: Mg^{2+} , Ni^{2+}, and Cu^{2+}. Through AFM analysis, Zhao and his co-workers revealed that each type of cation led to the DNA being immobilized onto the HOPG surface, but in different

patterns. For magnesium, the DNA molecules preferred to bind to the HOPG in looping patterns. It was thought that this behavior was derived from the crossover of intramolecular and intermolecular chains. The nickel cations enabled the DNA molecules to form various networks across the HOPG surface. Finally, for copper, the DNA tended to form flat chains with the chain links being composed of angular looped DNA molecules. Zhao's work revealed that DNA molecules could be immobilized onto HOPG through the use of certain divalent metal cations.[66]

Despite Zhao's work, most researchers decided to immobilize DNA on HOPG by modifying the HOPG's surface. Campos et al. used modified HOPG to immobilize DNA in 2015. Here, DNA origami structures were produced with pH-induced nanomechanical switching of i-motifs structures incorporated into them. While the interaction between DNA origami and HOPG was not the main focus of the study, the team bound DNA origami onto HOPG by modifying the HOPG surface with cysteamine.[67]

While DNA immobilization onto HOPG was possible through surface modification, the process of modifying the HOPG surface could be time-consuming. A major breakthrough was performed by our group in 2017 with HOPG and DNA origami. Here we showed a method of depositing DNA origami onto HOPG successfully without either surface-modification, or using excess metal cation in the DNA solution. Instead, our team exploited the fact that exfoliated HOPG was much more hydrophilic than surface HOPG. Using this knowledge, we applied DNA origami to exfoliated HOPG. Our results revealed that the deposited DNA origami nanostructures adsorbed onto the HOPG with no sign of extreme deformity. Additionally, the structures were able to maintain their morphology for at least a week. Most excitingly, the process promoted site-selective chemical vapor deposition onto SiO2. This was performed by carrying out SiO_2 CVD growth onto the HOPG bound DNA origami using tetraethyl

orthosilicate (TEOS), NH_4OH, water, and isopropanol. The results were successfully deposited SiO_2 onto the DNA origami structures (Figure 6c). It was found that the thickness of the SiO_2 was greater on the HOPG bound DNA origami when compared to the same procedure using Si-bound DNA origami. This was attributed to the inertness of HOPG which improves spatial selectivity and more aggressive reaction conditions to be used. Our findings were a major leap forward in developing DNA origami onto HOPG. While the study of DNA-HOPG interactions has not been mastered, there is a promising hope that HOPG may yet become a standard substrate for DNA origami adsorption.[68]

Substrates for DNA origami are not just limited to SiO2, mica, and HOPG. There are a wide variety of different substrates being tested regarding DNA interactions. Because of the plethora of currently studied substrates, it is beyond the scope of this thesis to review all of them. Rather, a select few projects will be mentioned to reveal the potential of using other substrates for immobilizing DNA origami. In 2014, Zhang et al. attempted to deposit DNA on native and passivated molybdenum disulfide substrates (Figure 6d). This is because molybdenum disulfide, MoS_2, is a promising material for future sensors. It was found that DNA nanostructures quickly lost their structural integrity upon interaction with MoS_2. To avoid this, Zhang used pyrene and 1-pyrenemethylamine to modify the MoS_2 surface and protect the structural integrity of the DNA nanostructures. He found that both served as effective protective agents with 1-pyrenemethylamine being the more effective of the two.[69] Another example of exploring different substrates was performed by Gallego et al. in 2017. Gallego investigated the ability of binding DNA origami structures to gold surfaces using thiol-modified oligonucleotides. Finally, certain polymers such as polystyrene are being investigated to see if DNA origami can effectively interact with the polymer surfaces.[70] DNA interactions with various substrates is a

growing area of importance in the realm of DNA nanotechnology. Understanding and discovering new methods and materials to bind DNA nanostructures will open the doors to new potential applicative pathways. This thesis will discuss one such project where the interaction of DNA and various organosilane-self-assembled monolayers will be analyzed.

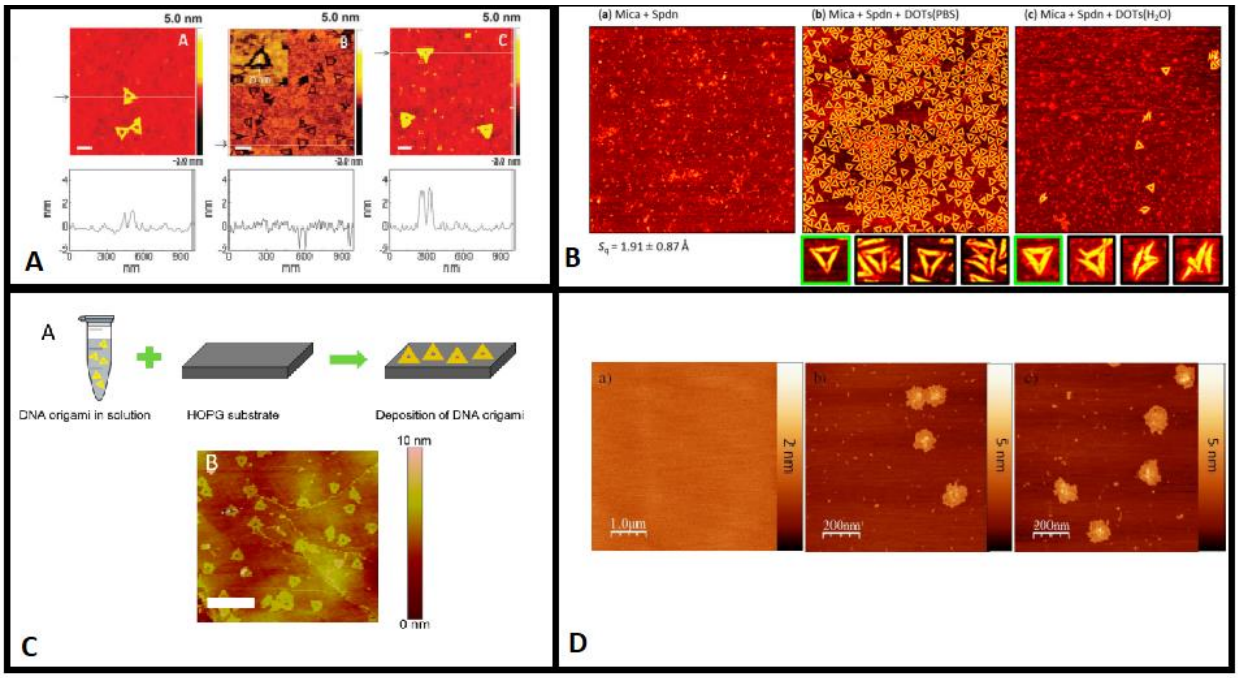

Figure 6. DNA origami interactions with various substrates. DNA origami used to pattern SiO_2 (a); Use of magnesium-free DNA origami on mica (b); Adsorption of DNA origami onto exfoliated HOPG (c); Adsorption of DNA origami onto molybdenum disulfide (d). Reprinted with permission from Surwade, S. P.; Zhao, S.; Liu, H. Molecular Lithography through DNA-Mediated Etching and Masking of SiO_2. *Journal of the American Chemical Society* **2011**, *133* (31), 11868–11871. © 2011. American Chemical Society (a), Reprinted by permission from John Wiley and Sons: ChemBioChem, *ChemBioChem*, DNA Origami-Based Protein Manipulation Systems: From Function Regulation to Biological Application, Ziqi Xu, Yide Huang, Hao Yin, et al. © 2022 (b), Reprinted by permission from Ricardo, K. B.; Xu, A.; Salim, M.; Zhou, F.; Liu, H. Deposition of DNA Nanostructures on Highly Oriented Pyrolytic Graphite. *Langmuir* **2017**, *33* (16), 3991–3997. © 2017. American Chemical Society (c), and reference 69 Copyright © 2014 Beilstein Journal of Nanotechnology, https://creativecommons.org/licenses/by-sa/4.0/deed.en (d)

2.0 ULTRATHIN CALCIUM PHOSPHATE FILM COATING OF DNA ORIGAMI NANOSTRUCTURES

2.1: INTRODUCTION

Thin films are layers of materials that range from a fraction of a nanometer to several micrometers in thickness. Thin film techniques have been practiced as early as 2667 B.C. by the Ancient Egyptians during the Third Dynasty of the Old Kingdom. During those days, thin film techniques were used to overlay gold onto various tombs, walls, and other decorative objects.[71] Since then, thin film materials and applications have expanded to phenomenal proportions. Thin film materials now range from metals and inorganics to polymers and organic molecules. Their applications, now beyond the use of decorative functions, include drug-delivery, energy generation, energy storage, optics, data storage, and circuitry. To expand and further the usefulness of thin films, these layered materials are often combined with other various forms of technology. One such area of technology that has been combined with thin films is DNA nanotechnology.

The use of DNA origami nanostructures as templates is a growing application in the field of DNA nanotechnology. As mentioned earlier, methods of nanofabrication such as metallization have been utilized with DNA origami nanostructures to develop many different types of materials in various patterns. However, the methods of depositing various nanomaterials onto DNA origami templates vary in effectiveness and complexity. Currently, there are several different deposition techniques used to deposit materials onto DNA nanostructures. These methods include: anisotropic electroless deposition, seeding, and chemical vapor deposition.[72 – 74] Most of the methods mentioned are effective, but extremely complex and difficult to execute.

Many researchers have tried to apply simpler, less complex methods of deposition to DNA origami templates. One example is layer-by-layer deposition. Layer by Layer Deposition

(LbLD) is a thin film fabrication technique which involves deposition of oppositely charged ions for the formation of alternating layers with concomitant washing steps in between (Figure 7a).[75 – 77] LbLD is a simple and robust approach to thin film deposition. Additionally, it is extremely effective in fabricating well-organized multilayers at the nanometer scale. LbLD has many advantages. One of the most significant advantages that LbLD has over other forms of deposition is that LbLD can deposit thin films onto surfaces of almost any topography without using high temperatures. Another advantage is that LbLD can control the thickness of the film being deposited. It is also relatively cheap to perform and simple in methodology to teach and master.[78]

LbLD is a technique that has been utilized for quite some time. Its first known application was in 1966 where J.J. Kirkland and R. K. Iler developed it to produce porous thin-layered glass beads for gas-liquid chromatography.[79] Since then, LbLD has expanded to other materials. The most common use of LbLD is with polyelectrolytes to develop various thin films. These thin films have been applied in a variety of applications. These include protein purification, corrosion control, biomedical applications, ultra-strong materials, and other applications.[80]

While LbLD has been used with many different polymers, there has not been much use of it in regards to DNA. That being said, LbLD has been utilized in conjuncture with DNA nanochemistry to some extent. These utilizations mainly revolve around DNA-polymer and DNA-polyelectrolyte interactions. In 2014, Roh and co-workers used LbLD combined with DNA nanostructures to develop DNA microsponge particles for cancer therapeutic delivery. To develop these microsponges, Roh designed microsponge-like structures of DNA containing large amounts of periodic antisense oligodeoxynucleotide (ODN) strand in the form of a long polymeric ssDNA. These microsponges then had additional outer layer shells added to the

microsponges' core through LbLD. Through a combination of DNA nanotechnology and LbLD, Roh developed a nanoparticle that possessed multifunctionality.[81 – 82]

Another form of LbLD exists called successive ionic layer adsorption and reaction (SILAR). While LbLD focuses on polyelectrolytes, SILAR mainly focuses on developing thin ionic films. SILAR was initially developed in 1984 by Y. F. Nicolau to produce ZnS and CdS thin films. The number of thin films able to be produced by SILAR has expanded to other sulfides, oxides, and phosphates (Figure 7b).[83]

While examples of DNA origami nanofabrication exist, there are few examples of inorganic salts being fabricated utilizing DNA origami and LbLD together. This seems relatively unusual since metal ions are known to bind strongly to DNA through electrostatic interactions and LbLD has been used in the past to generate ultrathin films. Such inorganic-DNA hybrid materials might be used in a variety of applications including MRI imaging and enzymatic sensors. Furthermore, the research of such materials could answer many chemistry-related questions in hybrid organic-inorganic materials as well.

One known example of inorganic salts being fabricated utilizing DNA origami was conducted by Wu et al. in 2020. Here, Wu and his co-workers bound calcium phosphate to DNA origami nanostructures using crystallization by particle attachment (Figure 7c).[84] CPA is a form of colloidal assembly. This means that individual particles interconnect with one another to form a larger structure. These species which attach to one another range from multi-ion complexes to fully formed nanocrystals. This allows for delicate morphology and precision nanoscale addressability.

The project's main goal consisted of controlling the mineralization of the calcium phosphate to the DNA nanostructure only. This was done by forming Ca-P nanoclusters

(Posner's clusters) in supersaturated solution with DNA nanostructures. Here, the Posner clusters are absorbed onto the phosphorylated DNA backbone by CPA. CPA was desired because it slowed down the rapid crystal growth which led to over crystallization on the DNA nanostructure. Furthermore, the DNA nanostructure solution was saturated with Mg^{2+} ions to prevent the Posner clusters rapidly growing along the DNA nanostructure. Instead, the Posner clusters grew slowly and meticulously onto the nanostructure through Mg^{2+}/Ca^{2+} exchange.

In addition to controlling the mineralization of the calcium phosphate, the mechanical strength and thermal stability of the DNA nanostructures were analyzed when bound to the calcium phosphate crystals. Wu discovered that the mineralization of the DNA nanostructures increased the mechanical strength of the DNA origami. The increased mechanical strength was the result of increased rigidity in the nanostructures caused by mineralization. Furthermore, while not explained in depth, the thermal stability of the nanostructures increased with mineralization as well. This was observable by exposing the mineralized nanostructures to extreme heat (700^{o}C). The structures were able to retain their shape and dimensions even while exposed to the increased temperature.

Despite Wu's success, there are limitations in the project. One of the most significant limitations is that the project was specifically designed to mineralize calcium phosphate and not a range of materials. The thermodynamic barriers overcome by CPA might not apply to other materials such as magnesium phosphate. Here, we demonstrate the use of LbLD to form various DNA nanostructures. While the studied salt was calcium phosphate, it is hoped that LbLD could be applied to form other salts on DNA nanostructures. This would allow for the creation of inorganic salts in specific patterns, shapes, and designs which would be highly beneficial in a variety of applications.

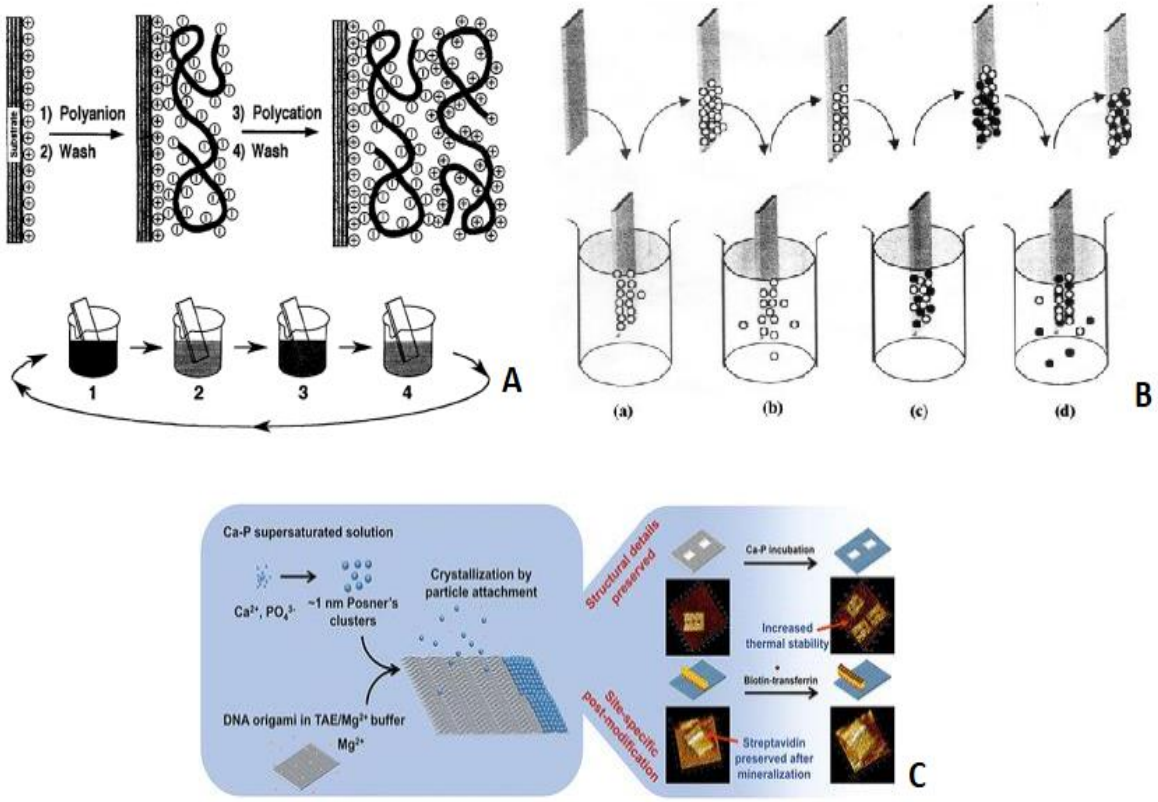

Figure 7. Layer-by-layer deposition techniques and projects. Layer-by-Layer Deposition (LbLD) procedure (a); SILAR procedure (b); Deposition of calcium phosphate onto DNA origami (c). Reprinted by permission from Springer Nature: Springer ebook, *Springer ebook*, Protein Multilayer Architectures on Electrodes for Analyte Detection, Sven C. Feifel, Andreas Kapp, Fred Lisdat. © 2013 (a), Reprinted by permission from Elsevier: Materials Science and Engineering: B, *Materials Science and Engineering: B*, Successive ionic layer adsorption and reaction (SILAR) trend for nanocrystalline mercury sulfide thin films growth, R.S. Patil,C.D. Lokhande,R.S. Mane,H.M. Pathan,Oh-Shim Joo,Sung-Hwan Han. © 2006 (b), Reprinted with permission from u, S.; Zhang, M.; Song, J.; Weber, S.; Liu, X.; Fan, C.; Wu, Y. Fine Customization of Calcium Phosphate Nanostructures with Site-Specific Modification by DNA Templated Mineralization. *ACS Nano*. **2020**, *15* (1), 1555– 1565. © 2020 American Chemical Society (c)

2.2: EXPERIMENTAL

2.2.1: Materials and Methods

Silicon wafers with native oxide layers were purchased from Vishay Siliconix Inc (625 ±15 μm). M13mp18 scaffold and synthetic staple DNA stands were used to fabricate the origami nanostructures. These were ordered from Bayou Biolabs. Buffer solution for DNA was made from 50 x TAE Buffer (Trist-acetate-EDTA), magnesium acetate tetrahydrate, and deionized water (DIW). The 50 x TAE Buffer was diluted to 1 x TAE Buffer using DIW. Piranha solution was made from sulfuric acid and hydrogen peroxide solution (30% H_2O_2). Calcium chloride, potassium phosphate, and potassium chloride were utilized for layer-by-layer deposition. Ethanol was utilized as a solvent. All chemicals used in this project were bought from Thermo Fisher Scientific.

2.2.2: DNA Nanostructure Solution

The creation of DNA nanostructures is based on previously published papers. Briefly summarizing, in an aliquot a solution of 180 μL of 1xTAE Mg^{2+} Buffer (pH = 8.5), 8.6 μL of M13mp18 ss DNA (1 μg/mL), 15 μL of 300nM DNA staple strand, and 77 μL of ultrapure water was mixed. The solution was thoroughly mixed and then separated into four aliquots with each aliquot containing 70 μL of solution. The aliquots were then annealed in an MJ Research Minicycler at 700C for 90 minutes. Following this, the four aliquots were combined into a single 30K Omega Nanosep centrifugal device. The solution was centrifuged and filtered for five minutes using a single speed bench top Fisher Scientific microcentrifuge at 6,000 rpm. Next, 400 μL of 1xTAE Mg^{2+} Buffer (pH =8.5) was mixed with the remaining 100μL of DNA solution and centrifuged again for five minutes. This process was repeated three times. This combination of centrifugation and washing was designed to remove excess staple strands in the DNA

nanostructure solution. It is essential that the centrifuging does not leave the centrifuge device dry. There should be at least 50 - 100 μL left in the device. Following the centrifuged process, the concentration of the DNA solution was calculated using a Thermo Scientific Genesys 10S UV-Vis Spectrophotometer. The concentration of the DNA solution was between 20 - 40 μg/mL. Finally, the final solution should be placed in a refrigerator at 40C for storage.

2.2.3: Preparation and Analysis of Silicon Wafer

A CZ silicon wafer from Vishay Siliconix Inc. (thickness 625 ±15 μm) is cleaned in a hot mixture of piranha solution (70:30 H_2SO_4: H_2O_2) for 45 minutes. Warning: hot piranha solution is extremely dangerous and volatile. Do not leave unattended or exposed to extreme heat. Next, the wafer is thoroughly washed with ultra-pure water and dried with N_2 gas. In a humid environment, the wafer is covered in a 20 μL 50:50 DNA: 100 mM $CaCl_2$ solution. This is allowed to stand for 30 to 45 minutes. The wafer is then washed using 90:10 Ethanol: Water solution and dried with N_2 gas. This process is repeated three to five times. Another method of washing involved taking five vials and filling them with 90:10 Ethanol: Water. The wafer is placed in each vial and washed for 90 seconds. After washing in the vials, the wafer is dried with N_2. Afterwards, 20μL of 1mM K_3PO_4: 200 mM KCl is deposited onto the wafer and allowed to stand for five minutes. Afterwards, the wafer is washed with a 90:10 Ethanol: Water solution and dried with N_2 gas. This process is repeated three times. Another method of washing used included the vial method described in the previous paragraph. The wafer is then analyzed using an Asylum MFP3D AFM. Cross sections were taken to identify the height of the nanostructure on the AFM images. These cross sections were taken using the Asylum AR 16.19.220 software.

2.3: RESULTS AND DISCUSSION

2.3.1: AFM Images and Structural Morphology of DNA Nanostructures

Samples were made by depositing a 50:50 DNA nanostructure: $CaCl_2$ solution onto SiO_2 substrate. The substrate was then washed with 90:10 ethanol: water solvent and dried with N_2 gas. Afterwards, the substrate was covered with K_3PO_4 solution and analyzed with AFM (Figure 8). Over one hundred samples were made and analyzed. On many of the samples prior to K_3PO_4 deposition, the DNA nanostructures were present on the wafer. Some nanostructures though when deposited onto the wafer were denatured and showed rounded edges. These denatured nanostructures varied in appearance, but the most common appearance of the nanostructures were clean triangles with sharp edges. However, after K_3PO_4 deposition, the surfaces appeared dirty with heavy aggregation being apparent (Figure 9a and 9b).

Several reasons were discussed as to why the AFM images were so dirty after depositing K_3PO_4. It was thought that the most likely reason was contamination on either the wafer surface or the cantilever tip. This was backed up by finding other AFM images affected by contamination on the surface. The contamination could be averted by cleaning the wafer surface with a stronger cleaning agent, washing the wafers longer, or lowering the setpoint on the AFM.

Longer washing was tested to see if this would result in clearer AFM images. Five vials were set up each containing around 30 mL of 90:10 Ethanol: Water solution. Each wafer upon deposition of nanostructure and K_3PO_4 was washed separately in each vial for about ninety seconds. It was thought that the constant drying in between washings might be responsible for the lack of nanostructure on the wafer so drying with N_2 air was not applied until the very end of the washings. The resulting AFM images were not only clear, but the nanostructure was retained with clear sharp edges and resolution (Figure 9c and 9d).

2.3.2: Nucleation of Calcium Phosphate

With the success of overcoming this first challenge, a statistical analysis was done of the wafers to see if nucleation of calcium phosphate was occurring. Two of the wafers tested were taken to see the height difference between the wafers coated with zero deposition layers and one deposition layer of K_3PO_4. For this analysis, thirty different cross sections were taken with their heights being measured. For the wafer with zero layers, it was discovered that the height of the nanostructures was on average 1.33 ± 0.2 nm. The wafer with one layer of K_3PO_4, was discovered to have nanostructures with an average height of 1.55 ± 0.3 nm (Figure 10a and 10c). While the height of the nanostructures had increased, the standard deviation of the heights was too large for the heights to be considered statistically significant. It was thought that the lack of height change could be due to there being only one deposition and not multiple deposition cycles.

To test this, nanostructures with multiple layers of Ca^{2+} and K_3PO_4 would be produced to see if the height of the nanostructure increased as the number of deposition cycles increased. A total of fifty samples with multiple layers of $CaCl_2$: K_3PO_4 were produced, but only a fraction of them showed signs of nucleation. Overall, the nanostructures seemed to vanish after the K_3PO_4 was exposed onto the wafer. There were some wafers where this was not the case. In these situations, the wafers showed signs of increased height on the AFM which might indicate the presence of calcium phosphate nucleation. Based on the cross sections of these successful nanostructures, there was an increase in nanostructure height between 1.15 - 2.14 nm per nucleation cycle (Figure 10b and 10d). However, too few samples were successful enough to pinpoint a general average in increased height. For most of the samples, the AFM images showed no change in the nanostructure height. Lack of detail was especially apparent on the

AFM images of samples with two or more depositions of K_3PO_4. Little to no resolution was seen on these samples, with many sporting raised aggregates on the surface.

2.3.3: Discussion

There is speculation as to why there has been so difficult to observe well-defined DNA nanostructures with potential calcium phosphate nucleation. The most likely issue is that the ions deposited on the surface of the SiO_2 as well as the nanostructures. This would make sense since the SiO_2 would attract the calcium cations due to its negatively charged surface. The over-adsorption of the ions on the both the substrate and the nanostructures would explain the low resolution and raised aggregates on the surface as the number of cycles increased. Since this could be the culprit for the results, it would be important to find a way to prevent the deposition of ion onto the surface except on the nanostructures. One way we could achieve this is by using self-assembled monolayers to cover the SiO_2 surface except where DNA origami were present. This would be possible by depositing the DNA origami onto the SiO_2 followed by covering the surface in a hydrophobic self-assembled monolayer. This would leave only the DNA nanostructures exposed. We performed such a procedure in a past project which will be discussed in the next chapter of this thesis. Another, though less likely, possibility is that the ionic layers are being washed off during the washing process. This washing phenomenon could be the result of several factors including kinetics, thermodynamics, equilibrium, or a combination of all three. Another potential reason for the lack of DNA nanostructures would be the presence of deionized water. Our team tested the effects of washing nanostructures with DI water. In this case, the DI water successfully washed off the impurities on the wafer, but also extremely decreased the density of the nanostructure after just five minutes of washing in DI water. The main goal of the washing is to remove the salt impurities without affecting the nanostructures to extreme degrees.

It was speculated that changing the pH level might induce or hinder nucleation of calcium phosphate. According to Wu, calcium phosphide was successfully deposited onto DNA nanostructures at a pH of 6.5. In Wu's project, a calcium chloride solution of 5 mM was added dropwise into a phosphate-DNA solution at a pH equal to 6.5. In this example, the calcium and the phosphorus bonded well together and to the DNA tetrahedron nanostructures at a desirably slow nucleation rate. This is because Wu found that more acidic pHs slowed nucleation while more basic pHs sped up nucleation. Currently, the pH of the DNA nanostructure solution is at 8.5.[84] Changing the pH of the solution to a higher pH such as 9.5 or 10 might be able to enhance nucleation of calcium phosphate onto the nanostructure.

Finally, the calcium phosphate might not be depositing due to the presence of magnesium ions. Wu states that magnesium ions prohibit the nucleation of calcium phosphide. This was overcome by utilizing calcium ions instead of magnesium ions during the DNA self-assembly process. Currently, the DNA nanostructure solution contains Mg-Tris buffer. It is quite possible that the magnesium ions present in the solution are inhibiting the nucleation of calcium phosphate to occur. To test this, a solution of DNA nanostructure with calcium-tris buffer would be produced and used instead of the usual DNA nanostructure solution using magnesium-tris buffer.

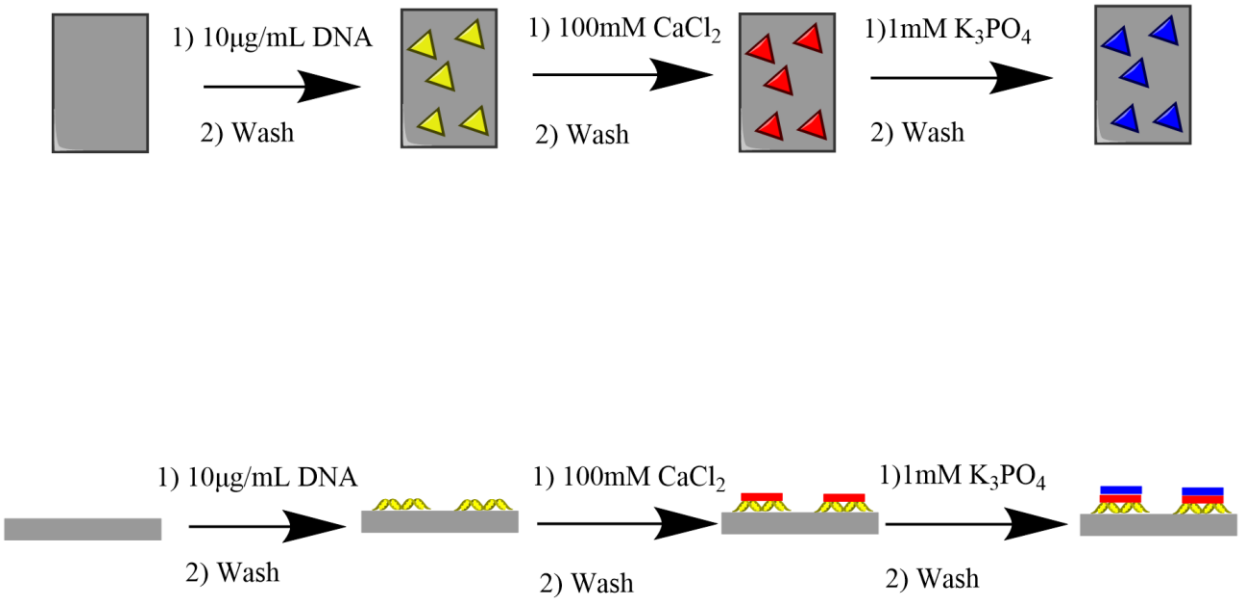

Figure 8. Procedure of calcium phosphate deposition onto DNA origami templates using LbLD.

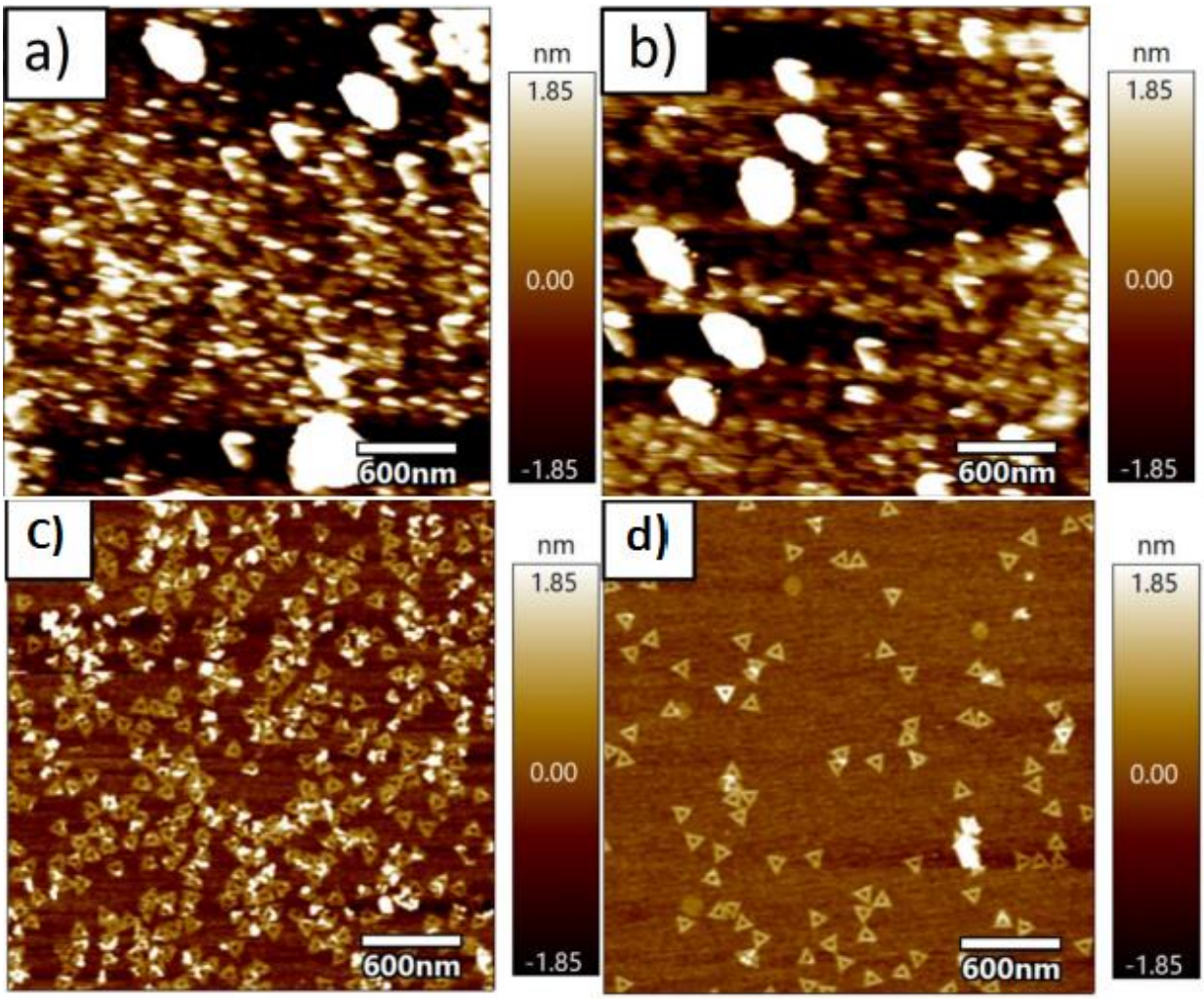

Figure 9. Comparison between wafer surface post-K_3PO_4 deposition utilizing new washing method. AFM images showing sample surfaces prior to utilizing new washing method (a and b); AFM images showing sample surfaces after utilizing new washing method (c and d).

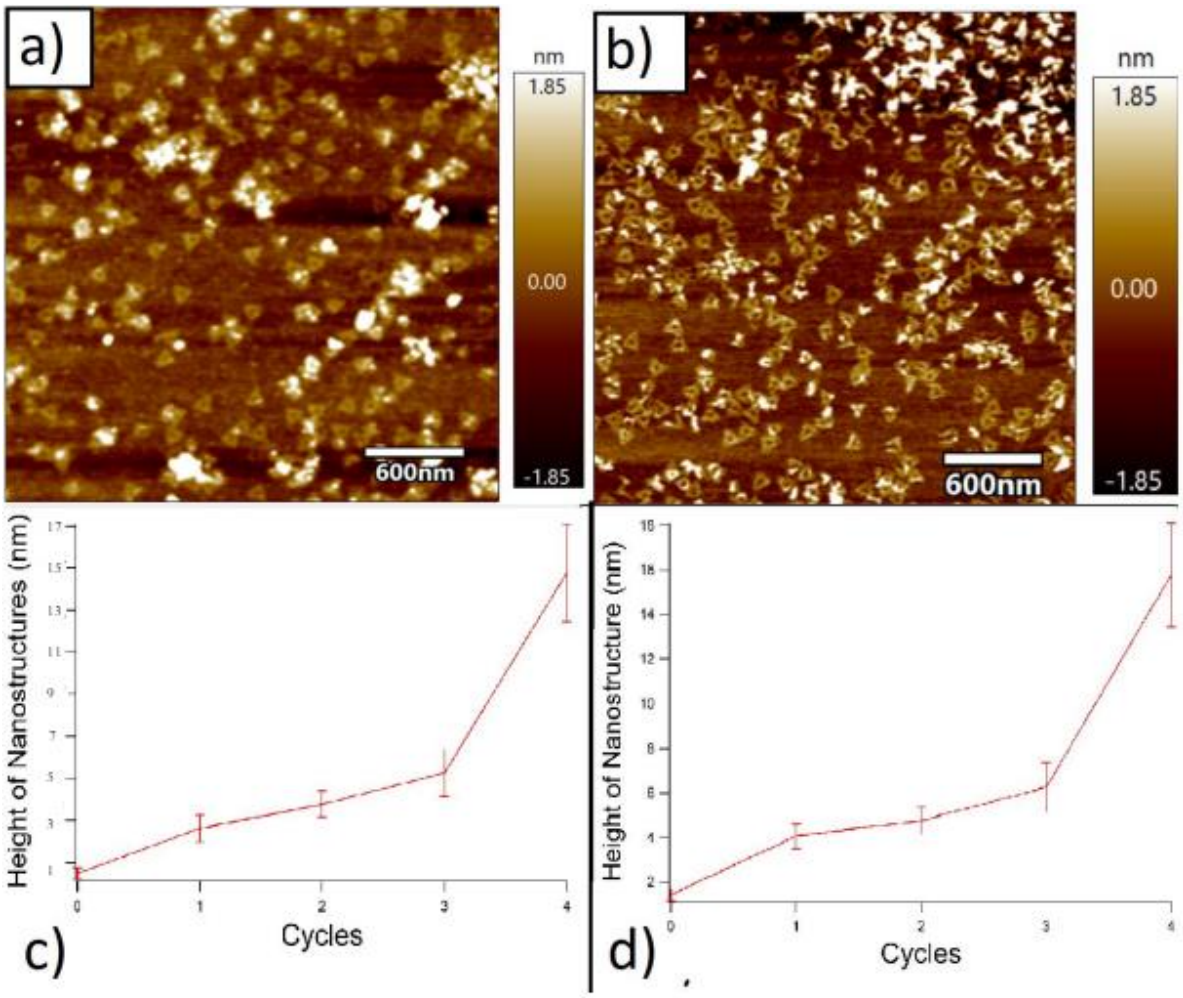

Figure 10. Results of calcium phosphate nucleation. AFM image of wafer surface and graph indicating film growth on first sample (a and c); AFM image of surface and graph indicating average film growth of all samples (b and d). a and b are AFM images of the first and second successful samples showing proper nucleation of calcium phosphate after one cycle of deposition respectively.

2.5: CONCLUSIONS

Here, we present a general method of applying LbLD to DNA origami nanostructures to fabricate inorganic salts in various shapes and designs. The idea of using DNA origami as templates for inorganic salt nanofabrication has promising uses in a variety of applications. DNA origami nanostructures have been utilized as templates before to develop and produce other materials. Most of these materials do involve metal ions and generating metal films on top of the DNA origami structure. Additionally, LbLD/SILAR has been found to be an effective technique in layering ions on top of each other to produce layers of thin films on different surfaces. The technique has been heavily applied to ionic compounds, and many research studies have shown that ionic salts are able to be fabricated using LbLD. Combining these two areas: DNA origami templates and LbLD, could generate salts in various shapes which could be used in applications such as MRI imaging or enzymatic sensors.

Unfortunately, this project did not produce the results we were hoping for. Poor AFM imaging and nucleation results along with insufficient time led to this project being unsuccessful. The problems surrounding the project were centered around lack of experience in sample preparation, the minimum available knowledge surrounding this topic, and insufficient time to master the techniques required for this project. These factors combined led to the project producing insufficient data to determine whether LbLD could be applied to DNA origami nanostructures to generate ionic salts.

With this being said, this does not mean that the project is over nor is the hope of using LbLD with DNA origami templates unachievable. It should be noted that this project was the first of its kind, and as with most initial projects regarding a new topic, sufficient time, knowledge, and mastering of techniques is required. Since this project, many techniques required for redoing this project have been mastered. Additionally, new knowledge has been

discovered and investigated which might benefit this project should it be revived or reattempted again. Finally, if proper time is given to this project, better results will be collected. While these results might or might not prove that LbLD could be applied to DNA origami, the results would show whether or not the project should be continued, revised, abandoned, etc.

It should also be noted that a variation of this project has been discussed and is potentially in line of being initiated. As mentioned before, it is thought that the most likely reason for the lack of successful nucleation samples was due to both the surface and the nanostructures experiencing electrostatic interactions with the deposited ions. To prevent this, we would apply a hydrophobic self-assembled monolayer to the SiO_2 surface after depositing the DNA origami. This would prevent the SiO_2 surface itself from interacting with any deposited ions, leaving only the DNA nanostructures as possible binding sites. This might induce DNA-cation interaction which might improve the LbLD of the salt. Additionally, a variation of the project utilizing polymers instead of ionic species is also under construction.

The idea of utilizing LbLD with DNA origami is not farfetched nor is it certain that ions cannot be bound to DNA origami to produce ionic salts. The foundations for this new idea have been clearly researched and have generated promising results. Furthermore, the chemistry behind the idea is plausible and makes logical sense. In order for this project to succeed, sufficient time, effort, and training is required. However, if these three needs are met, this project could reveal new potential applications in the field of nanofabrication and DNA nanotechnology which could impact the world.

3.0 DNA ORIGAMI NANOSTRUCTURE INTERACTIONS WITH VARIOUS SILANE SELF-ASSEMBLED MONOLAYERS

3.1: INTRODUCTION

The interactions between nanostructures and the substrates are extremely important because various materials for applicative purposes possess different interactive behaviors with DNA nanostructures. Additionally, expanding the realm of materials that DNA nanostructures can adsorb onto opens up new potential application areas. This has led many researchers either trying or developing new surfaces for DNA origami nanostructures to interact with. Furthermore, different surfaces possess different properties which can lead to a range of potential benefactors.

A self-assembled monolayer (SAM) is a one molecule thick layer of material that bonds to a surface in an ordered way as a result of physical or chemical forces during a deposition process. SAMs are created from the molecular assemblies of certain molecules. Regarding this, the molecules used to form the SAM possess three parts: the head group, the tail, and the functional group (Figure 11).[85 – 86] First, chemisorption of the head groups occurs onto the substrate from either the vapor or liquid phase. This is followed by a slow organization of the tail groups. Over time, this organization leads to the development of close-packed molecular nucleated areas. This continues until the substrate is covered in a single monolayer of material (Figure 11).

SAMs were initially developed in 1946 where W.A. Zisman published the preparation of a monomolecular layer by adsorption (self-assembly) of a surfactant onto a clean metal surface. He did this by using particular amphiphilic compounds to form well-ordered monolayer thin films directly from the solution he was using. However, the work he produced was not seen as chemically important and therefore, the potential of SAMs was not recognized for some time. In 1978, Haller with IBM reported his work where alkylsilane monolayers were formed on

silicon and gallium arsenide semiconductor surfaces. This was followed up by Nuzzo and Allara in 1983 where they were able to develop well organized monolayer films of dialkyl disulfides onto gold surfaces. These projects brought SAMs into the research spotlight, and many people began trying to apply SAMs in various ways.[87 – 89]

More recently, SAMs have become extremely popular for forming thin-films on which nanostructures and nanoparticles can be deposited onto. This has taken an extreme interest in the realm of material science. Researchers have found that certain adsorbate molecules can be tailored to attract two different materials. Because of this, SAMs are used to attract certain materials onto various surfaces. This is made possible by using the head groups to attach to the substrate, while the tail groups are modified to attract certain nanoparticles. This technique functionalizes the surface and allows for nanostructures of certain materials to "bond" to the surface.[90 – 91]

One of the most common forms of SAM-nanostructure interaction researched currently is the interaction between metal nanoparticles and thiolated SAMs.[92 – 94] However, thiolates are not the only studied SAMs. Other SAMs that have been investigated include fatty acids, phosphates, and organosilanes. Organosilane SAMs are commonly used to functionalize various silicon dioxide surfaces such as clean glass. Organosilanes adsorb onto silicon dioxide through condensation. Here, the SiOH groups of the silicon dioxide surface react with either $R{-}SiCl_3$ or $R{-}Si(O(CH_2)_nCH_3)_3$ through a dehydration process which in turn forms strong chemical Si-O-Si bonds (Figure 12a).[94 – 97]

It should be noted that organosilanes can be difficult to produce due to their sensitivity to water. Excess water in the presence of the SAMs will cause them to polymerize and deposit undesired polysiloxane onto the surface. However, too little water will cause the formation of

incomplete monolayers. As a result, people have tried to find optimal water conditions for growing organosilane SAMs. McGovern et al. discovered that for organosilane SAMs, a moisture quantity of 1.5 μg/ mL provided the optimum condition to grow closely packed monolayers of organosilanes.[98]

Aside from this difficulty, organosilane SAMs are relatively popular amongst material scientists. This is because organosilane SAMs possess remarkable properties such as mechanical and chemical stability due to the strong immobilization through siloxane bonds. Additionally, organosilane SAMs on SiO_2 possess strong photo resistance. This has taken interest by many in the application of topographical etching.[99]

The number of projects and experiments concentrated around organosilane SAMs is enormous. Most of these projects revolve around investigating the photo resistant properties, electrochemical properties, and optimizing the self-assembly process of organosilane SAMs. The interactions between organosilane SAMs and nanoparticles have not been nearly as studied.

The few studies that have been conducted around organosilane SAMs and nanoparticle interaction mostly consist of nanoscale patterning. Studies regarding nanoscale patterning can trace their roots back to the 1990s. One of the first nanoscale patterning with organosilane SAMs was performed by J.Liu et al. in 1998. Liu thought of a way to pattern gold film by utilizing 3-aminopropyl-trimethoxysilane (APTES) SAM on SiO_2 substrates. This involved covering regions of the SiO_2 substrate with APTES SAM and then exposing the surface to Au colloid solutions.[100] The results were that the APTES SAM regions attracted the gold particles thus forming gold covered regions on the SiO_2. Another project was performed in 2009 where Morrill et al. created APTES SAMS onto nanostructured titania and tin oxide nanowires. These

functionalized metal oxide surfaces were then decorated with borohydride-reduced silver nanoparticles.[101]

Other forms of nanoscale patterning with organosilane SAMs were also investigated. In 2005, Zhang et al. used organosilane SAMs along with electron beam lithography to pattern various proteins. Here, Zhang used chemical vapor deposition to deposit a 1*H*,1*H*,2*H*,2*H*-perfluorodecyltriethoxysilane (FDTES) SAM onto a silicon surface. Following this, he modified the residue at the c-terminus of a green fluorescent protein from the jellyfish, *Aequorea victoria*, in order for it to bind to the FDTES SAM. He was then able to use electron beam lithography to pattern the proteins into various designs and groups (Figure 12b).[102]

DNA nanostructures and nanoscale patterning with organosilane SAMs was investigated by our team in 2016. Here, DNA origami was deposited onto SiO_2 wafers and then covered with octadecyltrichlorosilane via chemical vapor deposition. Afterwards, the DNA nanostructures were removed by sonication in DIW. This left negative toned patterns on the OTC modified surface. The surface was finally exposed to APTES vapors which bound to the exposed SiO_2 surface. This left SAM patterns on the substrate's surface consisting of mixed organosilane SAMs (Figure 12c and 12d).[103]

Despite our project, DNA nanostructures and their interactions with organosilane SAMs have not been heavily investigated. This is mainly because DNA nanostructures require a charged hydrophilic surface for proper interaction. As of now, most DNA nanostructures use cations, usually magnesium, to form salt bridges which bond to negatively charged hydrophilic surfaces such as mica and silicon oxide. It has been found that very select few organosilanes bind DNA nanostructures through electrostatic interactions, but these are normally amine-terminated organosilanes such as APTES.[104 – 105] Additionally, the stability and strength of the

DNA nanostructures when bound to such organosilanes has not been investigated. However, most organosilanes are uncharged and hydrophobic which are undesirable for DNA nanostructure adsorption. Because of this, many researchers have not found interest in studying the interactions between DNA nanostructures and organosilanes.

However, recently, some research has been done to investigate whether hydrophobic surfaces can adsorb DNA nanostructures. This is because early studies revealed that strong hydrophobicity of certain polymer surfaces could enhance the adsorption of DNA strands. This interaction was heavily studied by J.F. Allemand et al. in 1997. Allemand and his team investigated the interactions between ssDNA, dsDNA, and various surfaces including hydrophobic ones. They found that DNA strands interact with hydrophobic surfaces through the nucleotide bases. This finding led to some people believing that DNA nanostructures might be able to be adsorbed onto hydrophobic surfaces. Additionally, later scarce studies with HOPG suggested that DNA nanostructures can adsorb onto hydrophobic surfaces through $\pi - \pi$ interactions. With these two factors in mind, it was thought that certain hydrophobic surfaces, such as phenyl terminated SAMs, could adsorb DNA nanostructure.[106]

Our team investigated the interactions of DNA nanostructures with various hydrophobic polymers in 2020. Here, we deposited DNA nanostructures on SiO_2 wafers which had their surfaces modified with a random phenyl-containing polymer. These polymers varied, but most were polystyrene based copolymers. Pure polystyrene was also investigated. We found that on the hydrophobic surfaces, the main contributing factor to the adsorption of the DNA was $\pi - \pi$ interaction while the preservation of the nanostructures' structural integrity was determined by the available surface charge on the surface. This led us to the conclusion that certain hydrophobic surfaces would be capable of adsorbing DNA origami nanostructures provided that

pi interaction was capable between the structures and the surface. Additionally, we concluded that in order for structural integrity to be sustained, sufficient surface charge would be required.[107]

The growing evidence of DNA adsorption onto hydrophobic surfaces along with knowing that certain organosilanes can adsorb DNA nanostructures leads to many questions surrounding the interactions between DNA nanostructures and organosilane SAMs. These questions surround topics such as which types of organosilane SAMs could effectively adsorb DNA nanostructures along with the chemical stability of the nanostructures when adsorbed to the SAM. If certain organosilane SAMs could be found which bind DNA nanostructures effectively, these SAMs might be substituted in the place of other surfaces for adsorbing DNA. Furthermore, a discovery of such SAMs would expand the realm of applicative surfaces capable of adsorbing DNA. Finally, understanding the interaction between DNA nanostructures and organosilane SAMs, will shed more light on how DNA nanostructure adsorb to certain surfaces and whether chemical groups hinder or enhance adsorption.

Here we demonstrate the interaction between DNA origami nanostructures and various organosilanes. The organosilanes chosen for this experiment are octadecyltrichlorosilane (OTC), (3-aminopropyl) triethyloxysilane (APTES), phenyltrichlorosilane (PTCS), and 6-phenylhexyltrichlorosilane (6-PHTCS). The organosilanes chosen vary in their terminal end groups which will help reveal whether certain end groups absorb DNA better than others (Figure 13). The organosilane SAMs are analyzed in terms of film growth and wettability over time. This will help determine the kinetics of the film growth along with the optimal conditions for growing effective monolayers. Additionally, the interaction between the SAMs and DNA nanostructures is observed to determine which SAMs effectively adsorb DNA nanostructure and

which do not. Finally, the chemical stability of the DNA nanostructures is also tested in regards to ionic strength, exposure to water, and exposure to various solvents (Figure 14).

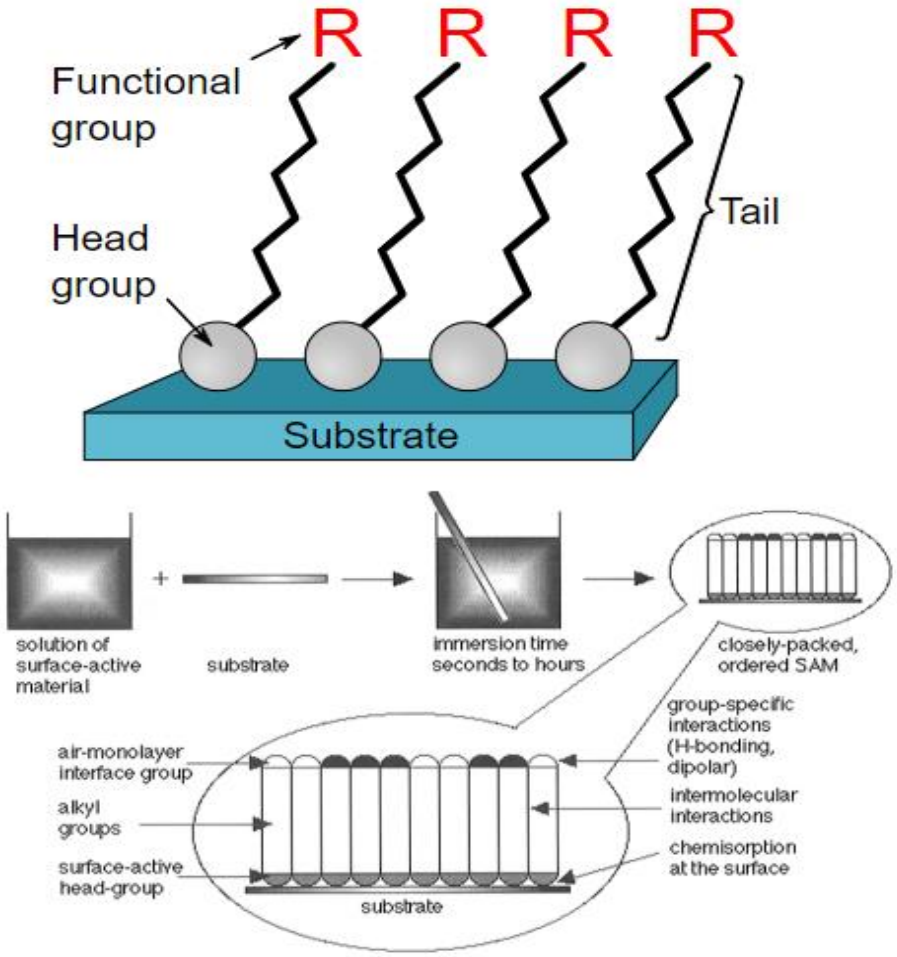

Figure 11. Characteristics of self-assembled monolayers. Diagram of SAM molecule (top); Procedure of SAM process (bottom). Reprinted with permission from Copyright © Vladsinger, https://creativecommons.org/licenses/by-sa/4.0/deed.en (top) Reprinted with permission from Ulman, A. Formation and Structure of Self-Assembled Monolayers. *Chemical Reviews* **1996**, *96* (4), 1533–1554. © 1996. American Chemical Society (bottom)

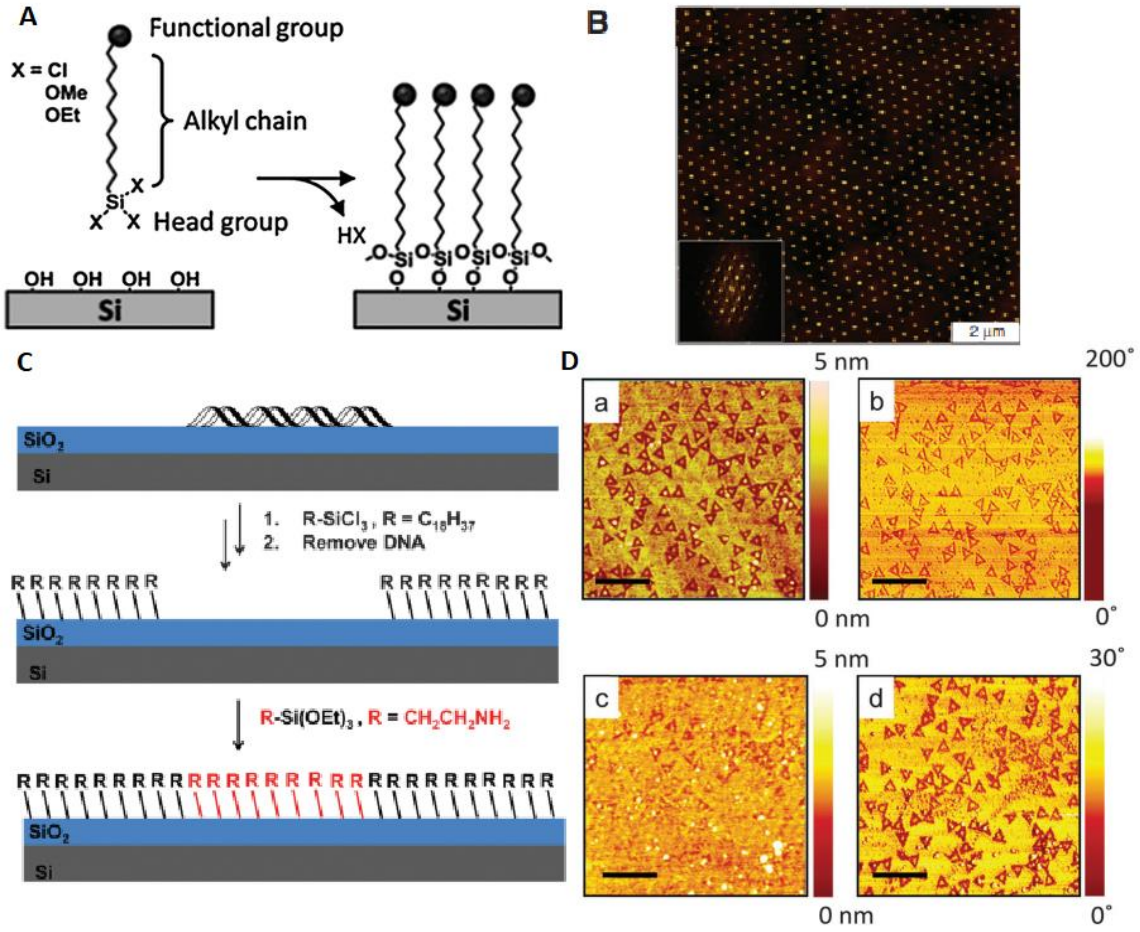

Figure 12. Organosilane self-assembled monolayers. Chemistry of organosilane SAM assembly (a); Use of organosilane SAM for nanoscale patterning (b); Procedure for nanoscale patterning of organosilane SAMs using DNA origami (c); AFM images of organosilane nanoscale patterning utilizing DNA origami (d). Reprinted with permission from reference 94 Copyright © 2014 Material Horizons, https://creativecommons.org/licenses/by-nc/3.0/ (a), Reprinted with permission from John Wiley and Sons: Small, *Small*, Nanoscale Patterning of Protein Using Electron Beam Lithography of Organosilane Self-Assembled Monolayers, Iwao Ohdomari, Takashi Funatsu, Yuzo Kanari, et al. © 2005 (b), and reference 103 Copyright © 2016 Chem Comm (c and d)

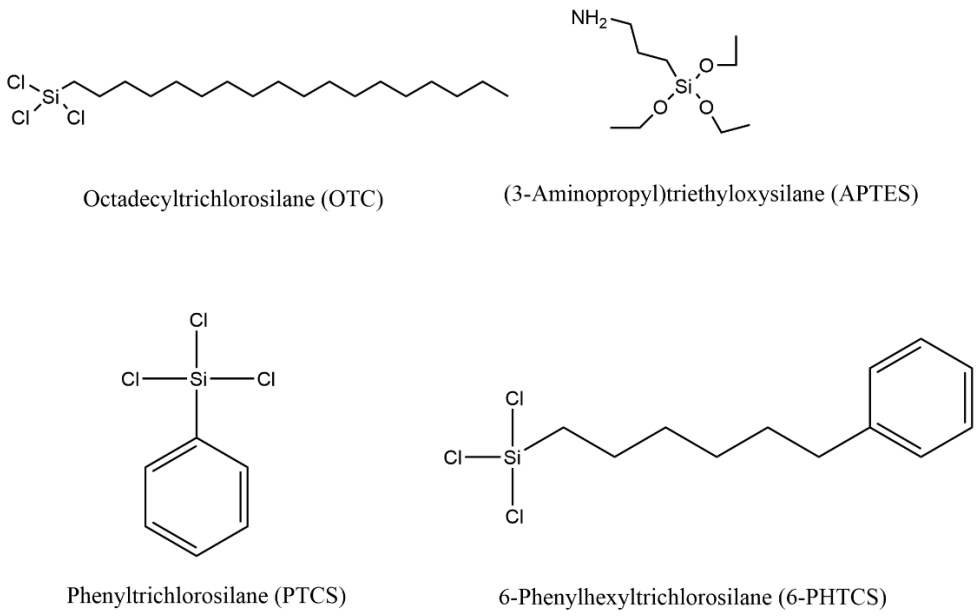

Octadecyltrichlorosilane (OTC)

(3-Aminopropyl)triethyloxysilane (APTES)

Phenyltrichlorosilane (PTCS)

6-Phenylhexyltrichlorosilane (6-PHTCS)

Figure 13. Structures of organosilane SAMs analyzed for project.

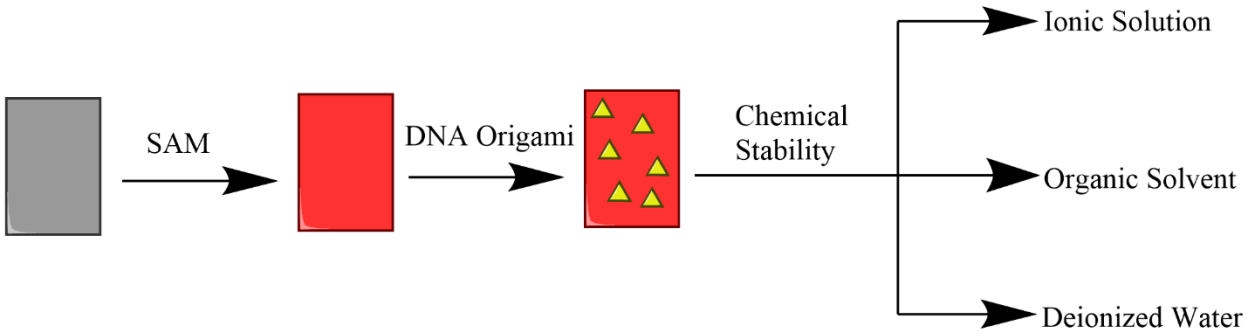

Figure 14. Procedure for DNA origami interactions with various organosilanes.

3.2: EXPERIMENTAL

3.2.1: Materials and Methods

Silicon wafers with native oxide layers were purchased from Vishay Siliconix Inc (625 ±15 μm). M13mp18 scaffold and synthetic staple DNA stands were used to fabricate the origami nanostructures. These were ordered from Bayou Biolabs. Buffer solution for DNA was made from 50 x TAE Buffer (Trist-acetate-EDTA), magnesium acetate tetrahydrate, and deionized water (DIW). The 50 x TAE Buffer was diluted to 1 x TAE Buffer using DIW. Piranha solution was made from sulfuric acid and hydrogen peroxide solution (30% H2O2) purchased from Sigma-Aldrich. SAMs were created from octadecyltrichlorosilane (≥99.5%), 3-aminopropyl-trimethoxysilane, and phenyltrichlorosilane (≥95%). Methanol, ethanol, hexane (mixture of isomers, ≥98.5%), and toluene (≥99.5%), chloroform (≥99.5%), and 2-propanol were utilized as solvents. Sodium chloride (≥99.0%) was used to test ionic strength of nanostructures. All chemicals that were used in this project were bought from Thermo Fisher Scientific.

3.2.2: DNA Nanostructure Solution

The creation of DNA nanostructures is based on previously published papers. Briefly summarizing, in an aliquot a solution of 180 μL of 1xTAE Mg^{2+} Buffer (pH = 8.5), 8.6 μL of M13mp18 ss DNA (1 μg/mL), 15 μL of 300nM DNA staple strand, and 77 μL of ultrapure water was mixed. The solution was thoroughly mixed and then separated into four aliquots with each aliquot containing 70 μL of solution. The aliquots were then annealed in an MJ Research Minicycler at 70C for 90 minutes. Following this, the four aliquots were combined into a single 30K Omega Nanosep centrifugal device. The solution was centrifuged and filtered for five minutes using a single speed bench top Fisher Scientific microcentrifuge at 6,000 rpm. Next, 400 μL of 1xTAE Mg^{2+} Buffer (pH =8.5) was mixed with the remaining 100 μL of DNA solution and centrifuged again for five minutes. This process was repeated three times. This combination

of centrifugation and washing was designed to remove excess staple strands in the DNA nanostructure solution. It is essential that the centrifuging does not leave the centrifuge device dry. There should be at least 50 - 100 μL left in the device. Following the centrifuged process, the concentration of the DNA solution was calculated using a Thermo Scientific Genesys 10S UV-Vis Spectrophotometer. The concentration of the DNA solution was between 20 - 40 μg/mL. Finally, the final solution should be placed in a refrigerator at 40C for storage.

3.2.3: Preparation of Silicon Wafer

A CZ silicon wafer from Vishay Siliconix Inc. (thickness 625 ±15 μm) is first sonicated in deionized water for 30 minutes. Following this, the wafer is cleaned in a hot mixture of piranha solution (70:30 H_2SO_4: H_2O_2) for 45 minutes. Warning: hot piranha solution is extremely dangerous and volatile. Do not leave unattended or exposed to extreme heat. Next, the wafer is thoroughly washed with ultra-pure water and dried with N_2 gas. Immediately following this washing, wafers are baked in an oven for 30 minutes at 120^{o}C to drive off any remaining water.

3.2.4: Ellipsometry Measurement of Native Oxide Layer

Silicon wafer after baking in the oven is removed and placed in an airtight glass vial. The wafer is then analyzed with an Alpha-SE Ellipsometer with an angle offset of 65 degrees to measure the thickness of native oxide. The program model, "NTVE_JAW" was used with the ellipsometer to measure the thickness of the native oxide layer. Following this analysis, the wafer is returned to the oven and baked at 120^{o}C for thirty minutes to remove any potential water obtained through air exposure.

3.2.5: Assembly of Octadecyltrichlorosilane SAM

Wafer is immediately removed from the oven and placed in an airtight glove box. The wafer is exposed to a 1 mM octadecyltrichlorosilane (OTC) solution mixed with either anhydrous hexane or anhydrous toluene for desired time. The wafer is then rinsed thoroughly with excess anhydrous hexane or toluene before being baked in the oven at 120^{o}C for

approximately five minutes. Following, the wafer is washed in isopropanol and then sonicated in chloroform for thirty minutes. Finally, the wafer is washed with isopropanol and dried with nitrogen gas.

3.2.6: Assembly of Phenyltrichlorosilane SAM

Wafer is immediately removed from the oven and placed in an airtight glove box. The wafer is exposed to a 1 mM phenyltrichlorosilane (PTCS) solution mixed with either anhydrous hexane or anhydrous toluene for desired time. The wafer is then rinsed thoroughly with excess anhydrous hexane or toluene before being baked in the oven at 120^{o}C for approximately five minutes. Following, the wafer is washed in isopropanol and then sonicated in chloroform for thirty minutes. Finally, the wafer is washed with isopropanol and dried with nitrogen gas.

3.2.7: Assembly of 6-Phenylhexyltrichlorosilane SAM

Wafer is immediately removed from the oven and placed in an airtight glove box. The wafer is exposed to a 1 mM 6-phenylhexyltrichlorosilane (6-PHTCS) solution mixed with either anhydrous hexane or anhydrous toluene for desired time. The wafer is then rinsed thoroughly with excess anhydrous hexane or toluene before being baked in the oven at 120^{o}C for approximately five minutes. Following, the wafer is washed in isopropanol and then sonicated in chloroform for thirty minutes. Finally, the wafer is washed with isopropanol and dried with nitrogen gas.

3.2.8: Assembly of (3-Aminopropyl)triethoxysilane With Toluene Solvent

Wafer is immediately removed from the oven and placed in an airtight glove box. The wafer is exposed to a 1 mM (3-Aminopropyl)triethoxysilane (APTES) solution mixed with anhydrous toluene for desired time. The wafer is then rinsed thoroughly with excess anhydrous toluene before being washed in isopropanol. Wafer is then sonicated in chloroform for thirty minutes. Finally, the wafer is washed with isopropanol and dried with nitrogen gas.

3.2.9: Assembly of (3-Aminopropyl)triethoxysilane With Methanol Solvent

An APTES stock solution is created consisting of 50% methanol, 47.5% APTES, and 2.5% deionized water. This solution is then stored at 4^{o}C for at least one hour. Wafer is removed from the oven and placed in a glass vial. A 1:500 solution of APTES stock: methanol is created and wafer is placed in solution for desired time. Following, the wafer is rinsed with excess methanol and dried with nitrogen gas. The wafer is then sonicated in deionized water for thirty minutes. Finally, the wafer is washed with deionized water and dried with nitrogen gas.

3.2.10: Ellipsometry and Water Contact Angle Measurements

Silanized wafers are analyzed in regards to the SAM film thickness and water contact angle. For ellipsometry measurements, an Alpha-SE Ellipsometer with an angle offset of 65 degrees is used to measure the film thickness. Two program models were used to measure the film thickness of the samples. The first model, "NTVE_JAW," was used for the native oxide layer while a second model, "Cauchy - ZDOL (A = 1.30)," was added on top to measure the actual film. Five different spots on the wafer have their film measured and then the average of those five measurements is taken. For water contact angles, a VCA Optima contact angle tester is used to take the angle measurements. Three measurements are taken for each wafer and then the average of those three is recorded.

3.2.11: Analysis of SAM Chemical Composition via X-ray Photoelectron Spectroscopy

Wafer surfaces are analyzed with a Thermo ESCALAB 250Xi XPS. This is to determine the chemical composition of the wafer's surface and thereby revealing whether the SAM is present. Parameter wise, the XPS was used with a standard lens mode, AI K Alpha source gun, and a 650 μm spot size. Additionally, a pass energy value of 50.0 eV was used as an analyzer mode with an energy step size of 0.1 eV.

3.2.12: Deposition of DNA Nanostructure onto Wafer

Wafer is placed in a humid environment and has 20 μL of a 10 μg/mL solution of DNA nanostructure deposited onto its surface (5 μg/mL for amine terminated SAMs). The wafer is allowed to sit for 20 minutes. Following this, the wafer is thoroughly washed in 90:10 ethanol: water solution and dried with nitrogen gas.

3.2.13: Topographical Analysis of Wafer with Atomic Force Microscopy

Wafers are analyzed using an Asylum MFP3D AFM. Cross sections are taken to identify the height of the nanostructure on the AFM images. These cross sections are taken using the Asylum AR 16.19.220 software. For DNA covered wafers, both the center and edge of the wafer are analyzed. This is to determine whether the distribution and condition of the DNA nanostructures is uniform across the entire surface.

3.2.14: Stability of DNA Nanostructures in Organic Solvents

The DNA origami nanostructures assembled on SAM covered wafers are immersed in hexane, ethanol, or toluene solvents for 2, 4, or 24 h. The substrates with DNA nanostructure are then dried with an N_2 stream.

3.2.15: Stability of DNA Nanostructures in Deionized Water

The DNA origami nanostructures assembled on SAM covered wafers are immersed in deionized water for 10 s, 5 min, or 1 h. The substrates with DNA nanostructure are then dried with an N_2 stream.

3.2.16: Influence of Ionic Strength on the Stability of DNA Nanostructures

The DNA origami nanostructures deposited on SAM covered wafers are placed inside a sodium chloride solution of desired concentration (0.01−0.2 M) for 10 s followed by blow-drying with N_2 gas. Depending on surface cleanness, most of the samples are washed once or twice in the 9/1 (v/v) ethanol/water solution for 3 s to remove any potential salt impurities. The washed wafers are then redried using N_2 gas to obtain clean AFM images.

3.3: RESULTS

For the project's nanostructures, our shape of choice was a DNA equilateral triangle origami structure. This structure was chosen for several reasons. First, the design of this DNA nanostructure minimizes bending within the structure and prevents aggregation between them as well. Secondly, our group has used DNA origami triangles as the primary template for a number of bottom-up nanofabrication work, including etching and masking of SiO_2 and templated chemical vapor deposition of inorganic oxides. Dimensionally, each edge has a length of approximately 140 nm and consists of 9 parallel double stranded DNA. Theoretically, the height of the DNA nanostructure should be around 1.5 - 2.0 nm, but the observed height on the AFM could vary significantly due to the difference in sample-tip and substrate-tip interaction.

3.3.1: Characteristics of SAMs

Each organosilane SAM was first analyzed in regards to film thickness (Figure 15 and Table 1) and water contact angle (Figure 16 and Table 2) over time. Six samples of each organosilane were created and left in the appropriate silanization solution for 1 hour, 3 hours, 6 hours, 16 hours, 20 hours, and 24 hours. This was performed to analyze the growth rate of the SAMs as well as determine the best time duration for successful monolayer deposition without the formation of multilayers. Additionally, the amine-terminated organosilane (APTES) was also characterized with XPS. This was done to determine the chemical composition of the surface.

The OTC film grew to a thickness of approximately 1.34 ± 0.026 nm within the first hour before plateauing to a thickness of around 1.94 ± 0.047 nm around six hours. There appears to be a linear increase in height between six and sixteen hours with the thickness of the film at sixteen hours around 3.10 ± 0.047 nm. The film growth then seems to plateau around 20 hours with a thickness of approximately 3.59 ± 0.027 nm. The water contact angle of OTC reveals an

increase over time with an exponential decay in the rate. Within the first hour, the OTC possesses a water contact angle of approximately 53.19 ± 0.84 degrees. From there, the water contact angle continues to increase, until it begins to plateau at approximately 16 hours with a value around 105.33 ± 0.95 degrees. The value of the water contact angle seems to slightly vary between samples, but not enough to be considered statistically significant.

The film thickness of the PTCS seems to possess a similar, yet slightly different trend then that of OTC. As with OTC, there is a rapid initial growth within the first hour, here with PTCS possessing film thickness of around 1.16 ± 0.06 nm. This growth appears to plateau around six hours with a film thickness of approximately 1.59 ± 0.05 nm. The main difference between OTC and PTCS is the sharp increase in film thickness between twenty and twenty-four hours. Here, the film increases from 2.20 ± 0.15 nm to 3.12 ± 0.11 nm. The water contact angle for the PTCS possesses an increasing trend with an exponential decay in regards to rate. Within the first hour, the water contact angle is around 73.03 ± 1.40 degrees with the angle plateauing around six hours with a value of 80.40 ± 0.70 degrees.

The results for the 6-PHTCS were initially very similar to both the film growth of OTC and PTCS. Initially, the film grew to about 1.44 ± 0.02 nm within the first hour. Afterwards, the film grew to a value which plateaued between 1.54 ± 0.02 nm to 1.64 ± 0.02 nm between 3 - 6 hours. The growth then grew from 1.62 ± 0.03 nm to 3.04 ± 0.04 nm between six to twenty hours. This was different from PTCS as between 6 - 20 hours, PTCS experienced a plateau in film thickness. The final height recorded after twenty-four hours was 3.18 ± 0.013 nm. The water contact angle for the 6-PHTCS grew to around 92.47 ± 0.6 degrees within the first hour. Afterwards, the water contact angle plateaued between 97.60 ± 0.5 degrees to 99.53 ± 0.4 degrees between three and twenty-four hours.

The film thickness for APTES shows a similar trend to that of PTCS albeit at a slower rate and a smaller magnitude. Within the first hour, the APTES grows to a film thickness of approximately 0.82 ± 0.05 nm with it plateauing around nine hours with a thickness of 1.36 ± 0.13 nm. The growth seems to then experience a sharp increase between twenty hours and twenty-two hours where the film increases from 1.49 ± 0.04 nm to 1.92 ± 0.01 nm. The growth then seems to plateau afterwards with a final thickness of 1.95 ± 0.03 nm at twenty-four hours. The water contact angle for APTES follows a trend which is consistent with the average thickness. Initially, the contact angle increases to 0.42.7 ± 0.8 degrees. A slow increase with an exponential decay in rate occurs between one hour and six hours before finally plateauing around sixteen hours with a value of approximately 63.2 ± 0.3 degrees.

The XPS data for APTES revealed that the intensity of nitrogen grew to $3.26*10^3$ Count/sec within the first hour. This intensity continued to grow until it plateaued around six hours with an intensity of $7.56*10^3$ Count/sec. The intensity of the nitrogen then began to drastically increase at around sixteen hours with an initial intensity of $8.93*10^3$ Count/sec and a final intensity reading of $1.21*10^4$ Count/sec at twenty-four hours (Figure 17 and Table 3). Sonication with deionized water was also applied during the APTES SAM process because it was thought that the water would help remove certain impurities, particularly unbound APTES. Different periods of sonication times were tested. These ranged from 0 minutes to 90 minutes. The goal was to find a sonication time period that effectively cleaned the surface, but did not remove the APTES SAM. For each wafer sonicated, an XPS of the surface was also taken to determine whether the APTES SAM was still present and not compromised by the sonication. The spectra for each sample revealed that nitrogen intensity for each sample

sonicated was between $8.55*10^3$ - $1.08*10^4$ Count/sec (Figure 18 and Table 4). This strongly indicated that the APTES SAM was relatively intact after the sonication process.

3.3.2: DNA Origami Nanostructure Interaction with Organosilane SAMs

AFM imaging of DNA nanostructure was performed to observe the interactive behavior of the nanostructure with each organosilane SAM. Additionally, each sample had images taken at the center of the wafer and the edge of the wafer. This was to see if the surface density of nanostructure was uniformly distributed throughout the wafer. The concentration of the DNA nanostructure solution was fixed to 10 μg/mL (5 μg/mL for amine terminated SAMs) to optimize the density of the adsorbed origami on the surface while also preventing multilayering of the nanostructure. The heights of the nanostructures were also taken using cross-sections on the AFM program.

The DNA nanostructure on the OTC seemed to deform upon interaction (Figure 19). This was observed by finding aggregates of material on the SAM's surface after DNA deposition. These aggregates ranged in height, with most between 6 - 13 nm. Additionally, the aggregates were uniformly distributed throughout both the wafer's center and edge showing no bias towards any one region of the surface. It was thought necessary to verify that these aggregates were deformed DNA nanostructures and not impurities of any sort. For confirmation, new samples were made where AFM images were taken at each stage of the experimental process where impurities could occur. Furthermore, the samples had the DNA nanostructure solution deposited onto them without the DNA components. This was done to determine if the solution itself was responsible for the aggregates. After running several samples, it was found that the aggregates only appeared once DNA nanostructure was deposited onto the SAM's surface (Figure 20d).

Initially, the PTCS SAM showed strong interactions with DNA nanostructure (Figure 19). Here, the nanostructures adsorbed onto the SAM surface strongly along with having their structural integrity well preserved. The height of these nanostructures ranged between 1 - 3 nm. It was also revealed that the DNA nanostructure was uniformly distributed throughout the entire surface. Initially, "islands" of aggregates were observed on the SAM's surface. It was later thought that these islands were aggregates forming due to solvent evaporation during the silanization process. Sonication with chloroform was found to remove these aggregates (Figure 21 and Figures 22 a – c). However, later samples began to show variations in the interactive behavior. This came in the form of some samples possessing intact nanostructure while others would show deformed nanostructure (Figure 22 d). In some instances, the same sample could have nanostructure intact on one area and deformed nanostructure on another. Usually in these cases, the deformed nanostructure was seen at the center of the sample while intact nanostructure was seen at the sample's edge (Figures 22 e – f, 22 i – j) although in one instance, the opposite was seen (Figures 22 g – h). The later samples usually had deformed nanostructures observed on both the center and edges of the sample (22 k), but a few samples showed structurally intact nanostructures on both the center and edges of the sample (22 l).

6-PHTCS showed similar results to PTCS. Several of the samples possessed deformed nanostructure at the sample's center (Figure 23 a), and more intact nanostructure at the edges (Figure 22 b). In contrast, some samples possessed intact nanostructures throughout the entire sample's surface (22 c – e) and others possessed completely deformed nanostructures throughout the sample's surface (22 f – g). It should be noted that many of the intact nanostructures lacked certain details which are normally retained. For example, on many of the intact structures, the hole in the triangles' center was not observed nor were the edges of many triangles straight

(Figure 22 h). Furthermore, the nanostructures were not intact to the extent found on PTCS with many showing signs of deformation although not to the extent where the structures' shape could not be identified. The height of the intact nanostructures was the same as those found on the other SAMs, usually ranging between 1.5 - 2 nm. The deformed nanostructures' height varied, but were generally between 2.5 - 6 nm.

APTES showed the strongest interaction with DNA nanostructures. It was found that DNA nanostructures strongly adhered to methanol-solvated APTES (Figure 19). These nanostructures ranged in height between 0.6 - 1.5 nm. Additionally, the nanostructures were found to be uniformly distributed throughout the surface. However, very little, if any, nanostructure was observed on toluene-solvated APTES SAMs (Figure 24). The toluene-solvated APTES samples also possessed aggregates on the surface while the methanol-solvated APTES samples did not.

3.3.3: Effect of Rinsing with Organic Solvents

Solution chemistry plays a major role in many bottom-up nanofabrication processes. Many former projects have proven that the deposition of DNA nanostructures on various surfaces is affected by the solution applied. One extreme concern of solution phase processing deposited DNA nanostructure is the risk of lifting-off the structures from the surface. Since the interactions between organosilane SAMs and deposited DNA nanostructure is the primary focus of this project, we found it appropriate to test the effects of various organic solvents on the deposited DNA nanostructures.

For this part of the project, only the organosilanes which showed structurally intact deposited DNA nanostructures were tested. Therefore, we did not test the DNA nanostructures adsorbed onto OTC SAM. Three organic solvents were chosen: ethanol, hexane, and toluene. We chose these solvents because they are heavily used in either DNA origami

nanofabrication, organosilane SAMs, or both. Additionally, ethanol is a polar organic solvent while both hexane and toluene are nonpolar organic solvents. Using these three different solvents would reveal the stability of the DNA nanostructures in both polar and nonpolar organic solvents. To assess the nanostructures' stability in organic solvents, DNA origami triangles were deposited onto silicon wafers covered in either APTES or PTCS SAM. The substrates were immersed in organic solvents for various time lengths depending on the SAM being utilized. DNA nanostructures were characterized with AFM to evaluate their number density and the overall shape of the structures.

APTES showed a general trend in both surface density and structural integrity of nanostructures when exposed to the organic solvents (Figure 25). We observed that APTES initially had a surface density of 30.75 nanostructure/μm^2 before being exposed to ethanol. The surface density showed no relative change after exposure to ethanol for one hour. Furthermore, the structural integrity of the nanostructures did not change after one hour exposure to ethanol. The nanostructures possessed a relative height between 1 - 2 nm. However, after two hours of exposure, the surface density dramatically decreased to 10.75 nanostructure/μm^2. The nanostructures' structural integrity also appeared compromised. Many of the nanostructures showed signs of deformation along with many features, such as the hold in the triangle's center, not being observable. The height of the nanostructures also decreased to around 0.5 - 1.5 nm. Finally, aggregates with heights over 2 - 3 nm were observed all over the surface. The nanostructures on APTES when exposed to hexane showed extremely different results. Here, the surface density, 55 nanostructure/μm^2, was relatively the same after the APTES-covered wafer was exposed to hexane for up to two hours. The nanostructures appeared to maintain their

structural integrity in hexane as well. Height-wise, the nanostructures were shorter in height, averaging between 0.8 - 1.2 nm.

For both PTCS and 6-PHTCS, we observed that the nanostructures on the surface did not change in either surface density nor structural integrity no matter which solvent we used (Figures 26 and 27). No signs of deformation were also observed. Here, the nanostructures maintained their details and characteristics while their dimensions remained relatively the same, with heights ranging between 1 - 2 nm. These results suggested that polar and nonpolar organic solvents do not affect the stability of DNA nanostructures when adsorbed onto PTCS or 6-PHTCS SAMs. We decided to test these findings by taking the solvent exposure to the extreme. We did this by placing PTCS and 6-PHTCS wafers in ethanol, hexane, and toluene for over 48 hours and then analyzing their nanostructures (Figures 28 and 29). Even after over 48 hours of exposure, the nanostructures on both SAMs did not seem to be affected by the solvents.

3.3.4: DNA Nanostructures in Aqueous Solutions

DNA nanostructures are known to be removed from most surfaces while in the presence of aqueous solutions. To evaluate the stability of the DNA nanostructures in aqueous solutions, nanostructures were deposited onto APTES or PTCS coated silicon oxide wafers. These wafers had AFM images taken of their surface prior to exposure with aqueous solutions. Following this, the wafers were either exposed to DIW or aqueous ionic solution. The wafers were then removed and then analyzed with AFM again to observe both the surface density and structural integrity of the nanostructures after exposure.

3.3.4a: DNA Nanostructures in DIW

The nanostructures adsorbed onto wafers were exposed to DIW for either 10 seconds, 5 minutes, or 1 hour. We observed on the APTES wafers, that the DNA nanostructures after exposure to DIW for 10 seconds did not change regarding surface density. However, several

nanostructures did appear to show signs of deformation. After five minutes of exposure to DIW, there was no indication of any DNA nanostructure on the surface. This was obviously observed for the 1-hour exposure too (Figure 30).

For the nanostructures on PTCS, the behavior was very similar to those observed on APTES (Figure 31). The surface density was relatively unchanged after exposure to DIW for 10 seconds. Structurally, the nanostructures on PTCS still possessed integrity, but not to the same extent observed on the APTES. For the PTCS samples exposed to DIW for both five minutes and one hour, the nanostructures were completely removed and not observed on the surface.

Initially, it was expected that the nanostructure adsorbed onto 6-PHTCS would behave similarly to those adsorbed onto PTCS. This is because both organosilanes possess phenyl-terminated tail groups with the only difference being that the phenyl on 6-PHTCS is connected to the silicon central atom via hexyl-chain rather than being bound directly as in PTCS' case. However, the nanostructure behaved differently enough to be considered distinguishable (Figure 32). Within 10 seconds of exposure to DIW, the nanostructures on the surface showed extreme signs of deformation. This was observable by the deformity in the nanostructures' shape to the point where their initial triangular structure could not be identifiable. Additionally, many of the nanostructures appeared to accumulate together to form misshapen aggregates which could be described as "blobs." After five minutes of DIW exposure, the surface possessed regions of aggregates albeit not everywhere. In those areas where the aggregates were not observed, the surface appeared similar to that of both PTCS and APTES after five minutes of DIW exposure. After one hour of DIW exposure, the surface contained small regions of aggregates with most possessing a height between 1 - 1.5 nm. This behavior was not seen on any of the other SAMs.

3.3.4b: DNA Nanostructures in Aqueous Ionic Solution

DNA nanostructures were adsorbed onto either APTES or PTCS covered silicon oxide wafers and then had their AFM images taken. Following this, the wafers were exposed to either 0.01 M NaCl, 0.05 M NaCl, or 0.2 M NaCl for ten seconds. The wafers were then reanalyzed with AFM to observe any changes in relative surface density or structural integrity.

We observed on the APTES wafers that after exposure to 0.01 M NaCl, relatively no DNA nanostructures were observed. However, for APTES wafers exposed to 0.05 M NaCl, some DNA nanostructure remained on the surface of the wafer although with an overall lower surface density and observed deformation in the structural integrity. Finally, for the APTES exposed to 0.2 M NaCl, the nanostructures seemed to maintain both their structural integrity and surface density as prior to exposure. The nanostructures observed on the APTES after ionic exposure appeared rougher and more irregular in shape. The surface on the nanostructures appeared to be grinded. Nonetheless, the height of the nanostructures seemed relatively the same before and after ionic exposure, ranging between 1 - 2 nm in height (Figure 33).

For PTCS, there was no observed nanostructure after ionic exposure of any concentration (Figure 34). Unlike PTCS though, 6-PHTCS showed relatively different results (Figure 35). Initially, after being exposed to 0.01 M NaCl, no nanostructure was observed on the surface of 6-PHTCS. However, exposure to 0.05 M NaCl resulted in extreme deformation of the nanostructures. This was observable by the complete loss of structural integrity. However, unlike the observations seen with DIW exposure, these nanostructures did not seem to form blobby aggregates. Instead, these nanostructures appeared almost as if they had disintegrated. Additionally, these nanostructures behaved almost identically to nanostructures exposed to ionic solution when deposited onto silicon oxide. For the samples exposed to 0.2 M

NaCl, no observable DNA nanostructures were seen. There were though blobby aggregates observed on the surface ranging in heights between 2 - 5 nm.

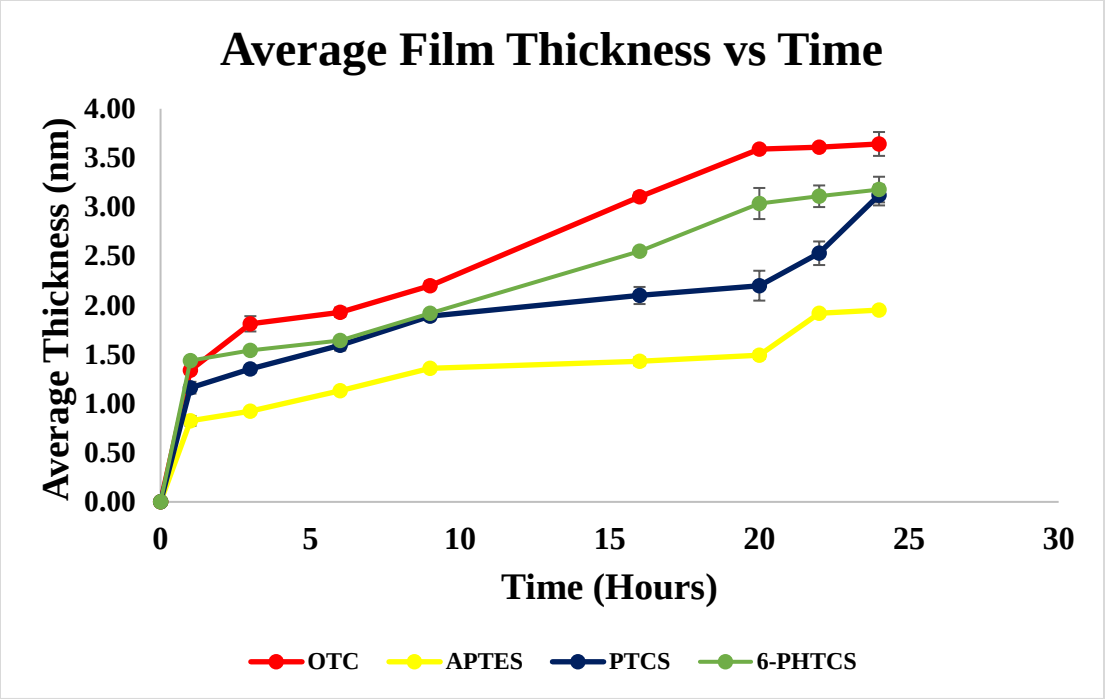

Figure 15. Characteristics of SAM growth using ellipsometry. The figure shows the growth of film over time on the surface of SiO_2. This helped us determine the appropriate time periods for developing monolayers of organosilanes, but also avoiding the growth of multilayers on the surface.

Table 1. Film Thickness of Organo Silanes

Organosilane	1 Hour	3 Hour	6 Hour	9 Hour	16 Hour	20 Hour	22 Hour	24 Hour
OTC	1.34 ± 0.03 nm	1.81 ± 0.08 nm	1.93 ± 0.05 nm	2.20 ± 0.05 nm	3.10 ± 0.05 nm	3.59 ± 0.03 nm	3.61 ± 0.02 nm	3.64 ± 0.12 nm
APTES	0.82 ± 0.05 nm	0.92 ± 0.03 nm	1.13 ± 0.02 nm	1.36 ± 0.01 nm	1.43 ± 0.04 nm	1.49 ± 0.04 nm	1.92 ± 0.02 nm	1.95 ± 0.03 nm
PTCS	1.16 ± 0.06 nm	1.35 ± 0.04 nm	1.59 ± 0.05 nm	1.89 ± 0.04 nm	2.10 ± 0.09 nm	2.20 ± 0.15 nm	2.53 ± 0.12 nm	3.12 ± 0.11 nm
6-PHTCS	1.44 ± 0.02 nm	1.54 ± 0.02 nm	1.64 ± 0.02 nm	1.92 ± 0.02 nm	2.55 ± 0.02 nm	3.04 ± 0.16 nm	3.11 ± 0.11 nm	3.18 ± 0.13 nm

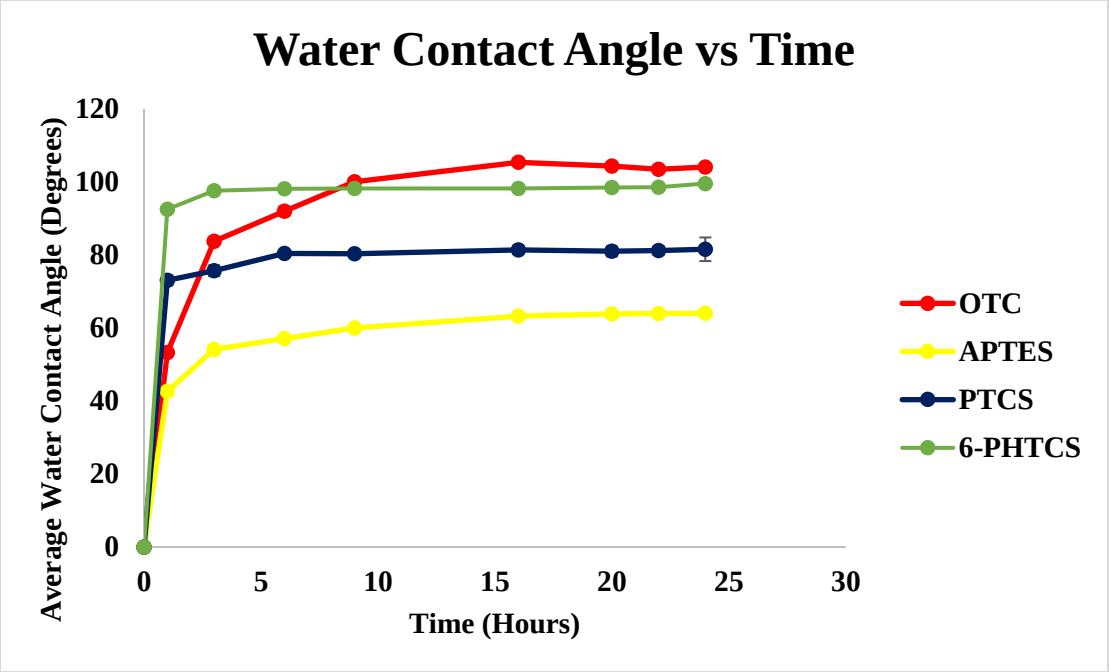

Figure 16. Characteristics of SAM using water contact angle. The figure shows the water contact angle of the functionalized SiO_2 surface over time. This helped us understand the wettability of the surface depending on what organosilane was formed.

Table 2. Water Contact Angle of Organosilanes

Organosilane	1 Hour	3 Hour	6 Hour	9 Hour	16 Hour	20 Hour	22 Hour	24 Hour
OTC	53.2 ± 0.8°	83.7 ± 0.8°	91.9 ± 1.2°	100.1 ± 0.9°	105.3 ± 0.9°	104.3 ± 0.5°	103.4 ± 0.4°	104.1 ± 0.4°
APTES	42.7 ± 0.7°	54.1 ± 0.5°	57.1 ± 0.4°	60.0 ± 0.3°	63.2 ± 0.3°	63.8 ± 0.1°	63.9 ± 0.1°	64.0 ± 0.1 °
PTCS	73.0 ± 1.4 °	75.6 ± 1.5°	80.4 ± 0.7°	80.3 ± 0.9°	81.3 ± 1.2°	80.9 ± 1.4°	81.2 ± 1.2°	81.5 ± 3.2°
6-PHTCS	92.4 ± 0.1°	97.6 ± 0.2°	98.1 ± 0.6°	98.2 ± 0.5°	98.2 ± 0.2°	98.5 ± 0.5°	98.5 ± 0.6°	99.5 ± 0.4°

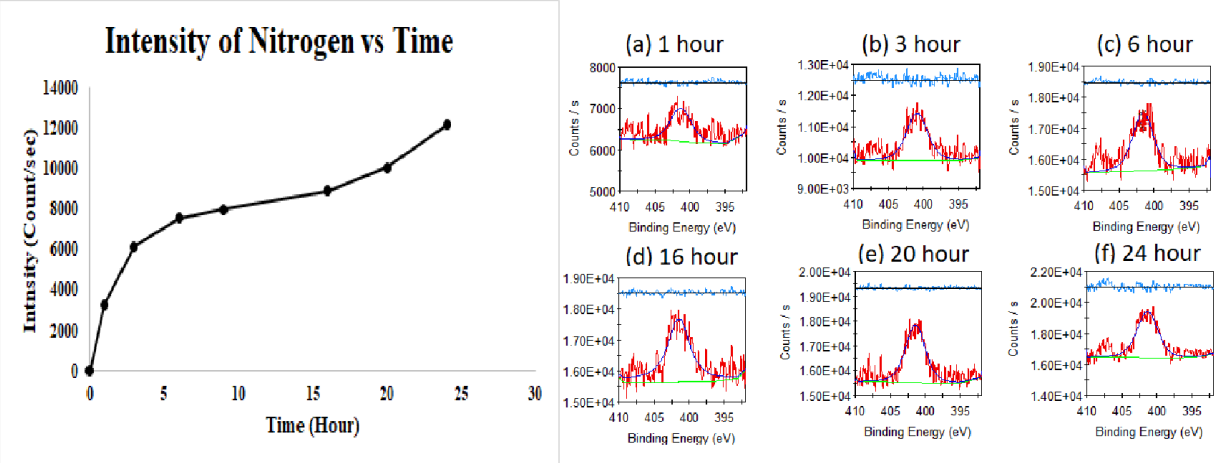

Figure 17. XPS analysis of APTES over time. The figure above shows the relation between the intensity of nitrogen on the SiO_2 surface over various times of exposure to APTES.

Table 3. Intensity of Nitrogen over Time

Time (Hour)	0 Hour	1 Hour	3 Hour	6 Hour	9 Hour	16 Hour	20 Hour	24 Hour
Intensity (Count/sec)	0	3263.22	6160.72	7566.15	8000	8893.67	10073.05	12158.97

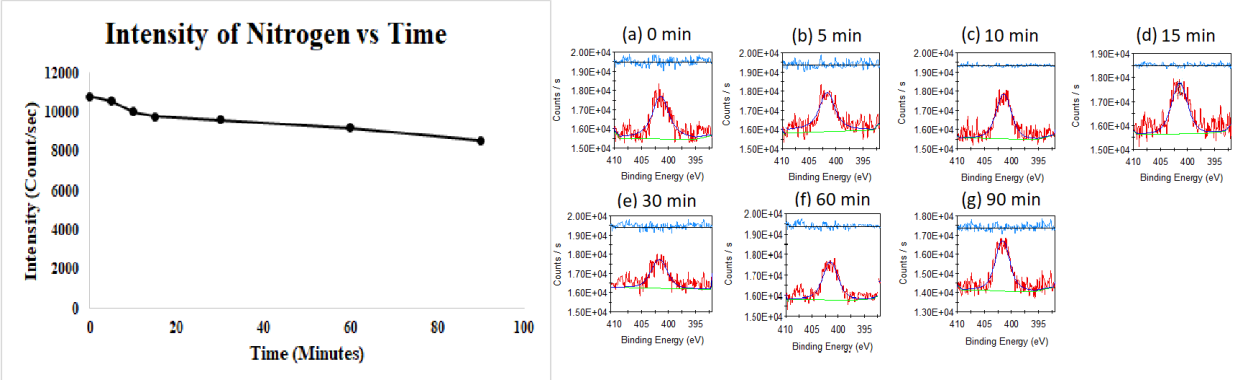

Figure 18. XPS analysis of APTES and sonication in deionized water over time. The figure shows the intensity of nitrogen, and therefore the presence of APTES, after various durations of sonication in deionized water.

Table 4. Intensity of Nitrogen over Time of Sonication in DIW

Time (Minute)	0	5	10	15	30	60	90
Intensity (Count/sec)	10821.48	10577.65	10008.13	9788.488	9603.32	9216.113	8557.24

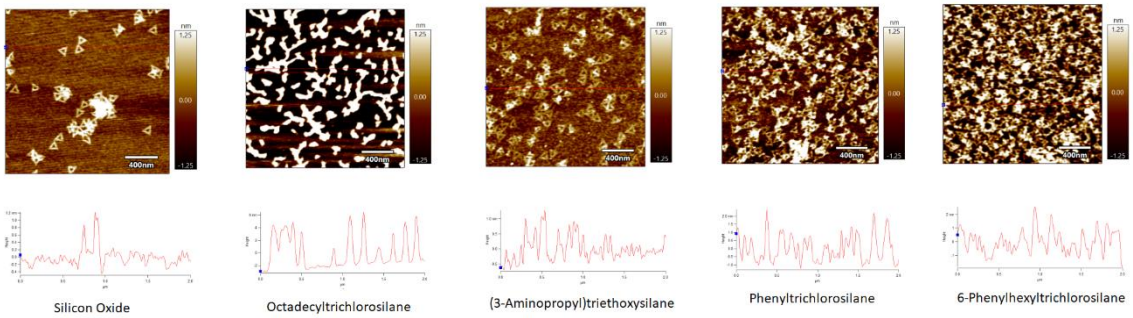

Figure 19. Interaction of DNA origami nanostructures with organosilane SAMs. The following shows the interactions between DNA origami nanostructures and the organosilanes investigated throughout this project. Each figure has a scale height of 2.50 nm. Red line represents location of cross-section.

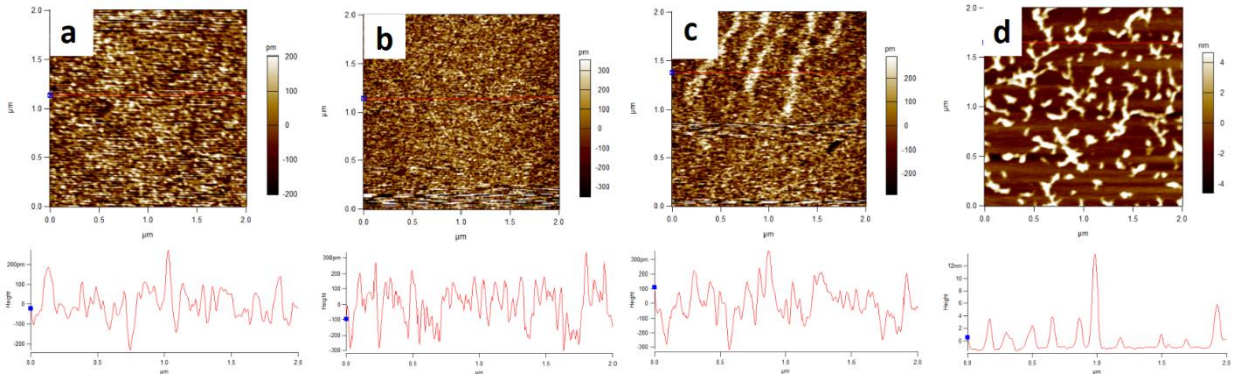

Figure 20. Process of DNA origami deposition onto OTC. The figure shows an example of a sample that undergoes the steps of DNA origami deposition onto OTC SAM. (a) SiO_2 surface only after cleaning. (b) SiO_2 surface with OTC SAM. (c) Deposition of tris-buffer solution onto OTC SAM. (d) Deposition of DNA nanostructure onto OTC SAM. Red line represents location of cross-section.

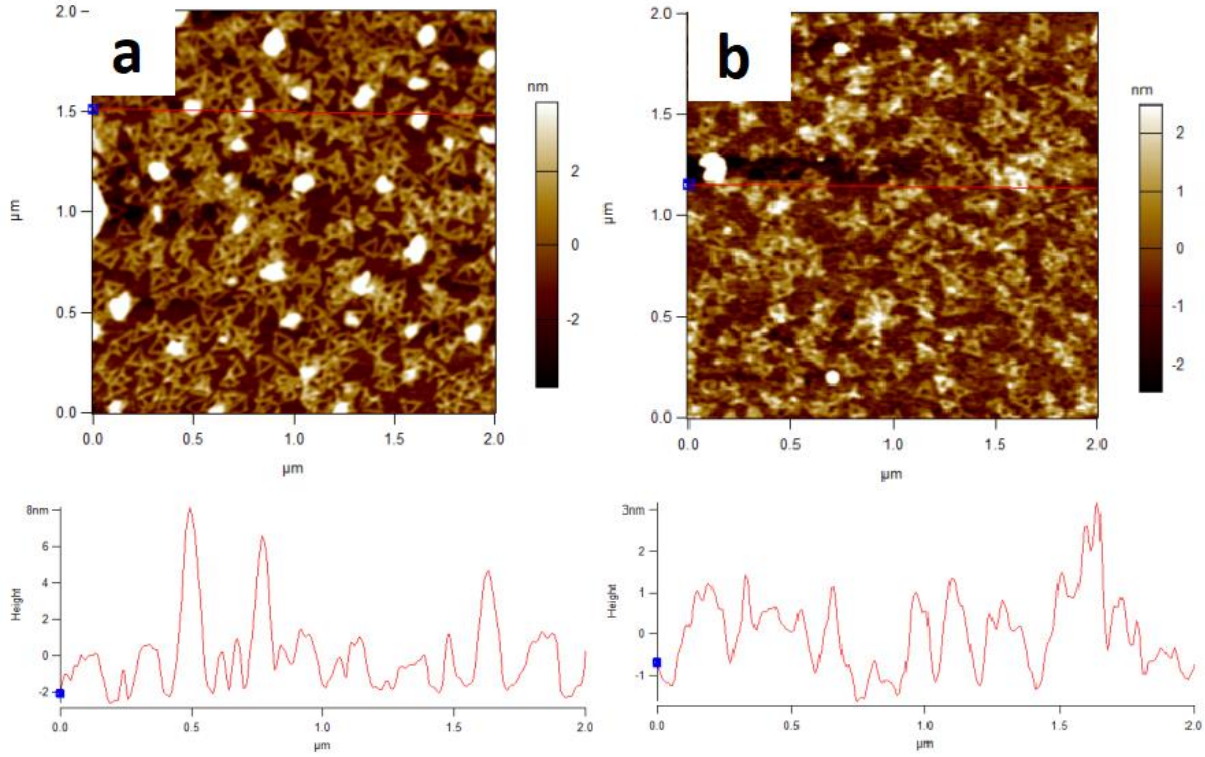

Figure 21. PTCS interaction with DNA nanostructure and removal of aggregates. DNA was initially found to interact well with PTCS monolayer. However, it was noticed that aggregates tended to form throughout the surface (a). It was discovered that sonication in chloroform for thirty minutes after PTCS was assembled on the surface removed the aggregates mostly (b). Red line represents location of cross-section.

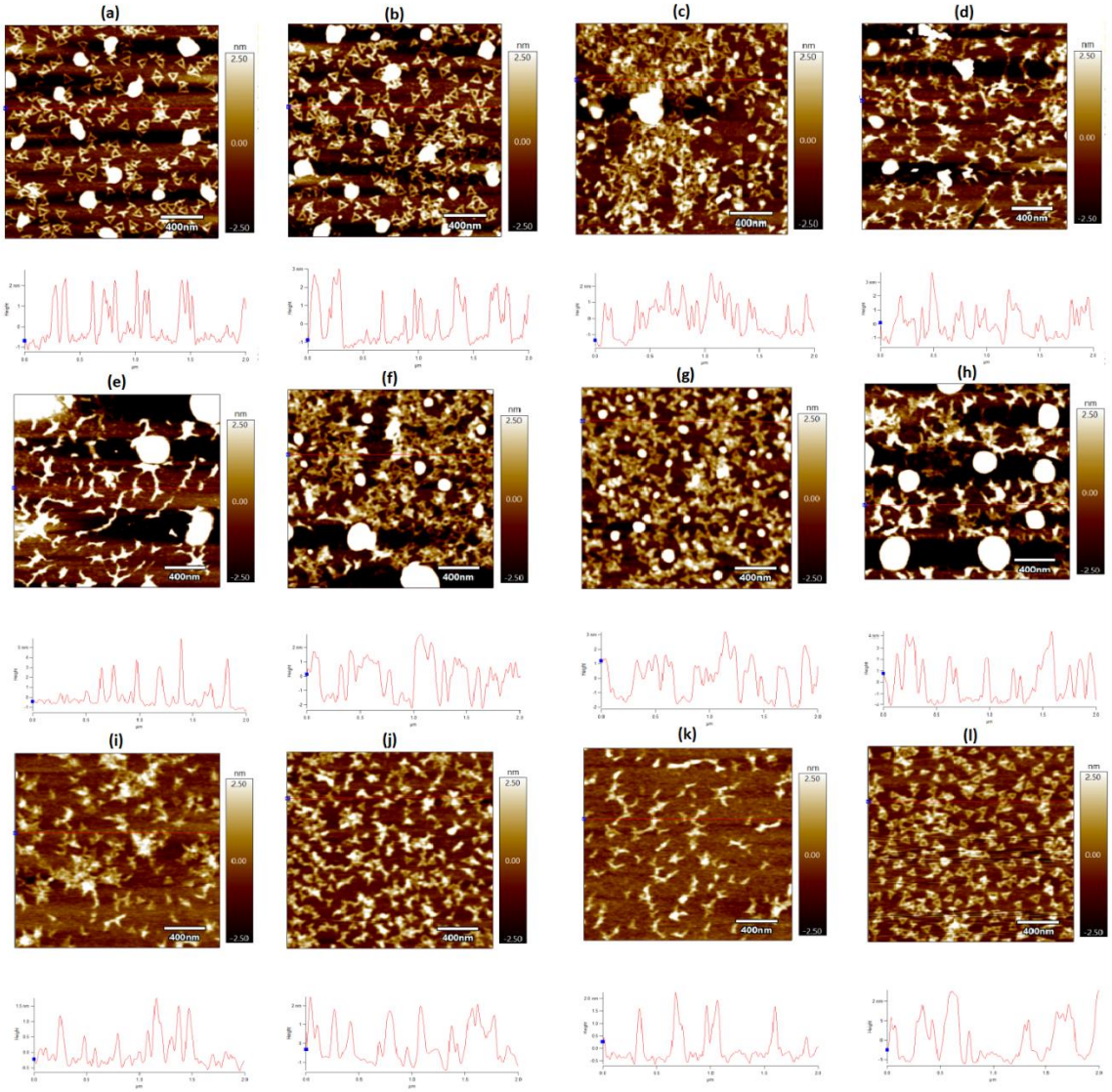

Figure 22. Variation in DNA origami interaction with PTCS. Examples of uniformly distributed intact nanostructures (a – b, l); Example of uniformly distributed deformed nanostructure (d and k); Examples of deformed nanostructure found at samples' center (e and i); Examples of intact nanostructures found at samples' edges (f and j); Example of sample showing intact nanostructure at sample center and deformed nanostructure at sample edge (g and f).

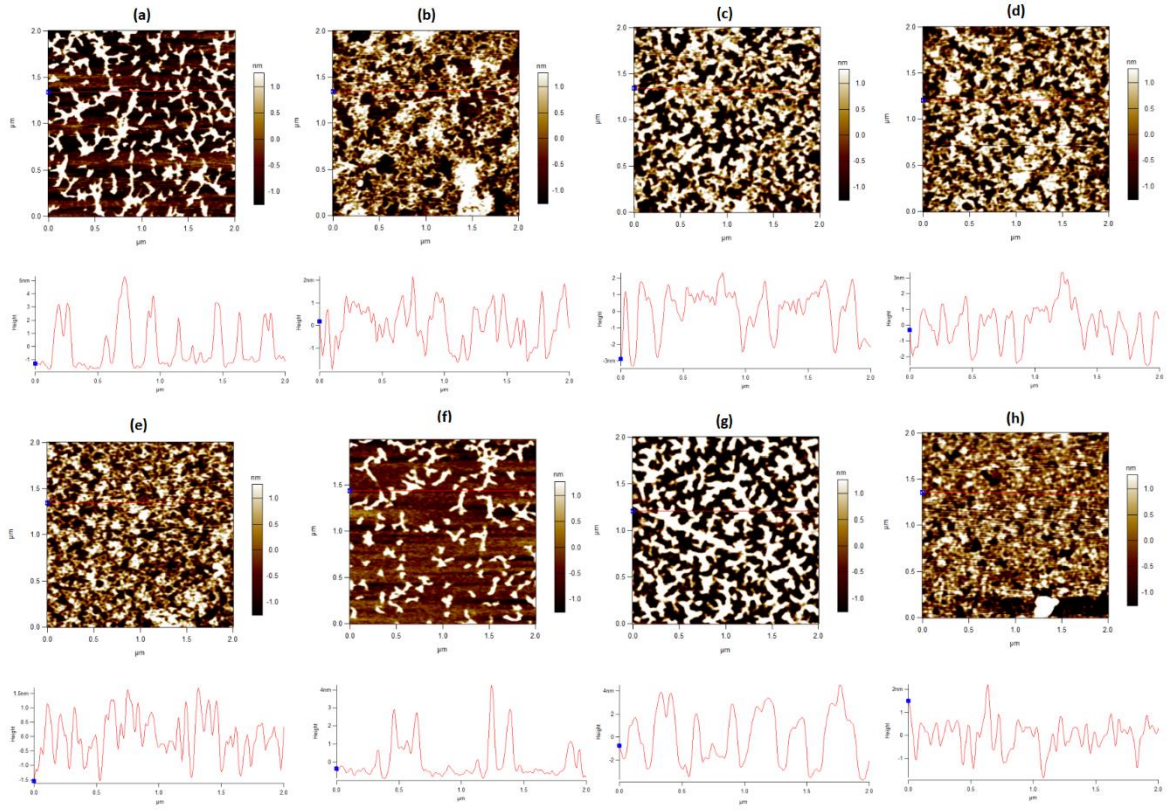

Figure 23. Variations in DNA origami interactions with 6-PHTCS. Examples of deformed nanostructure found at samples' center (a and c); Examples of intact nanostructures found at samples' center (b and d); Example of uniformly distributed intact nanostructure (e); Examples of uniformly distributed deformed nanostructure (f and g); Example of intact nanostructures showing lack of detail (h).

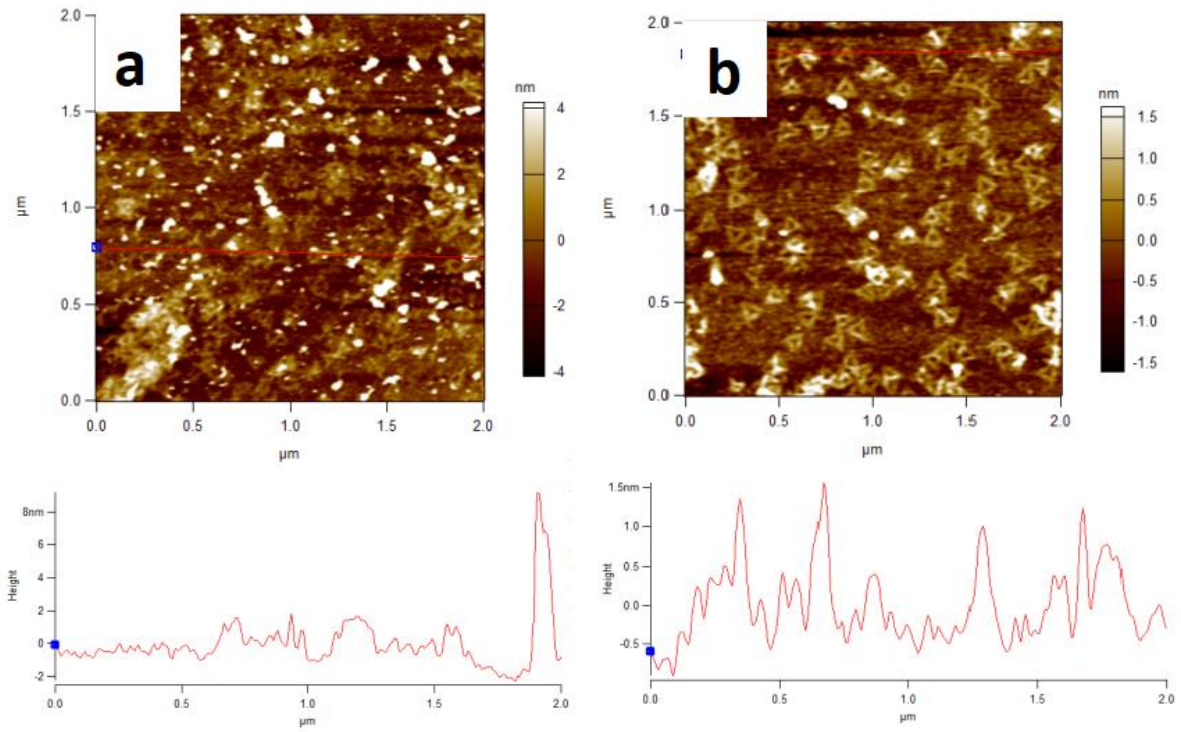

Figure 24. Variation in DNA interaction between APTES using toluene or methanol as solvent. DNA nanostructure adsorbed onto toluene-solvated APTES (a); DNA nanostructure adsorbed onto methanol-solvated APTES (b).

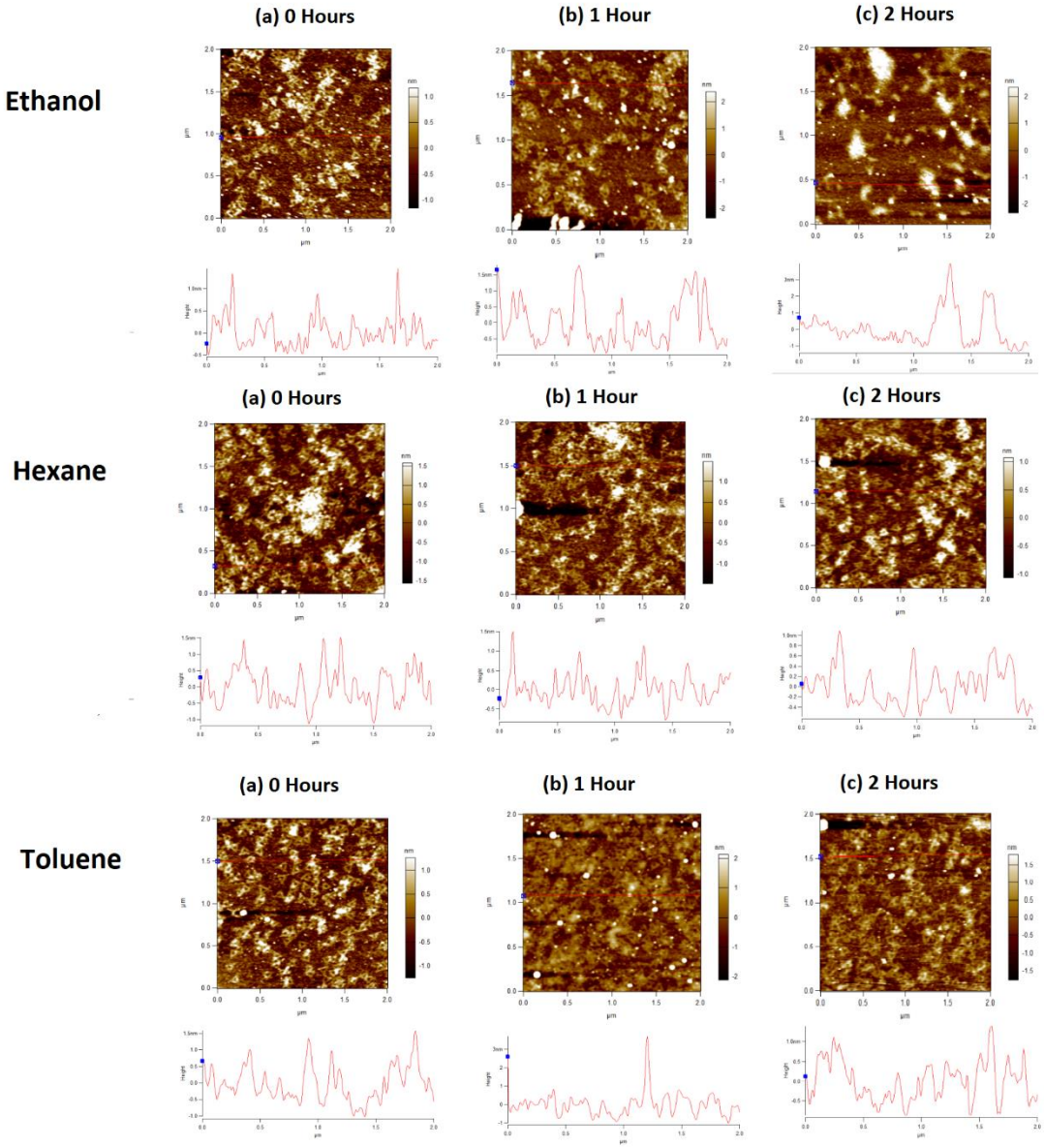

Figure 25. Stability of DNA nanostructures on APTES SAM in organic solvents. AFM images of DNA origami triangles immersed in ethanol (top), hexane (middle), and toluene (bottom) for (a) 0 h, (b) 1 h, and (c) 2 h. The red horizontal lines on the AFM images indicate the location of the cross sections.

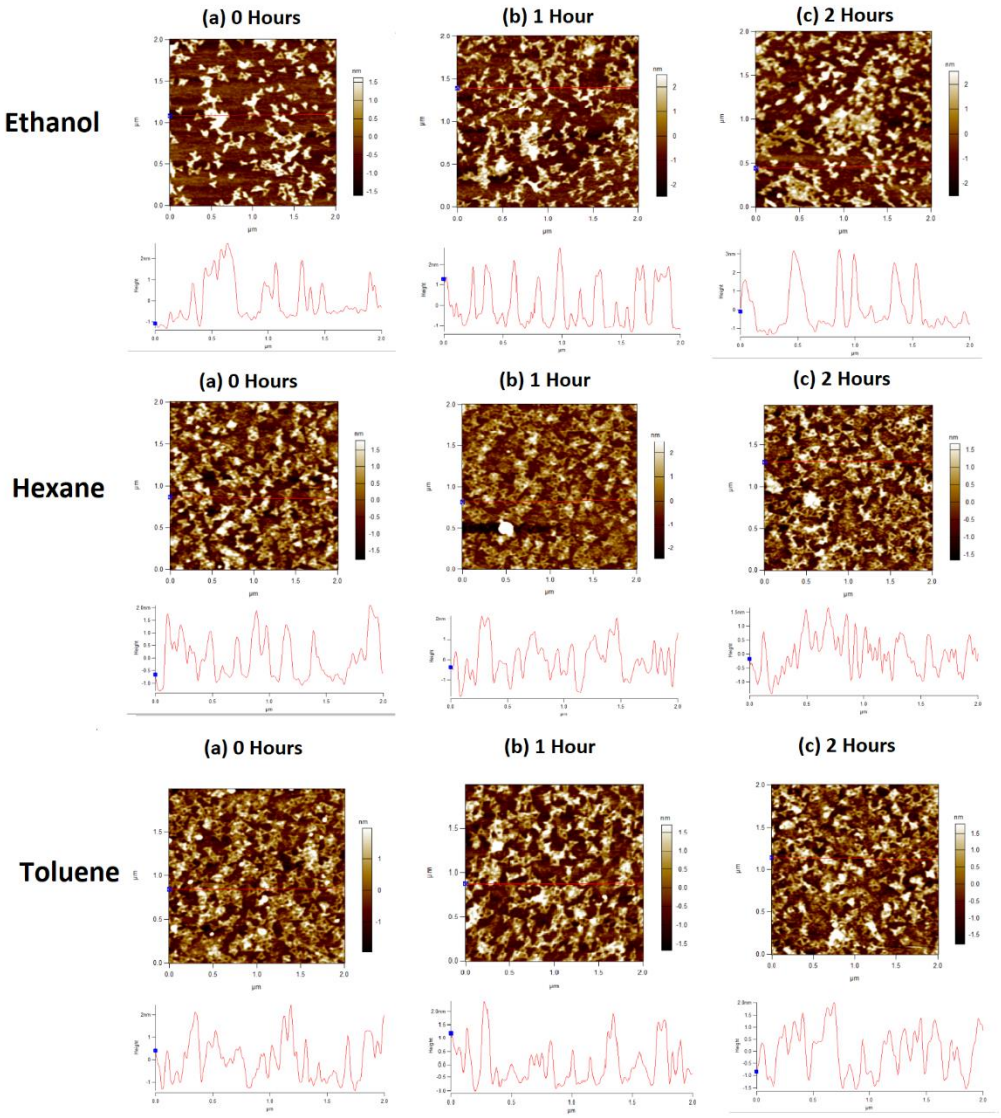

Figure 26. Stability of DNA nanostructures on PTCS SAM in organic solvents. AFM images of DNA origami triangles immersed in ethanol (top), hexane (middle), and toluene (bottom) for (a) 0 h, (b) 1 h, and (c) 2 h. The red horizontal lines on the AFM images indicate the location of the cross sections.

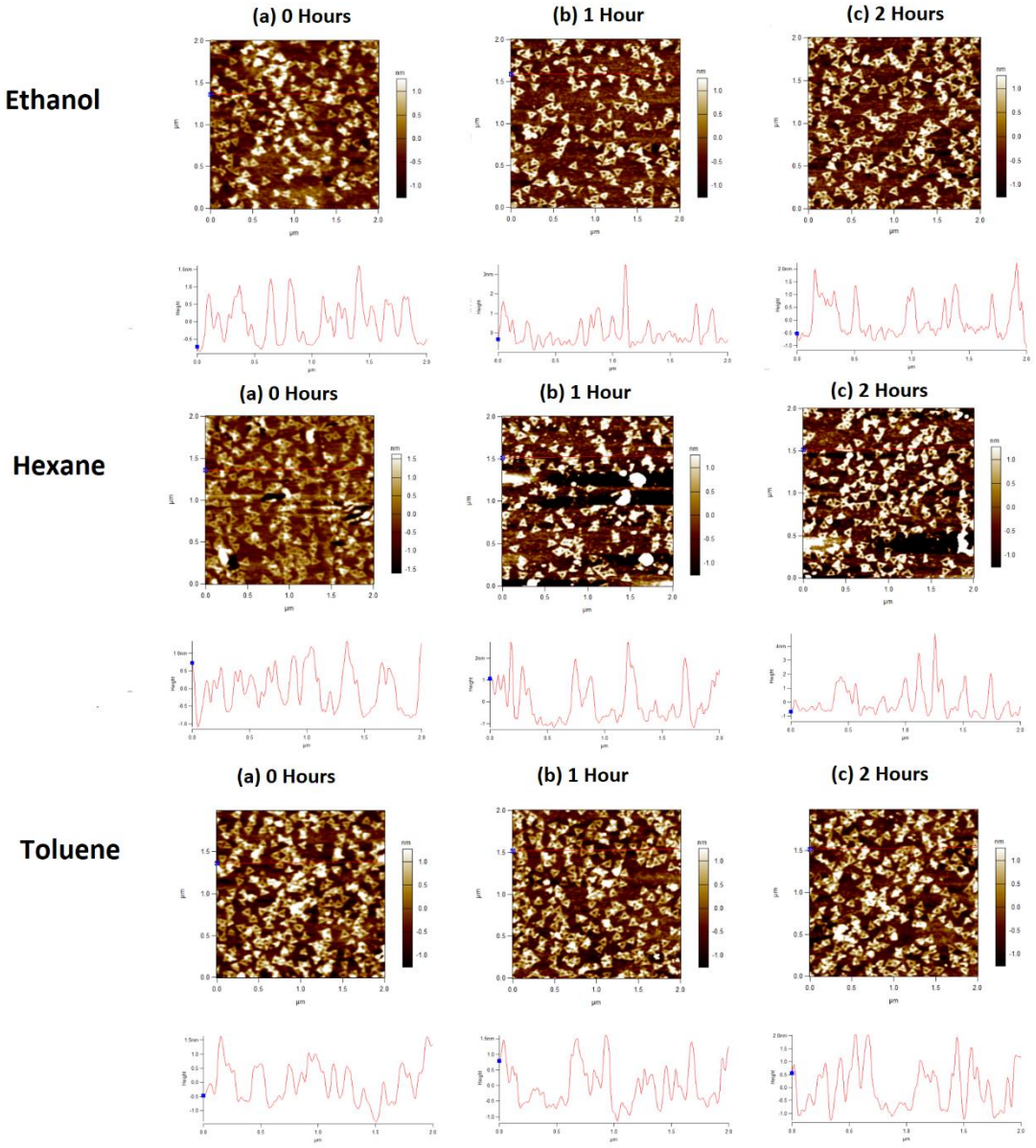

Figure 27. Stability of DNA nanostructures on 6-PHTCS SAM in organic solvents. AFM images of DNA origami triangles immersed in ethanol (top), hexane (middle), and toluene (bottom) for (a) 0 h, (b) 1 h, and (c) 2 h. The red horizontal lines on the AFM images indicate the location of the cross sections.

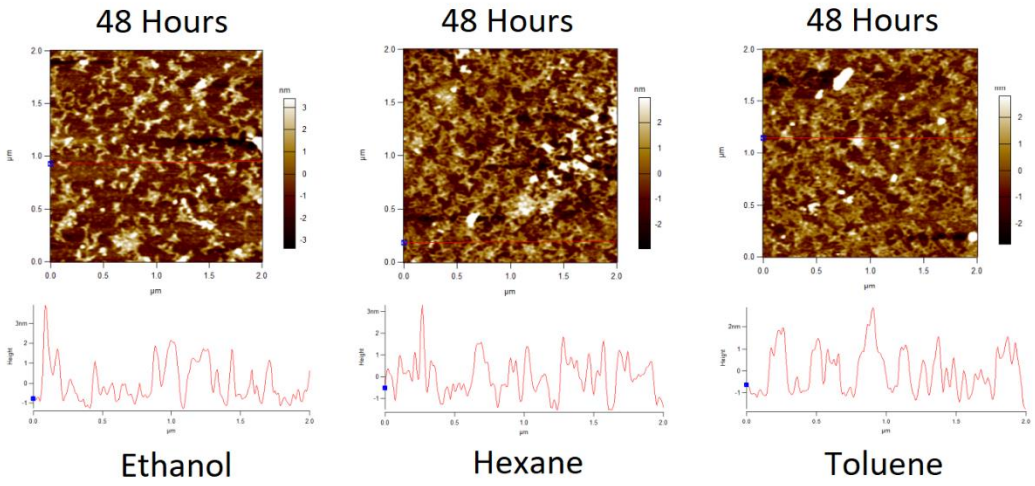

Figure 28. Stability of DNA nanostructures on PTCS SAM in organic solvents after immersion for 48 hours. AFM images of DNA origami triangles immersed in ethanol (left), hexane (middle), and toluene (right). The red horizontal lines on the AFM images indicate the location of the cross sections.

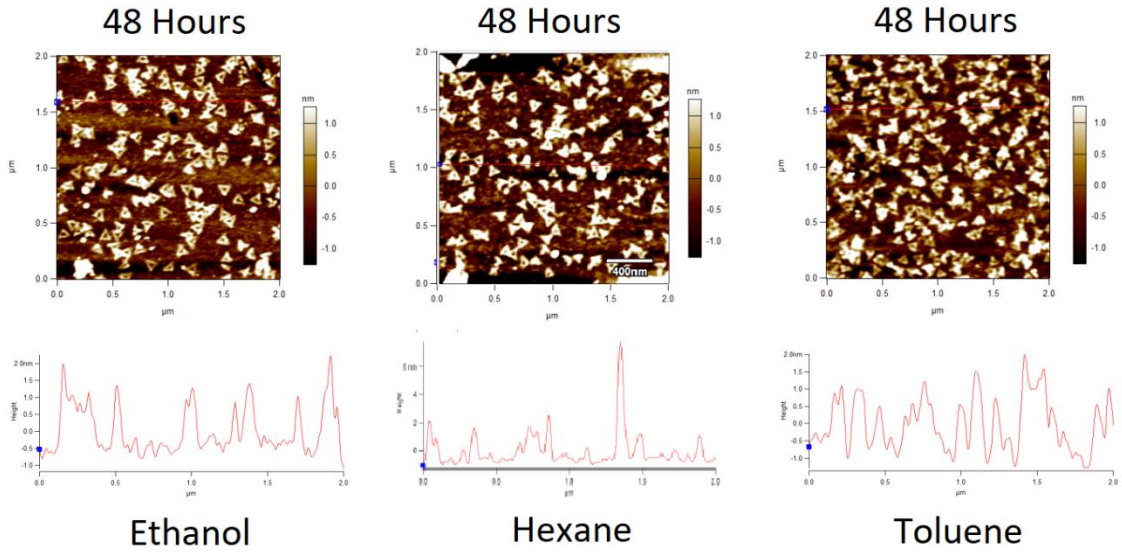

Figure 29. Stability of DNA nanostructures on 6-PHTCS SAM in organic solvents after immersion for 48 hours. AFM images of DNA origami triangles immersed in ethanol (left), hexane (middle), and toluene (right). The red horizontal lines on the AFM images indicate the location of the cross sections.

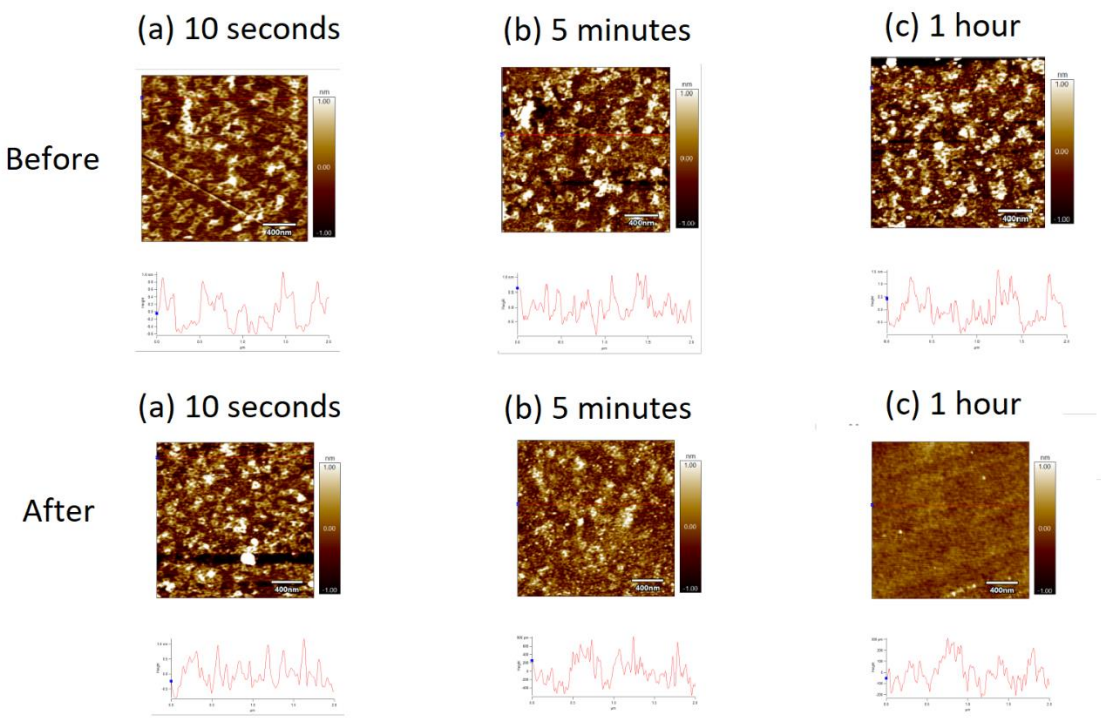

Figure 30. Stability of DNA nanostructure on APTES SAM in deionized water. Top row shows DNA samples on APTES SAM before exposure to deionized water. The bottom row shows the same wafers exposed to deionized water for 10 seconds (a), 5 minutes (b), and 1 hour (c).

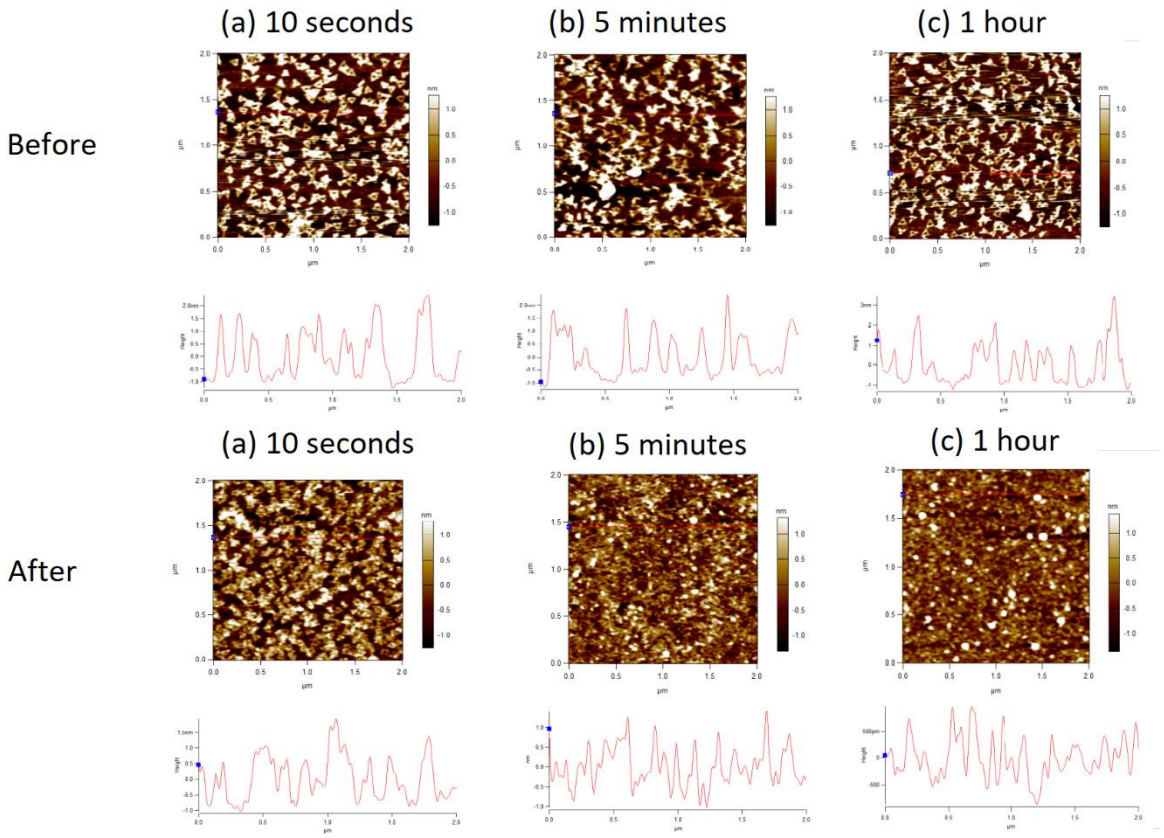

Figure 31. Stability of DNA nanostructure on PTCS SAM in deionized water. Top row shows DNA samples on PTCS SAM before exposure to deionized water. The bottom row shows the same wafers exposed to deionized water for 10 seconds (a), 5 minutes (b), and 1 hour (c).

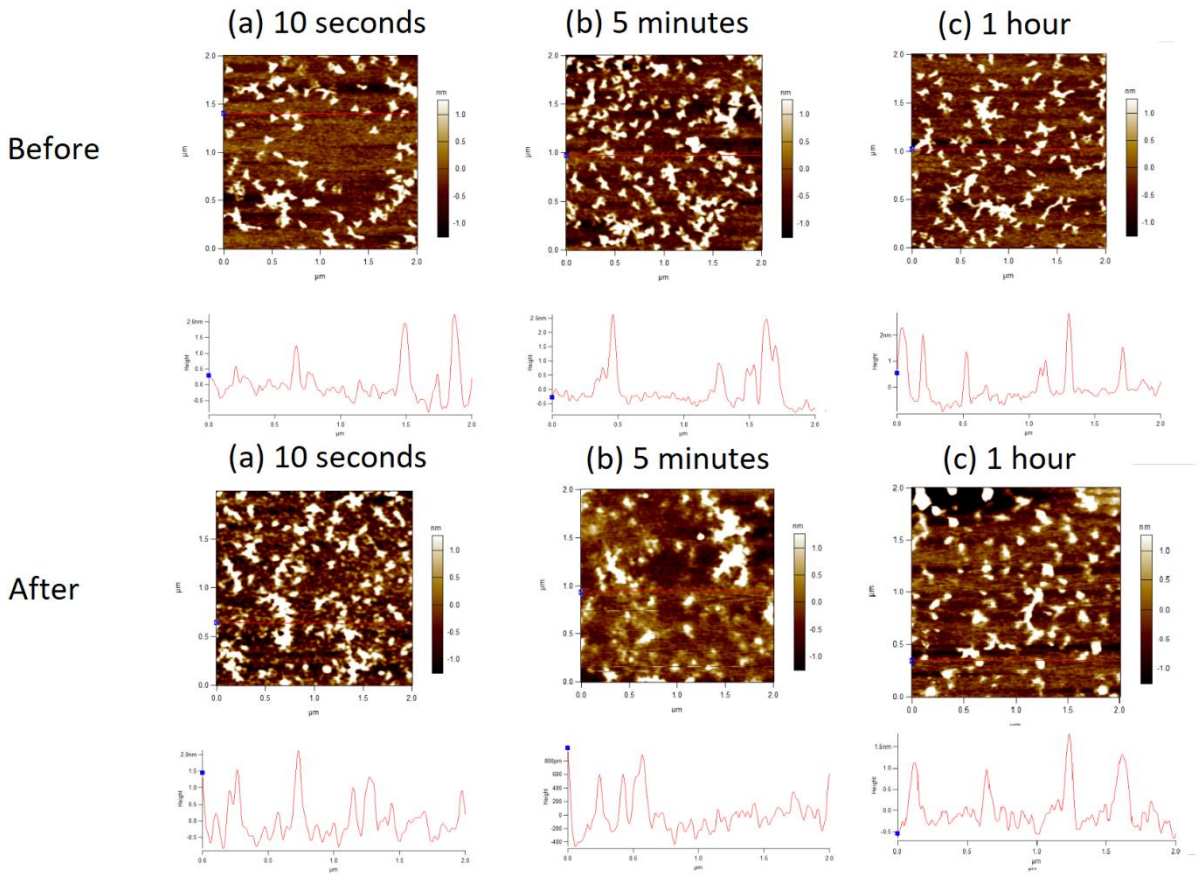

Figure 32. Stability of DNA nanostructure on 6-PHTCS SAM in deionized water. Top row shows the same DNA samples before exposure to deionized water. The bottom row shows the same wafers exposed to deionized water for 10 seconds (a), 5 minutes (b), and 1 hour (c).

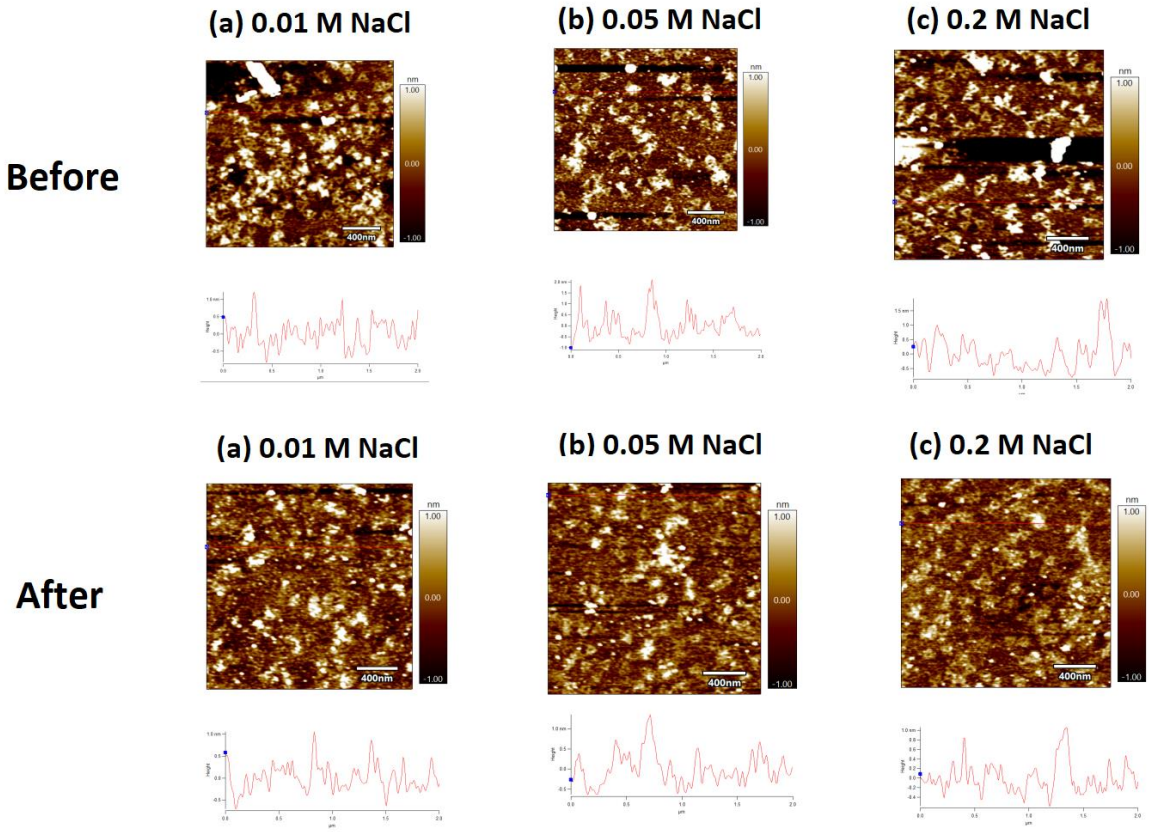

Figure 33. Effect of ionic strength on DNA nanostructures bound to APTES SAM. Top row shows DNA samples on APTES SAM before exposure to ionic solutions. The bottom row shows the same wafers exposed to ionic solutions with concentrations of 0.01 M NaCl (a), 0.05 M NaCl (b), and 0.2 M NaCl (c). All samples experienced the same duration of exposure which was 10 seconds.

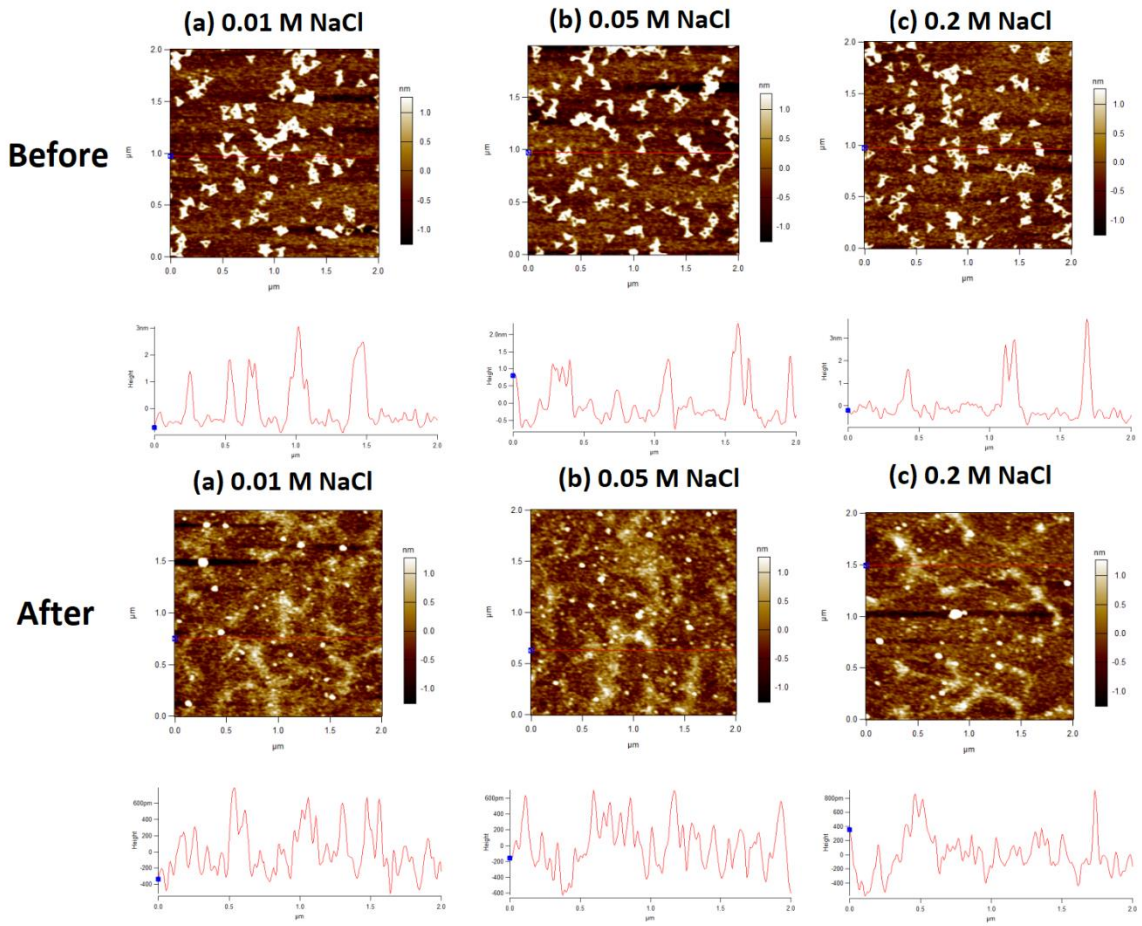

Figure 34. Effect of ionic strength on DNA nanostructures bound to PTCS SAM. Top row shows DNA samples on PTCS SAM before exposure to ionic solutions. The bottom row shows the same wafers exposed to ionic solutions with concentrations of 0.01 M NaCl (a), 0.05 M NaCl (b), and 0.2 M NaCl (c). All samples experienced the same duration of exposure which was 10 seconds.

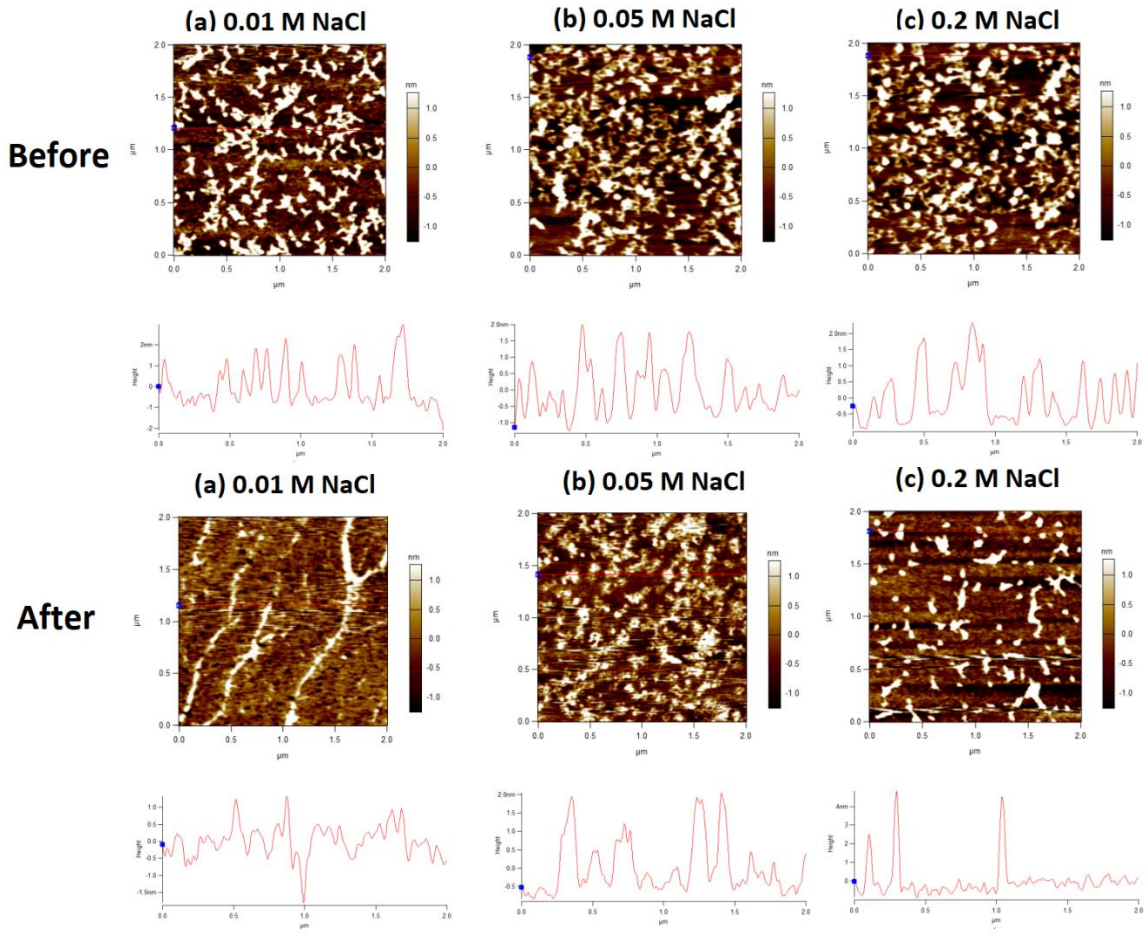

Figure 35. Effect of ionic strength on DNA nanostructures bound to 6-PHTCS SAM. Top row shows DNA samples on 6-PHTCS SAM before exposure to ionic solutions. The bottom row shows the same wafers exposed to ionic solutions with concentrations of 0.01 M NaCl (a), 0.05 M NaCl (b), and 0.2 M NaCl (c). All samples experienced the same duration of exposure which was 10 seconds.

3.4: DISCUSSION

3.4.1: Characteristics of SAMs

Given that different self-assembled monolayers were analyzed, it is not surprising that the growth rates and kinetics of the SAMs were relatively different. In SAM formation, several factors are involved with the growth of the film. These factors include chemical bond formations with the substrate and intermolecular interactions. Additionally, other processes are involved such as the solution-phase transport of adsorbate molecules to the solid-liquid interface and adsorption rate to the surface. In SAM formation, there is an evolution of molecular order in terms of both adsorption and surface coverage. This shows itself as monolayers growing in a stepwise process rather than a continuous pathway.

Regarding all the SAMs analyzed, based on the film growth and water-contact angle, monolayer begins to occur within one hour of silanization. The OTC and the 6-PHTCS seem to grow monolayers between 3 - 6 hours, with a slow linear trend in film growth afterwards till approximately twenty hours where a second layer is formed. This is apparent by the plateauing of the film growth between the given time periods. On the other hand, PTCS and APTES possess very similar trends where growth occurs for approximately nine hours before a monolayer is formed. Afterwards, a second layer of film seems to grow after approximately twenty hours with APTES experiencing a second layer growth after 22 hours.

Additionally, the more hydrophobic SAMs appear to have a higher magnitude of film thickness in comparison to the growth of APTES. In regards to the water-contact angle, the trend unsurprisingly fits the trend found on the film-growth. Here, the highest contact angles are found on the more hydrophobic SAMs while the APTES SAM possesses lower contact angles. Rate-wise, the SAMs possessing phenyl groups possess a slightly different trend in regards to water-contact angle. Here, both phenyl-terminated SAMs immediately experienced a

peak contact-angle value or near-peak contact angle value within the first hour of self-assembly followed by a general plateau after six hours. The other SAMs showed a slower trend where plateauing of the contact-angle values occurred around sixteen hours.

The trend in film growth observed amongst the SAMs analyzed can be explained by several factors. Organosilane SAM growth is dictated by two competitive reactions. The first is the aggregation process of hydrolyzed molecules in the precursor solution and the second reaction being the dehydration reaction of the hydrolyzed molecules forming the SAM. These two reactions are then further influenced by three factors: the interactions between the headgroups and SiO2, the interactions between the alkyl chains in the silane molecule, and the interaction between the end groups of the silane. It is important that a healthy balance is struck between all three factors to enable effective film growth.[108]

The film growth is seen to be higher amongst OTC, PTCS, and 6-PHTCS. This is likely because these three silanes are chlorosilanes meaning they have Si–Cl head groups. The chloro-groups are extremely hydrolysable which in turn leads to higher adsorption between the SiO_2 and the silane molecules. This is understandable since chloro-groups are better leaving groups than the ethoxy-groups found on APTES.[109 – 110] OTC possesses the highest film growth of the three trichlorosilanes due to its long alkyl chain. Past research has revealed that longer alkyl chains on silanes promote stronger van-der Waals intermolecular forces between the silane molecules.[111] As a result, the silane molecules are more densely packed and more uniform in orientation. This denser and more uniform packing promotes thicker film growth.

The PTCS shows the smallest film growth of the trichlorosilanes. This is most likely because its end group is a phenyl group directly attached to the Si central atom. The phenyl group of PTCS is bulky and sterically hinders the packing ability of the SAM.[107, 112 – 113]

Therefore, the bulky phenyl group leads to a more disordered state in the SAM and a lower surface density. As a result, the film growth is not as great as seen in OTC. The 6-PHTCS, while containing a phenyl group, also contains a hexyl chain which enables for stronger van-der-Waals forces which counteracts the steric hindrance caused by the phenyl end group. This explains why the 6-PHTCS film growth is in between the OTC and PTCS. Interestingly, the film growth of 6-PHTCS is fairly high and is more similar to that of OTC rather than PTCS. This might infer that alkyl chain length has a greater influence in film growth over the steric hindrance caused by the phenyl group.

3.4.2: DNA Origami Nanostructure Interaction with Organosilane SAMs

The data collected reveals that DNA nanostructures behave differently depending on the self-assembled monolayer utilized. This is in terms of both interaction and chemical stability. Regarding the general interaction between the nanostructures and the SAMs along with maintaining structural integrity, it is apparent that the worst interaction occurred between the nanostructures and OTC. This was then followed by 6-PHTCS, then PTCS, and APTES. The deformation of the DNA nanostructures seen on OTC is likely the result of DNA destabilization. DNA is not only stabilized by hydrogen bonding, but also hydrophobic interactions known as hydrophobic base stacking. These "hydrophobic pockets" stabilize the DNA double helices. However, research has revealed that long carbon chains can interact with the hydrophobic pockets thus destabilizing the DNA structure. The destabilization comes in the form of the DNA molecule folding on top of itself.[114 – 115] This would explain why the deformed DNA observed on the OTC surface is significantly higher.

Unsurprisingly, the nanostructures adsorbed onto APTES showed excellent structural integrity. Here, little to no deformation was observed. This is because the surface of the APTES is positively charged due to the protonation of the amine group on the APTES. This charged

amine group interacts well with the negatively charged phosphate-backbone of the DNA.[116] It should be noted that the contaminates seen on some of the samples have been observed before by other researchers as well. They have concluded that these contaminants are precipitation products of APTES reacted with trace water.[117] These particles are extremely stable and require extreme methods to wash off or remove.

It was of extreme interest that the APTES method using toluene showed significantly different results from the APTES method using methanol. We made several samples of APTES with toluene as the solvent and several samples of APTES with methanol as the solvent. In each case, little to no nanostructures were observed on the APTES samples using toluene as solvent while nanostructure was clearly observed on the APTES samples using methanol as the solvent. Initially, it was thought that the methanol solvent method was not depositing APTES onto the SiO_2, and the nanostructures were adsorbing onto SiO_2. However, this was ruled out after XPS revealed that APTES was present on the SiO_2 surface. This led us to believe that the solvents used affected the growth of the APTES and the adsorption of DNA origami. Past research studies have shown that alcohol-solvated APTES SAM growth increases the density of APTES found on the SiO_2 surface.[118] An SiO_2 surface with a higher density of APTES would lead to a more positively charged, and therefore interactive, surface for DNA origami nanostructures. In order to determine if toluene and methanol affected the surface density of APTES, we created several samples of APTES using either toluene or methanol as the solvent. Afterwards, we immediately used XPS to compare the intensity of nitrogen found on the surfaces. We found that in all cases, the methanol-solvated APTES samples had on average a nitrogen intensity 2.2 times than that found on toluene-solvated APTES (Figure 36). This

suggests that the methanol-solvated APTES have a higher density on the SiO_2 surface which improves the adsorption of DNA origami nanostructure.

With both PTCS and 6-PHTCS, we experienced random variation in the structural integrity of the nanostructures. This led us to attempting to modify the DNA adsorption process to enable better structural preservation of the nanostructures. A past experiment by one of our former team members showed that depositing unfiltered DNA onto polystyrene film would allow for adsorption of completely intact DNA nanostructure. This is because the unfiltered ssDNA strands left in the solution were adsorbed onto the polystyrene creating a layer for the nanostructures to effectively adsorb onto.[107] Using this same technique for both PTCS and 6-PHTCS, we created unfiltered DNA nanostructure solution and deposited onto samples of SiO_2 with either SAM. Our results revealed completely intact nanostructure on the surfaces of both SAMs. Six separate samples for each SAM were created and repeated using the same technique. In every case, structurally intact nanostructure was observed on both the center and edges of the wafers' surface with uniform surface density of the nanostructures (Figure 37). This experiment revealed that unfiltered DNA solution could be used to adsorb structurally intact DNA nanostructure onto both PTCS and 6-PHTCS SAMs.

We cannot explain why the phenyl-terminated SAMs experienced such random results with DNA adsorption. There has been practically no past research investigating how DNA nanostructures interact with phenyl-terminated silanes. Fortunately, one of our former team members recently discovered how DNA nanostructures interact with phenyl-terminated hydrophobic surfaces. It was discovered that DNA strands can effectively bind to phenyl-terminated surfaces through $\pi - \pi$ stacking. However, sufficient surface charge is required for the nanostructures to retain their structural integrity.[107] Without sufficient surface charge, the

hydrophobic surfaces induce the DNA strands to stretch. This induced stretching collapses the DNA strands' double helices required for structural preservation and deforms the DNA nanostructures. Given this information, it is likely that a combination of strong hydrophobic interactions and insufficient surface charge lead to the observed deformed DNA nanostructures on the phenyl-terminated samples.

With this being said, it would be expected then for all of the phenyl-terminated samples to show only deformed DNA nanostructures. However, several of the samples showed structurally intact nanostructures. Two theories have been made that might explain the unusual phenomenon observed. The first theory is that the SAM is not fully developed on the SiO_2 wafer, and the DNA nanostructures are actually adsorbing onto SiO_2 pockets on the surface. Past research has revealed that certain phenyl-terminated silanes, such as PTCS, experience disordered film growth which can lead to non-uniform layers of film.[119 – 120] The second idea is that in some samples, enough ssDNA strands are adsorbed onto the SAM allowing for adsorption of the actual nanostructure.

Tests would need to be done to see whether either of these two theories are true. For the SAM-theory, the SAMs should be analyzed with IR mapping.[121] This would allow us to determine whether certain areas of the surface possessed phenyl-functional groups, and therefore SAM, while other areas did not. If the test showed that certain areas of the surface did not possess phenyl-groups, it would support the idea that the nanostructures were adsorbing onto regions of SiO_2 instead of SAM thus preserving the structures' integrity. For the ssDNA-theory, we would need to discover a way to detect whether ssDNA strands were present on the surface of the SAM. This might be able to be done by using fluorescence-enhanced DNA detection applied by certain biochemists. To do this, we would first need to modify the DNA strands by

attaching florescent labels to the ssDNA. This would allow us to "track" and "monitor" the adsorption of the DNA onto the SiO_2 surface. We could easily label the ssDNA using fluorescent reagents such as *N*-[2-(iodoacetamido)ethyl]-7-diethylaminocoumarin-3-carboxamide (IDCC) which can be bound to the cytosine base of the DNA strands. After modifying the ssDNA strands, we would deposit unfiltered DNA nanostructure onto the phenyl-terminated SAMs. We could then use a simultaneous combination of AFM and super-resolution fluorescence microscopy to determine if a layer of ssDNA was present on the surface.[122 – 124] If so, this would further support the idea that ssDNA is responsible for the adsorption of structurally intact DNA on the SiO_2 surface.

3.4.3: Effect of Rinsing with Organic Solvents

The DNA nanostructures, when present on all the forms of the SAMs, did not show any change upon interaction with ethanol, hexane, or toluene in terms of either structural integrity or surface density. This led to us concluding that organic solvents do not have a strong influence on the interaction between DNA nanostructures and organosilane SAMs. The only exception was with APTES after two hours of exposure to ethanol. Here, the DNA appeared to be removed from the surface with various aggregates being observed. This observation was unusual since all the other SAMs showed no other similar results. Additionally, past experiments showing the chemical stability of DNA nanostructures and ethanol revealed that the nanostructure stayed intact and was not removed from the surface.

We do not understand why there was an absence of DNA nanostructure on the APTES surface after long exposure to ethanol. Past research has shown that DNA nanostructures adsorbed onto SiO_2 were not affected by ethanol exposure.[125] In fact, ethanol is commonly used to induce DNA precipitation.[126] This led us to believe that the ethanol was removing the APTES SAM that the DNA nanostructures were adsorbed to. Ethanol, and other alcohols, have been

used in past experiments to remove excess APTES from surfaces. This is because the ethanol disrupts the equilibrium of the condensation reaction between APTES molecules, thus removing them from the surface.[127 – 128] While this usually is used to remove excess APTES silanes on surfaces, the prolonged exposure to ethanol might affect the APTES bound to the SiO_2 surface and lead to a slow removal of the SAM. That being said, this is only speculation, and further testing for need to be conducted. The most effective way to answer this is to create APTES sample, without DNA, and analyze the intensity of nitrogen on the surfaces using XPS. The wafers would then be subjected to ethanol exposure using the same time frame, two hours, as in the experiment. Afterwards, the exposed wafers would be reexamined with XPS and have their nitrogen intensity reanalyzed. If there was a significantly lower intensity in the presence of nitrogen after ethanol exposure, this would support the idea that the ethanol was removing the APTES from the surface.

3.4.4: DNA Nanostructures in DIW

With the interactions between DNA nanostructures and DIW, the results from both APTES and PTCS were expected.[125] In both cases, DNA nanostructure was affected by the presence of water and was gradually removed from the surface as exposure progressed. For both, nanostructure was apparent on both up to ten seconds of exposure. The nanostructure was not apparent on either SAM after five minutes of DIW exposure. This is understandable since DIW exposure easily overcomes any forces which allow the DNA nanostructures to adsorb onto the surface. The 6-PHTCS showed extremely different results, and it is uncertain as to why.

3.4.5: DNA Nanostructures in Aqueous Ionic Solutions

In regards to ionic strength, APTES seemed to perform the best. In low concentrations of NaCl, the nanostructure appeared to be removed from the surface while at higher concentrations, the nanostructures seemed to stay on the surface and relatively intact. DNA origami structures

are usually stabilized by the presence of Mg^{2+}, but it has been found that other cations may suffice for preserving DNA origami nanostructure. Monovalent cations, such as Na^{+} can stabilize the DNA nanostructure, but usually their concentration has to be above 200 mM.[129] The nanostructures' rougher appearance and irregularity in shape was also seen in past experiments with DNA nanostructures and ionic strength. It is thought that these two characteristics are the result of either sodium replacing the Mg^{2+} interacting with the DNA or the accumulation of sodium on the DNA nanostructures.

The results from PTCS revealed that no DNA nanostructure was apparent after exposure to ionic solution of any strength. It is unknown as to why the nanostructure was removed from the PTCS surfaces immediately. It is possible that the removal was caused by the presence of water, but the presence of ions might disrupt the $\pi - \pi$ stacking between the DNA and PTCS. This being said, there is no evidence that this latter statement is true. Currently, there are no universally accepted explanations for the factors that govern $\pi - \pi$ stacking nor any universally accepted factors which promote or hinder the non-covalent interaction.[130 – 131] Therefore, the idea that the ions cause disruption in the $\pi - \pi$ stacking is merely speculation, and further information or testing would need to be required to verify this claim. However, if ionic disruption of the $\pi - \pi$ stacking was the cause of DNA nanostructure removal, then it would be expected that similar results would be observed on the 6-PHTCS. Ironically, the exact opposite was seen on 6-PHTCS where the DNA nanostructure remained on the surface albeit deformed at higher ionic strengths.

With this being said, it is likely that the presence of ions seems to affect or at least influence the interaction between DNA nanostructures and phenyl-terminated silanes. If ions had no effect on the interactions, then it is appropriate to assume that the ionic strength results would mirror those observed with DIW exposure. As of right now, there is not enough

information to discern the results observed on the two surfaces nor what role the ions play in the SAM – DNA interactions, but hopefully future research and investigations will reveal the answer to this question.

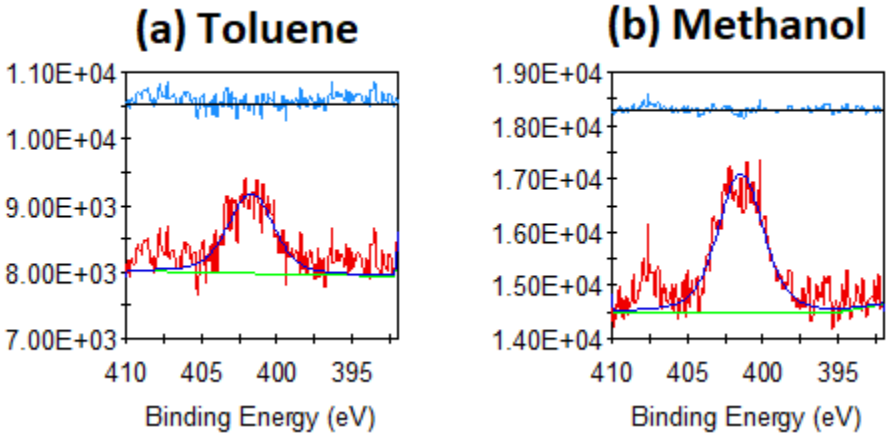

Figure 36. XPS spectrum of nitrogen intensity for toluene solvated-APTES (a) and methanol-solvated APTES (b)

Table 5. Intensity of Nitrogen Between Toluene and Methanol	
Solvent	Average Intensity (Count/sec)
Toluene	4864.07
Methanol	10586.93

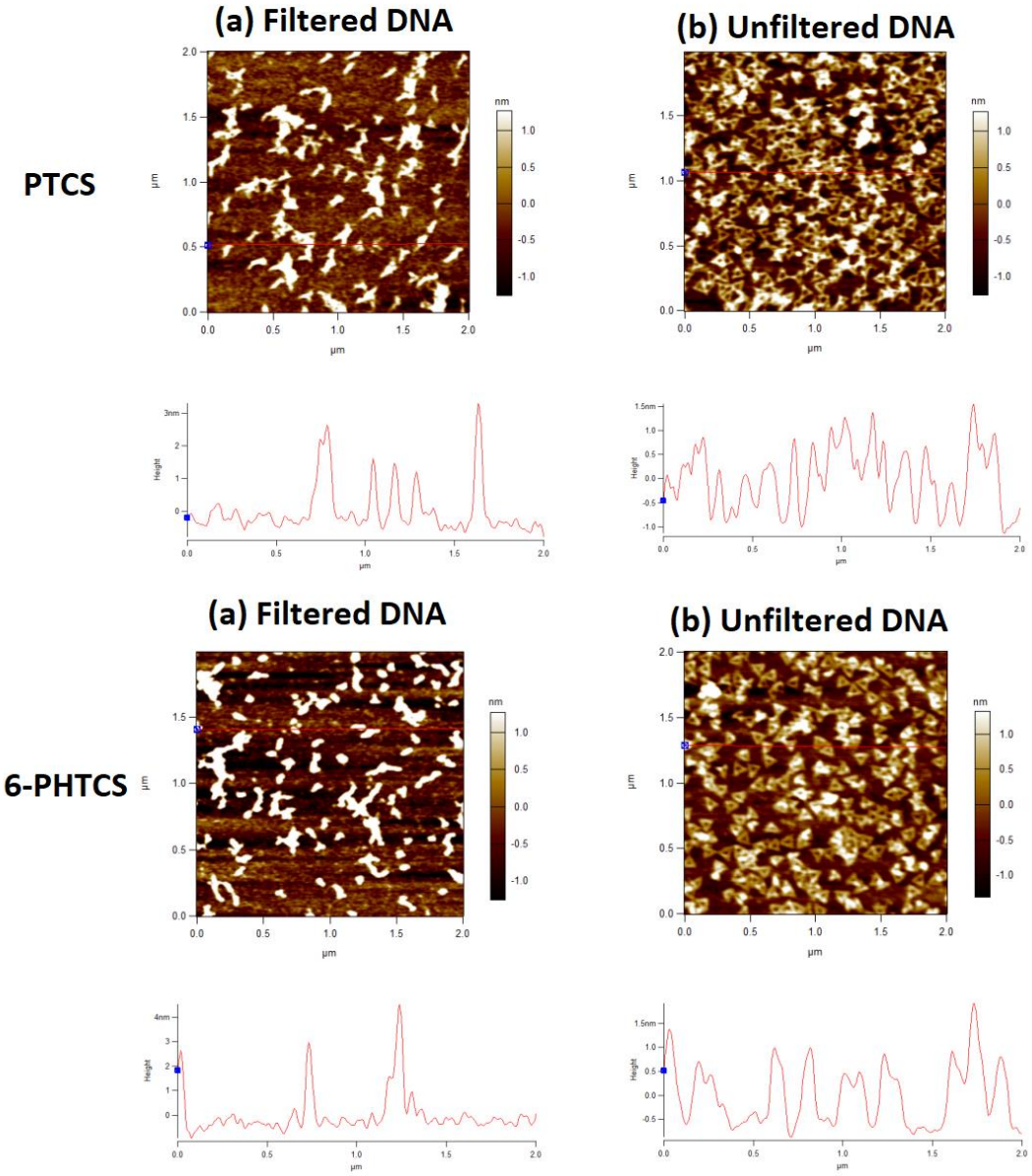

Figure 37. Adsorption of filtered DNA vs unfiltered DNA on phenyl-terminated silanes. The figure above shows the difference in interactive behavior between filtered DNA (a) and unfiltered DNA (b) when adsorbed onto PTCS (top) and 6-PHTCS (bottom).

3.4: CONCLUSIONS

This project was performed to investigate how DNA origami nanostructures interact with various organosilane SAMs. Each SAM contained certain functional tail-groups which might affect the interactive behavior of the DNA nanostructures. We analyzed the film growth of the SAMs to determine optimal conditions for proper monolayers. We observed how DNA origami nanostructures interacted with each SAM in terms of both surface density and structural integrity. Finally, we analyzed and investigated certain chemical stability parameters of the nanostructures when adsorbed to each SAM.

Throughout the project, a multitude of conclusions were made and confirmed. Regarding the characteristics of the SAMs, we concluded that trichlorosilanes had greater film thickness due to their more hydrolysable chloro-groups. We also found that APTES SAM was not significantly affected by DIW sonication for up to ninety minutes. Regarding DNA origami-SAM interaction, we found that APTES was the most successful in terms of nanostructure surface density and maintaining structural integrity. Furthermore, we concluded that methanol-solvated APTES allows for better DNA origami adsorption over toluene-solvated APTES due to the methanol inducing tighter packing of the APTES SAM. We found that OTC was the worst in preserving structural integrity of DNA nanostructures due to the long alkyl chains disrupting the stability of the DNA nanostructures. In regards to chemical stability, DNA nanostructures were not affected by organic solvents up to forty-eight hours when deposited onto PTCS or 6-PHTCS SAMs. Additionally, nanostructures were not affected by either toluene or hexane when deposited onto APTES SAM, and were stable in ethanol for up to an hour when deposited onto APTES SAM. Finally, it was discovered that using unfiltered DNA enabled better adsorption of structurally intact nanostructures on phenyl-terminated SAMs. It might be beneficial though

to discover other methods besides this to enable effective deposition of DNA nanostructure onto phenyl-terminated SAMs.

Throughout this experiment, we obtained results which could be further confirmed by utilizing different tests which could be easily conducted in the future. We believe that the DNA nanostructure was not observed on the surface of the APTES after two-hour exposure to ethanol due to the ethanol removing the APTES SAM. To test this, we would utilize XPS to compare the nitrogen intensity of APTES SAM before and after ethanol exposure. Currently, we are still uncertain as to why PTCS and 6-PHTCS gave such random results. PTCS and 6-PHTCS produced some samples showing intact nanostructures, deformed nanostructures, or a mixture of both. The PTCS overall had more success over 6-PHTCS in terms of maintaining structural integrity of the nanostructures.

We believe that the variation in results is the cause of either incomplete monolayers being formed on the surfaces, or the layering of ssDNA strands on the surface enabling the adsorption of structurally intact DNA nanostructures. We believe that either of these hypotheses could be confirmed by either using continuum IR microscopy or florescent DNA. Other future studies would include discovering other factors which might affect DNA adsorption onto phenyl-terminated SAMs, and modifying or altering certain factors to enable maximum DNA adsorption onto phenyl-terminated silanes.

Currently, we have a few results which cannot be confirmed at this time without additional data. These unknowns mainly revolve around the unusual behavior shown by the nanostructures adsorbed onto 6-PHTCS and their stability in both DIW and ionic solutions. Additionally, we are unsure as to why PTCS and 6-PHTCS show different results in regards to ionic solution exposure. Until further knowledge surrounding 6-PHTCS or the interaction

between DNA and phenyl-terminated silanes is uncovered, these findings will remain inconclusive.

Aside from additional research on phenyl-terminated silanes, this project could be further expanded upon. For example, one possibility would be investigating SAMs that possess other functional groups such as phosphates or sulfides. There are also various applications which could be tested. For example, it would be interesting to see if various SAMs could be used for DNA origami template lithography. These projects could be investigated later down the road by the current team or future researchers in the group. The field of DNA nanotechnology is greatly expanding. However, currently, there is a limited range of materials that DNA can properly interact with. This greatly limits the potential applications in this field of study. With a wider range of available surface materials for DNA adsorption, DNA nanotechnology could be expanded into other applications. This is why analyzing and discovering new materials for DNA nanostructures to interact with is essential for DNA nanotechnology. The investigation of organosilanes as potential surfaces for DNA nanostructures could lead to fantastic findings and discoveries which will not only benefit this field of study, but the future of mankind as well.

4.0: CONCLUSION

In this thesis, my research focused on DNA origami nanostructures interactions with various materials. These materials were either deposited onto nanostructures, or acted as surfaces for which nanostructures could adsorb onto. The information provided from this research could be used to help expand the realm of DNA nanotechnology by developing new methods to deposit material onto DNA nanostructures, or investigate new materials which could be used as substrates for DNA nanostructure adsorption. In both cases, the field of DNA nanotechnology would benefit as either study could potentially lead to new applicative achievements. Below, I summarize the main conclusions of each of my projects along with discussing the future directions of this thesis.

4.1: ULTRATHIN CALCIUM PHOSPHATE FILM COATING OF DNA ORIGAMI NANOSTRUCTURES

In chapter two, I discussed, developed, and demonstrated a facile method of coating ultrathin films of calcium phosphate on DNA origami nanostructures. Here, calcium cations and phosphate anions were applied to DNA origami templates using layer-by-layer deposition in hopes of forming ultrathin calcium phosphate films in the shape of the DNA origami template. However, due to complications and lack of experience in methodology, this project did not produce desired results. In the future, this project will hopefully be either repeated or improved upon. The idea of developing ultrathin films of inorganic materials utilizing DNA origami templates could lead to many desirable applications. As mentioned in chapter two, a variation of this project involving polymers is already being investigated. With this being said, due to the potential of success, this project should not be abandoned nor be considered a failure. With sufficient time, knowledge, and mastering of techniques, this project could be revived and reattempted.

4.2: DNA ORIGAMI NANOSTRUCTURE INTERACTIONS WITH VARIOUS SILANE SELF-ASSEMBLED MONOLAYERS

In chapter three, I discussed and presented my findings regarding how DNA origami nanostructures interact with various organosilane self-assembled monolayers. Here, DNA origami nanostructures were applied to different organosilanes to investigate the interactive behavior and chemical stability of the nanostructures when applied to these materials. It was found that APTES behaved very similarly to SiO_2, with the exception of long exposure to ethanol. Additionally, it is currently thought that the long exposure to ethanol leads to the removal of the APTES layer and with it the DNA nanostructures, but further testing would need to be performed to confirm this. The interactions between DNA origami nanostructures and phenyl-terminated silanes vary and produce random results, but it was discovered that unfiltered DNA can promote DNA adsorption. Finally, we found that hydrophobic silanes possessing long alkyl chains destabilize DNA nanostructures by disrupting the hydrophobic base stacking necessary for DNA double helix stability.

The findings of this project can be applied as a foundation for future investigations into analyzing DNA nanostructure interactive behavior with silane self-assembled monolayers. Additionally, the work surrounding the phenyl-terminated silanes has provided an avenue for other researchers to carry on the research surrounding the cause of the varying results observed. Furthermore, future projects revolving around phenyl-terminated silanes will be conducted to find ways to either optimize or improve DNA interaction between PTCS and 6-PHTCS. Finally, the kinetics and rate of film growth for the silanes were also investigated to determine optimal conditions for developing monolayers. This could be beneficial in better understanding the growth mechanisms of these self-assembled monolayers and discovering ways to optimize film growth. Future directions involving this project could include but are not

limited to: investigating new silanes for DNA interaction, determining whether multilayered SAMs affect DNA nanostructure interactive behavior, and developing methods to optimize DNA interaction with the SAMs studied.

4.3: FINAL REMARKS

Overall, my research provides new insight into how DNA origami nanostructures interact with various materials. I hope these results will be built upon and result in additional research to reveal the true potential of DNA nanostructures and their practical applications.

BIBLIOGRAPHY

1. Watson, J. D.; Crick, F. H. C., Molecular Structure of Nucleic Acids. *Resonance* **2004,** *9* (11), 96-98.

2. Watson, J.D.; Crick, F.H.C. The Structure of DNA. *Quant Biol* **1953**. (18), 123 – 131.

3. Travers, A.; Muskhelishvili, G. DNA Structure and Function. *FEBS Journal* **2015**. *282* (**12)**, 2279 – 2295.

4. Seeman, N. C., Nanotechnology and the Double Helix. *Scientific American* **2004,** *290* (6), 64-75.

5. Rothemund, P. W. K., Folding DNA to create nanoscale shapes and patterns. *Nature* **2006,** *440* (7082), 297-302

6. Andersen, E. S.; Dong, M.; Nielsen, M. M.; Jahn, K.; Lind-Thomsen, A.; Mamdouh, W.; Gothelf, K. V.; Besenbacher, F.; Kjems, J., DNA origami design of dolphin-shaped structures with flexible tails. *ACS nano* **2008,** *2* (6), 1213-1218.

7. Andersen, E. S.; Dong, M.; Nielsen, M. M.; Jahn, K.; Subramani, R.; Mamdouh, W.; Golas, M. M.; Sander, B.; Stark, H.; Oliveira, C. L.; Pedersen, J. S.; Birkedal, V.; Besenbacher, F.; Gothelf, K. V.; Kjems, J., Self-assembly of a nanoscale DNA box with a controllable lid. *Nature* **2009,** *459* (7243), 73-76.

8. Douglas, S. M.; Dietz, H.; Liedl, T.; Hogberg, B.; Graf, F.; Shih, W. M., Self-assembly of DNA into nanoscale three-dimensional shapes. *Nature* **2009,** *459* (7245), 414-418.

9. Han, D. R.; Pal, S.; Nangreave, J.; Deng, Z. T.; Liu, Y.; Yan, H., DNA Origami with Complex Curvatures in Three-Dimensional Space. *Science* **2011,** *332* (6027), 342-346.

10. Wei, B.; Dai, M. J.; Yin, P., Complex Shapes Self-Assembled from Single-Stranded DNA Tiles. *Nature* **2012,** *485* (7400), 623-626.

11. Hawker, C. J.; Wooley, K. L., The convergence of synthetic organic and polymer chemistries. *Science* **2005,** *309* (5738), 1200-1205.

12. Yan, H.; Park, S. H.; Finkelstein, G.; Reif, J. H.; LaBean, T. H., DNA-templated self-assembly of protein arrays and highly conductive nanowires. *Science* **2003,** *301* (5641), 1882-1884.

13. Wang, P.; Meyer, T. A.; Pan, V.; Dutta, P. K.; Ke, Y. The Beauty and Utility of DNA Origami. *Chem* **2017**, *2* (3), 359–382.

14. Escher, M.C. *Depth*. **1955**.

15. Seeman, N. C., Nucleic acid junctions and lattices. *Journal of Theoretical Biology* **1982,** *99* (2), 237-247.

16. Fu, T.-J.; Tse-Dinh, Y.-C.; Seeman, N. C., Holliday Junction Crossover Topology. *Journal of Molecular Biology* **1994,** *236* (1), 91-105.

17. Ma, R. I.; Kallenbach, N. R.; Sheardy, R. D.; Petrillo, M. L.; Seeman, N. C., Three-arm nucleic acid junctions are flexible. *Nucleic Acids Research* **1986,** *14* (24), 9745-9753.

18. Seeman, N.C. Construction of Three-Dimensional Stick Figures from Branched DNA. *DNA and Cell Biology* **1991**, *10* (7), 475–486.

19. Ding, B. Q.; Sha, R. J.; Seeman, N. C., Pseudohexagonal 2D DNA Crystals from Double Crossover Cohesion. *J. Am. Chem. Soc.* **2004,** *126* (33), 10230-10231.

20. He, Y.; Chen, Y.; Liu, H. P.; Ribbe, A. E.; Mao, C. D., Self-Assembly of Hexagonal DNA Two-Dimensional (2D) Arrays. *Journal of the American Chemical Society* **2005,** *127* (35), 12202-12203.

21. Rothemund, P. W. K., Folding DNA to create nanoscale shapes and patterns. *Nature* **2006,** *440* (7082), 297-302.

22. Douglas, S. M.; Dietz, H.; Liedl, T.; Högberg, B.; Graf, F.; Shih, W. M. Self-Assembly of DNA into Nanoscale Three-Dimensional Shapes. *Nature* **2009**, *459* (7245), 414–418.

23. Han, D.; Pal, S.; Nangreave, J.; Deng, Z.; Liu, Y.; Yan, H., DNA origami with complex curvatures in three-dimensional space. *Science* **2011,** *332* (6027), 342-346.

24. Martynenko, I. V.; Ruider, V.; Dass, M.; Liedl, T.; Nickels, P. C. DNA Origami Meets Bottom-up Nanopatterning. *ACS Nano* **2021**, *15* (7), 10769–10774.

25. Hernández-Ainsa, S.; Keyser, U. F. DNA Origami Nanopores: Developments, Challenges and Perspectives. *Nanoscale* **2014**, *6* (23), 14121–14132.

26. Sacca, B.; Niemeyer, C. M. Cheminform Abstract: DNA Origami: The Art of Folding DNA. *ChemInform* **2012**, *43* (14).

27. Ke, Y.; Ong, L. L.; Shih, W. M.; Yin, P. Three-Dimensional Structures Self-Assembled from DNA Bricks. *Science* **2012**, *338* (6111), 1177–1183.

28. Voigt, N., Tørring, T., Rotaru, A. *et al.* Single-molecule chemical reactions on DNA origami. *Nature Nanotech* **2010**, *5***,** 200–203.

29. Shih, W. M.; Lin, C. Knitting Complex Weaves with DNA Origami. *Current Opinion in Structural Biology* **2010**, *20* (3), 276–282.

30. Jia, S.; Wang, J.; Xie, M.; Sun, J.; Liu, H.; Zhang, Y.; Chao, J.; Li, J.; Wang, L.; Lin, J.; Gothelf, K. V.; Fan, C. Programming DNA Origami Patterning with Non-Canonical DNA-Based Metallization Reactions. *Nature Communications* **2019**, *10* (1).

31. Braun, E.; Eichen, Y.; Sivan, U.; Ben-Yoseph, G. DNA-Templated Assembly and Electrode Attachment of a Conducting Silver Wire. *Nature* **1998**, *391* (6669), 775–778.

32. Ke, Y.; Bellot, G.; Voigt, N. V.; Fradkov, E.; Shih, W. M. Two Design Strategies for Enhancement of Multilayer–DNA-Origami Folding: Underwinding for Specific Intercalator Rescue and Staple-Break Positioning. *Chemical Science* **2012**, *3* (8), 2587.

33. Liu, J.; Geng, Y.; Pound, E.; Gyawali, S.; Ashton, J. R.; Hickey, J.; Woolley, A. T.; Harb, J. N. Metallization of Branched DNA Origami for Nanoelectronic Circuit Fabrication. *ACS Nano* **2011**, *5* (3), 2240–2247.

34. Shen, B.; Linko, V.; Tapio, K.; Kostiainen, M. A.; Toppari, J. J. Custom-Shaped Metal Nanostructures Based on DNA Origami Silhouettes. *Nanoscale* **2015**, *7* (26), 11267–11272.

35. Vittala, S. K.; Zhao, Y.; Han, D. Programmed Assembly of DNA Templates by Silver Nanowires. *ChemPlusChem* **2022**, *87* (1).

36. Wu, Z.; Ge, S.; Chang, M.; Li, W.; Tao, K. Synthesis of Nickel Nanoparticles Supported on Metal Oxides Using Electroless Plating: Controlling the Dispersion and Size of Nickel Nanoparticles. *J. of Colloid and Interface Science* **2009**, *330*, 359 – 366.

37. Park, S. H.; Barish, R.; Li, H. Y.; Reif, J. H.; Finkelstein, G.; Yan, H.; LaBean, T. H. Three Helix Bundle DNA Tiles Self Assemble into 2D Lattice or 1D Templates for Silver Nanowires. *Nano Lett*. **2005**, *5*, 693-696.

38. Lee, J. S.; Abigail, K.R.; Jean, L.; Hurst, S. J.; Mirkin, C. A. Silver Nanoparticle – Oligonucleotide Conjugates Based on DNA with Triple Cyclic Disulfide Moieties. *Nano Lett*. **2007**, *7* (7), 2112 – 2115.

39. Pilo-Pais, M.; Goldberg, S.; Samano, E.; LaBean, T. H.; Finkelstein, G. Connecting the Nanodots: Programmable Nanofabrication of Fused Metal Shapes on DNA Templates. *Nano Letters* **2011**, *11* (8), 3489–3492.

40. Zhao, Y.; Zhang, C.; Yang, L.; Xu, X.; Xu, R.; Ma, Q.; Tang, Q.; Yang, Y.; Han, D. Programmable and Site-Specific Patterning on DNA Origami Templates with Heterogeneous Condensation of Silver and Silica. *Small* **2021**, *17* (47), 2103877.

41. Xu, Z.; Huang, Y.; Yin, H.; Zhu, X.; Tian, Y.; Min, Q. DNA Origami-Based Protein Manipulation Systems: From Function Regulation to Biological Application. *ChemBioChem* **2022**.

42. Aslan, H.; Krissanaprasit, A.; Besenbacher, F.; Gothelf, K. V.; Dong, M. Protein Patterning by a DNA Origami Framework. *Nanoscale* **2016**, *8* (33), 15233–15240.

43. Gopinath, A.; Rothemund, P. W. Optimized Assembly and Covalent Coupling of Single-Molecule DNA Origami Nanoarrays. *ACS Nano* **2014**, *8* (12), 12030–12040.

44. Pillers, M. A.; Lieberman, M. Thermal Stability of DNA Origami on Mica. *Journal of Vacuum Science & Technology B, Nanotechnology and Microelectronics: Materials, Processing, Measurement, and Phenomena* **2014**, *32* (4), 040602.

45. Kabiri, Y.; Ananth, A. N.; van der Torre, J.; Katan, A.; Hong, J. Y.; Malladi, S.; Kong, J.; Zandbergen, H.; Dekker, C. Distortion of DNA Origami on Graphene Imaged with Advanced TEM Techniques. *Small* **2017**, *13* (31), 1700876.

46. Surwade, S. P.; Zhao, S.; Liu, H. Molecular Lithography through DNA-Mediated Etching and Masking of SiO_2. *Journal of the American Chemical Society* **2011**, *133* (31), 11868–11871.

47. Diagne, C. T.; Brun, C.; Gasparutto, D.; Baillin, X.; Tiron, R. DNA Origami Mask for Sub-Ten-Nanometer Lithography. *ACS Nano* **2016**, *10* (7), 6458–6463.

48. Thomas, G.; Diagne, C. T.; Baillin, X.; Chevolleau, T.; Charvolin, T.; Tiron, R. DNA Origami for Silicon Patterning. *ACS Applied Materials & Interfaces* **2020**, *12* (32), 36799–36809.

49. Poppa, H.; Elliot, A. G. The Surface Composition of Mica Substrates. *Surface Science* **1971**, *24* (1), 149–163.

50. Green, N. S.; Pham, P. H.; Crow, D. T.; Burke, P. J.; Norton, M. L. Layered Graphene-Mica Substrates Induce Melting of DNA Origami. *Materials Research Express* **2018**, *5* (4), 045035.

51. Pastré, D.; Hamon, L.; Landousy, F.; Sorel, I.; David, M.-O.; Zozime, A.; Le Cam, E.; Piétrement, O. Anionic Polyelectrolyte Adsorption on Mica Mediated by Multivalent Cations: A Solution to DNA Imaging by Atomic Force Microscopy under High Ionic Strengths. *Langmuir* **2006**, *22* (15), 6651–6660.

52. Woo, S.; Rothemund, P. W. Self-Assembly of Two-Dimensional DNA Origami Lattices Using Cation-Controlled Surface Diffusion. *Nature Communications* **2014**, *5* (1).

53. Kielar, C.; Xin, Y.; Shen, B.; Kostiainen, M. A.; Grundmeier, G.; Linko, V.; Keller, A. On the Stability of DNA Origami Nanostructures in Low-Magnesium Buffers. *Angewandte Chemie* **2018**, *130* (30), 9614–9618.

54. Roodhuizen, J. A.; Hendrikx, P. J.; Hilbers, P. A.; de Greef, T. F.; Markvoort, A. J. Counterion-Dependent Mechanisms of DNA Origami Nanostructure Stabilization Revealed by Atomistic Molecular Simulation. *ACS Nano* **2019**, *13* (9), 10798–10809.

55. Xu, Z.; Huang, Y.; Yin, H.; Zhu, X.; Tian, Y.; Min, Q. DNA Origami-Based Protein Manipulation Systems: From Function Regulation to Biological Application. *ChemBioChem* **2022**.

56. Güell, A. G.; Tan, S.; Unwin, P. R.; Zhang, G. Electrochemistry at Highly Oriented Pyrolytic Graphite (HOPG): Toward a New Perspective. *Advances in Electrochemical Sciences and Engineering* **2015**, 31–82.

57. Gorodetsky, A. A.; Barton, J. K. Electrochemistry Using Self-Assembled DNA Monolayers on Highly Oriented Pyrolytic Graphite. *Langmuir* **2006**, *22* (18), 7917–7922.

58. Brglez, J.; Nikolov, P.; Angelin, A.; Niemeyer, C. M. Designed Intercalators for Modification of DNA Origami Surface Properties. *Chemistry - A European Journal* **2015**, *21* (26), 9440–9446.

59. Rahman, M.; Neff, D.; Green, N.; Norton, M. DNA Origami Reorganizes upon Interaction with Graphite: Implications for High-Resolution DNA Directed Protein Patterning. *Nanomaterials* **2016**, *6* (11), 196.

60. Green, N.S. et al.; Interactions of DNA with graphene and sensing applications of graphene field-effect transistor devices: A review. *Analytica chimica acta*. **2015**, *853*, 127 – 142.

61. Zhang, X.; Hongmei, H.; DNA molecules site-specific immobilization and their applications. *Open Chemistry*. **2014**, *12* (10), 977 – 993.

62. Umemura, K.; Hybrids of Nucleic Acids and Carbon Nanotube for Nanobiotechnology. *Nanomaterials*. **2015**, *5* (1), 321 – 350.

63. Khattat, M.M., Rafati, A., and Gill, P., Fabrication of DNA Nanotubes Using Origami-Based Nanostructures with Sticky Ends. *Journal of Nanostructure in Chemistry*. **2015**, *5*(2), 177 – 183.

64. Zhiguo, L., et al. Assembly of Single-Stranded DNA onto HOPG Surface at Different Temperature: Atomic Force Microscopy Study. *Scanning*. **2012**. *34(*5), 302 – 308.

65. Dubrovin, E.V. et al. The Effect of Underlying Octadecylamine Monolayer on the DNA Conformation on the Graphite Surface. *Colloids and Surfaces B: Biointerfaces*. **2010**. *76*, 63 – 69.

66. Zhao, L., et al. Influence of Mg^{2+}, Ni^{2+}, and Cu^{2+} on DNA Assembly onto HOPG Surfaces: Atomic Force Microscopy Study. **2012**. *34*, 68 – 75.

67. Campos, R.; Zhang, S.; Majikes, J. M.; Ferraz, L. C.; LaBean, T. H.; Dong, M. D.; Ferapontova, E. E. Electronically Addressable Nanomechanical Switching of I-Motif DNA Origami Assembled on Basal Plane HOPG. *Chemical Communications* **2015**, *51* (74), 14111–14114.

68. Ricardo, K. B.; Xu, A.; Salim, M.; Zhou, F.; Liu, H. Deposition of DNA Nanostructures on Highly Oriented Pyrolytic Graphite. *Langmuir* **2017**, *33* (16), 3991–3997.

69. Zhang, X.; Rahman, M.; Neff, D.; Norton, M. L. DNA Origami Deposition on Native and Passivated Molybdenum Disulfide Substrates. *Beilstein Journal of Nanotechnology* **2014**, *5*, 501–506.
70. Gállego, I.; Manning, B.; Prades, J. D.; Mir, M.; Samitier, J.; Eritja, R. DNA-Origami-Driven Lithography for Patterning on Gold Surfaces with Sub-10 Nm Resolution. *Advanced Materials* **2017**, *29* (11), 1603233.

71. Greene, J. E. Review Article: Tracing the Recorded History of Thin-Film Sputter Deposition: From the 1800s to 2017. *Journal of Vacuum Science & Technology A: Vacuum, Surfaces, and Films* **2017**, *35* (5).

72. Kuzyk, A.; Jungmann, R.; Acuna, G. P.; Liu, N. DNA Origami Route for Nanophotonics. *ACS Photonics* **2018**, *5* (4), 1151–1163.

73. Uprety, B.; Westover, T.; Stoddard, M.; Brinkerhoff, K.; Jensen, J.; Davis, R. C.; Woolley, A. T.; Harb, J. N. Anisotropic Electroless Deposition on DNA Origami Templates to Form Small Diameter Conductive Nanowires. *Langmuir* **2017**, *33* (3), 726–735.

74. Martynenko, I. V.; Ruider, V.; Dass, M.; Liedl, T.; Nickels, P. C. DNA Origami Meets Bottom-up Nanopatterning. *ACS Nano* **2021**, *15* (7), 10769–10774.

75. Chen, W.; McCarthy, T. J. Layer-by-Layer Deposition: a Tool for Polymer Surface Modification. *Macromolecules* **1997**, *30* (1), 78–86.

76. Dubas, S. T.; Kumlangdudsana, P.; Potiyaraj, P. Layer-by-Layer Deposition of Antimicrobial Silver Nanoparticles on Textile Fibers. *Colloids and Surfaces A: Physicochemical and Engineering Aspects* **2006**, *289* (1-3), 105–109.

77. Ostrander, J. W.; Mamedov, A. A.; Kotov, N. A. Two Modes of Linear Layer-by-Layer Growth of Nanoparticle−Polylectrolyte Multilayers and Different Interactions in the Layer-by-Layer Deposition. *Journal of the American Chemical Society* **2001**, *123* (6), 1101–1110.

78. Groth, T.; Lendlein, A. Layer-by-Layer Deposition of Polyelectrolytes — a Versatile Tool for the in Vivo Repair of Blood Vessels. *ChemInform* **2004**, *35* (18).

79. Kirkland, J. J. Porous Thin-Layer Modified Glass Bead Supports for Gas Liquid Chromatography. *Analytical Chemistry* **1965**, *37* (12), 1458–1461.

80. Trubetskoy, V. S.; Loomis, A.; Hagstrom, J. E.; Budker, V. G.; Wolff, J. A. Layer1by-Layer Deposition of Oppositely Charged Polyelectrolytes on the Surface of Condensed DNA Particles. *Nucleic Acids Research* **1999**, *27* (15), 3090–3095.

81. Cho, Y.; Lee, J. B.; Hong, J. Controlled Release of an Anti-Cancer Drug from DNA Structured Nano-Films. *Scientific Reports* **2014**, *4* (1).

82. Kim, T.; Nam, K.; Kim, Y. M.; Yang, K.; Roh, Y. H. DNA-Assisted Smart Nanocarriers: Progress, Challenges, and Opportunities. *ACS Nano* **2021**, *15* (2), 1942–1951.
83. Nicolau, Y. F.; Menard, J. C. Solution Growth of ZnS, Cds and zn1-Xcdxs Thin Films by the Successive Ionic-Layer Adsorption and Reaction Process; Growth Mechanism. *Journal of Crystal Growth* **1988**, *92* (1-2), 128–142.

84. Wu, S.; Zhang, M.; Song, J.; Weber, S.; Liu, X.; Fan, C.; Wu, Y. Fine Customization of Calcium Phosphate Nanostructures with Site-Specific Modification by DNA Templated Mineralization. *ACS Nano.* **2020**, *15* (1), 1555– 1565.

85. Hader, A.; Achik, I.; Hajjaji, A.; Boughaleb, Y. The Ordering Islands Growth Kinetics during Self-Assembled Monolayer Formation. *Optical Materials* **2012**, *34* (10), 1713–1716.

86. Greene, J. E. Review Article: Tracing the Recorded History of Thin-Film Sputter Deposition: From the 1800s to 2017. *Journal of Vacuum Science & Technology A: Vacuum, Surfaces, and Films* **2017**, *35* (5).

87. W.C. Bigelow, D.L. Pickett, W.A. Zisman, Oleophobic monolayers: I. Films adsorbed from solution in non-polar liquids. *Journal of Colloid Science.* **1946**. *1*(6). 513 – 538.

88. Haller, I. Covalently Attached Organic Monolayers on Semiconductor Surfaces. *Journal of the American Chemical Society* **1978**, *100* (26), 8050–8055.

89. Nuzzo, R. G.; Allara, D. L. Adsorption of Bifunctional Organic Disulfides on Gold Surfaces. *Journal of the American Chemical Society* **1983**, *105* (13), 4481–4483.

90. Ulman, A. Formation and Structure of Self-Assembled Monolayers. *Chemical Reviews* **1996**, *96* (4), 1533–1554.

91. Mrksich, M.; Whitesides, G. M. Using Self-Assembled Monolayers to Understand the Interactions of Man-Made Surfaces with Proteins and Cells. *Annual Review of Biophysics and Biomolecular Structure* **1996**, *25* (1), 55–78.

92. Eberle, F.; Metzler, M.; Kolb, D. M.; Saitner, M.; Wagner, P.; Boyen, H.-G. Metallization of Ultra-Thin, Non-Thiol Sams with Flat-Lying Molecular Units: PD on 1, 4-Dicyanobenzene. *ChemPhysChem* **2010**, *11* (13), 2951–2956.

93. Mwanda, J. A.; Cuesta, A. Electrochemical Metallization of Molecular Adlayers. *Current Opinion in Electrochemistry* **2019**, *17*, 72–78.

94. Nicosia, C.; Huskens, J. Reactive Self-Assembled Monolayers: From Surface Functionalization to Gradient Formation. *Mater. Horiz.* **2014**, *1*, 32–45.

95. Zhao, X.; Kopelman, R. Mechanism of Organosilane Self-Assembled Monolayer Formation on Silica Studied by Second-Harmonic Generation. *The Journal of Physical Chemistry* **1996**, *100* (26), 11014–11018.

96. Hinckley, A. P.; Muscat, A. J. Detecting and Removing Defects in Organosilane Self-Assembled Monolayers. *Langmuir* **2020**, *36* (10), 2563–2573.

97. Haensch, C.; Hoeppner, S.; Schubert, U. S. Cheminform Abstract: Chemical Modification of Self-Assembled Silane Based Monolayers by Surface Reactions. *ChemInform* **2010**, 41 (42).

98. Kitaev, V.; Seo, M.; McGovern, M. E.; Huang, Y.-jung; Kumacheva, E. Mixed Monolayers Self-Assembled on Mica Surface. *Langmuir* **2001**, *17* (14), 4274–4281.

99. Sugimura, H.; Ushiyama, K.; Hozumi, A.; Takai, O. Micropatterning of Alkyl- and Fluoroalkylsilane Self-Assembled Monolayers Using Vacuum Ultraviolet Light. *Langmuir* **2000**, *16* (3), 885–888.

100. Liu, J.; Zhang, L.; Gu, N.; Hong, Q.; Ren, J.; Wu, Y.; Mao, P.; Chen, D.; Lu, Z. Micro-Patterning of 3-Aminopropyltrimethoxy- Silane Self-Assembled Monolayers with Colloidal Gold. *Supramolecular Science* **1998**, *5* (5-6), 705–708.

101. Morrill, A. R.; Duong, D. T.; Lee, S. J.; Moskovits, M. Imaging 3-Aminopropyltriethoxysilane Self-Assembled Monolayers on Nanostructured Titania and Tin (IV) Oxide Nanowires Using Colloidal Silver Nanoparticles. *Chemical Physics Letters* **2009**, *473* (1-3), 116–119.

102. Zhang, G.-J.; Tanii, T.; Zako, T.; Hosaka, T.; Miyake, T.; Kanari, Y.; Funatsu, T.; Ohdomari, I. Nanoscale Patterning of Protein Using Electron Beam Lithography of Organosilane Self-Assembled Monolayers. *Small* **2005**, *1* (8-9), 833–837.

103. Surwade, S. P.; Zhou, F.; Li, Z.; Powell, A.; O'Donnell, C.; **Liu, H.*** "Nanoscale Patterning of Self-assembled Monolayers using DNA Nanostructure Templates" *Chem. Comm.*, **2016**, *52*, 1677-1680.

104. Kim, K. N.; Sarveswaran, K.; Mark, L.; Lieberman, M. Comparison of Methods for Orienting and Aligning DNA Origami. *Soft Matter* **2011**, *7* (10), 4636.

105. Sarveswaran, K.; Gao, B.; Kim, K. N.; Bernstein, G. H.; Lieberman, M. Adhesion of DNA Nanostructures and DNA Origami to Lithographically Patterned Self-Assembled Monolayers on Si[100]. *SPIE Proceedings* **2010**.

106. Allemand, J. F.; Bensimon, D.; Jullien, L.; Bensimon, A.; Croquette, V. Ph-Dependent Specific Binding and Combing of DNA. *Biophysical Journal* **1997**, *73* (4), 2064–2070.

107. Hui, L. et al. Deposit DNA Nanostructures on Hydrophobic Substrates.

108. Yang, S.-R.; Kolbesen, B. O. A Comparative Study of the Growth of Octadecyltrichlorosilane and 3-Mercaptopropyltrimethoxysilane Self-Assembled Monolayers on Hydrophilic Silicon Surfaces. *Applied Surface Science* **2008**, *255* (5), 1726–1735.

109. Kampyli, V.; Phillips, D. A. S.; Renfrew, A. H. M. Reactive Dyes Containing a 4-M-Carboxypyridinium-1,3,5-Triazine-2-Oxide Reactive Group: Exhaust Dyeing of Cotton under Alkaline and Neutral Fixation Conditions. *Dyes and Pigments* **2004**, *61* (2), 165–175.

110. Leaving Groups https://chem.libretexts.org/@go/page/1147 (accessed Apr 28, 2022).

111. Stenger, D. A.; Pike, C. J.; Hickman, J. J.; Cotman, C. W. Surface Determinants of Neuronal Survival and Growth on Self-Assembled Monolayers in Culture. *Brain Research* **1993**, *630* (1-2), 136–147.

112. Moineau, J.; Granier, M.; Lanneau, G. F. Organized Self-Assembled Monolayers from Organosilanes Containing Rigid π-Conjugated Aromatic Segments. *Langmuir* **2004**, *20* (8), 3202–3207.

113. Patrone, L.; Gadenne, V.; Desbief, S. Single and Binary Self-Assembled Monolayers of Phenyl- and Pentafluorophenyl-Based Silane Species, and Their Phase Separation with Octadecyltrichlorosilane. *Langmuir* **2010**, *26* (22), 17111–17118.

114. Ogino, M.; Taya, Y.; Fujimoto, K. Detection of Methylcytosine by DNA Photoligation via Hydrophobic Interaction of the Alkyl Group. *Organic & Biomolecular Chemistry* **2009**, *7* (15), 3163.

115. Balakrishnan, G.; Rajendran, T.; Senthil Murugan, K.; Sathish Kumar, M.; Sivasubramanian, V. K.; Ganesan, M.; Mahesh, A.; Thirunalasundari, T.; Rajagopal, S. Interaction of Rhenium(i) Complex Carrying Long Alkyl Chain with Calf Thymus DNA: Cytotoxic and Cell Imaging Studies. *Inorganica Chimica Acta* **2015**, *434*, 51–59.

116. Tang, B.; Tang, B.; Cheang; Wang, S.; Pro Xu. Promising Plasmid DNA Vector Based on APTES-Modified Silica Nanoparticles. *International Journal of Nanomedicine* **2012**, 1061.

117. Chu-jiang, C.; Zhi-gang, S.; Yu-shan, X.; Shu-lin, M. Surface Topography and Character of γ-Aminopropyltriethoxysilane and Dodecyltrimethoxysilane Films Adsorbed on the Silicon Dioxide Substrate via Vapour Phase Deposition. *Journal of Physics D: Applied Physics* **2006**, *39* (22), 4829–4837.

118. Miranda, A.; Martínez, L.; De Beule, P. A. A. Facile Synthesis of an Aminopropylsilane Layer on Si/SiO2 Substrates Using Ethanol as Aptes Solvent. *MethodsX* **2020**, *7*, 100931.

119. Dulcey, C. S.; Georger,, J. H.; Chen, M.-S.; McElvany, S. W.; O'Ferrall, C. E.; Benezra, V. I.; Calvert, J. M. Photochemistry and Patterning of Self-Assembled Monolayer Films Containing Aromatic Hydrocarbon Functional Groups. *Langmuir* **1996**, *12* (6), 1638–1650.

120. Xiang, J.; Zhu, P.; Masuda, Y.; Koumoto, K. Fabrication of Self-Assembled Monolayers (Sams) and Inorganic Micropattern on Flexible Polymer Substrate. *Langmuir* **2004**, *20* (8), 3278–3283.

121. Bartlam, C.; Morsch, S.; Heard, K. W. J.; Quayle, P.; Yeates, S. G.; Vijayaraghavan, A. Nanoscale Infrared Identification and Mapping of Chemical Functional Groups on Graphene. *Carbon* **2018**, *139*, 317–324.

122. Dillingham, M. S.; Tibbles, K. L.; Hunter, J. L.; Bell, J. C.; Kowalczykowski, S. C.; Webb, M. R. Fluorescent Single-Stranded DNA Binding Protein as a Probe for Sensitive, Real-Time Assays of Helicase Activity. *Biophysical Journal* **2008**, *95* (7), 3330–3339.

123. Gómez-Varela, A. I.; Stamov, D. R.; Miranda, A.; Alves, R.; Barata-Antunes, C.; Dambournet, D.; Drubin, D. G.; Paiva, S.; De Beule, P. A. Simultaneous Co-Localized Super-Resolution Fluorescence Microscopy and Atomic Force Microscopy: Combined Sim and AFM Platform for the Life Sciences. *Scientific Reports* **2020**, *10* (1).

124. Liu, J.; Qian, N.; Morrical, S. W. Dynamics of Bacteriophage T4 Presynaptic Filament Assembly from Extrinsic Fluorescence Measurements of GP32-Single-Stranded DNA Interactions. *Journal of Biological Chemistry* **2006**, *281* (36), 26308–26319.

125. Kim, H.; Surwade, S. P.; Powell, A.; O'Donnell, C.; Liu, H. Stability of DNA Origami Nanostructure under Diverse Chemical Environments. *Chemistry of Materials* **2014**, *26* (18), 5265–5273.

126. Gaillard, C.; Strauss, F. Ethanol Precipitation of DNA with Linear Polyacrylamide as Carrier. *Nucleic Acids Research* **1990**, *18* (2), 378–378.

127. Simon, A.; Cohen-Bouhacina, T.; Porté, M. C.; Aimé, J. P.; Baquey, C. Study of Two Grafting Methods for Obtaining a 3-Aminopropyltriethoxysilane Monolayer on Silica Surface. *Journal of Colloid and Interface Science* **2002**, *251* (2), 278–283.

128. Tomić, M.; Fohlerova, Z.; Gràcia, I.; Figueras, E.; Cané, C.; Vallejos, S. UV-Light Activated APTES Modified WO3-X Nanowires Sensitive to Ethanol and Nitrogen Dioxide. *Sensors and Actuators B: Chemical* **2021**, *328*, 129046.

129. Aghebat Rafat, A.; Pirzer, T.; Scheible, M. B.; Kostina, A.; Simmel, F. C. Surface-Assisted Large-Scale Ordering of DNA Origami Tiles. *Angewandte Chemie International Edition* **2014**, *53* (29), 7665–7668.

130. Martinez, C. R.; Iverson, B. L. Cheminform Abstract: Rethinking the Term “Pi-Stacking.” *ChemInform* **2012**, *43* (46).

131. Sinnokrot, M. O.; Valeev, E. F.; Sherrill, C. D. Estimates of the Ab Initio Limit for π–π Interactions: the Benzene Dimer. *Journal of the American Chemical Society* **2002**, *124* (36), 10887–10893.